



HUNGARIAN
ACADEMY
OF SCIENCES

Hungarian Agricultural Engineering

N^o 32/2017

Editors-in-Chief:
Dr László TÓTH
Dr. László KÁTAI

Managing Editor:
Dr. Csaba FOGARASSY

Secretary of Editorial board:
Dr. László MAGÓ

Editorial Board:

Dr. David C. FINGER
Dr. György SITKEI
Dr. Gábor KESZTHELYI-SZABÓ
Dr. László TÓTH
Dr. János BEKE
Dr. István SZABÓ
Dr. István J. JÓRI
Dr. Béla HORVÁTH
Dr. Péter SEMBERY
Dr. László FENYVESI
Dr. Csaba FOGARASSY
Dr. Zoltán BÁRTFAI
Dr. László MAGÓ
Dr. Bahattin AKDEMIR
Dr. R. Cengiz AKDENIZ
Dr. József NYERS
Dr. Mičo V. OLJAČA
Dr. Zdenek PASTOREK
Dr. Vijaya G.S. RAGHAVAN
Dr. Lazar SAVIN
Dr. Bart SONCK
Dr. Goran TOPISIROVIĆ
Dr. Valentin VLADUT

PERIODICAL OF THE COMMITTEE OF
AGRICULTURAL ENGINEERING OF
THE
HUNGARIAN ACADEMY OF SCIENCES

Published by

Szent István University, Gödöllő
Faculty of Mechanical Engineering
H-2103 Gödöllő, Páter K. u. 1.



Gödöllő
2017

Published online: <http://hae-journals.org>
HU ISSN 0864-7410 (Print)
HU ISSN 2415-9751(Online)

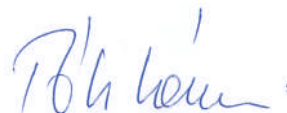
PREFACE

In the name of the Committee of Agricultural and Biosystem Engineering of the Hungarian Academy of Sciences we would like to welcome everyone who is interested in reading our journal. The Hungarian Agricultural Engineering (HAE) journal was published 30 years ago for the very first time with an aim to introduce the most valuable and internationally recognized Hungarian studies about mechanization in the field of agriculture and environmental protection. In the year of 2014 the drafting committee decided to spread it also in electronic (on-line and DOI) edition and make it entirely international. From this year exclusively the Szent István University's Faculty of Mechanical Engineering took the responsibility to publish the paper twice a year in cooperation with the Hungarian Academy of Sciences. Our goal is to occasionally report the most recent researches regarding mechanization in agricultural sciences (agricultural and environmental technology and chemistry, livestock, crop production, feed and food processing, agricultural and environmental economics and energy production) with the help of several authors. The drafting committee has been established with the involvement of outstanding Hungarian researchers who are recognized on international level as well. All papers are selected by our editorial board and a triple blind review process by prominent experts which process could give the highest guarantee for the best scientific quality. We hope that our journal provides accurate information for the international scientific community and serves the aim of the Hungarian agricultural and environmental engineering research.

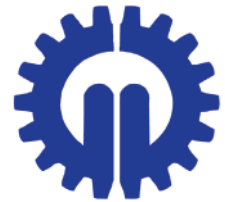
Gödöllő, 31.12.2017.



Dr. László KÁTAI
editor in chief



Dr. László TÓTH
editor in chief



A REVIEW OF PERFORMANCE HYBRID PHOTOVOLTAIC/THERMAL SYSTEM FOR GENERAL - APPLICATIONS

Author(s):

M.H.R. Alktranee

Affiliation:

Department of Mechanical, Technical Institute of Basrah, Southern Technical University, Basrah, Iraq.

Email address:

mohammed84alktranee@gmail.com

Abstract

Photovoltaic modules can generate more electricity when receives a big quantity of solar radiation, but the efficiency of (PV) modules will drop when the temperature of solar cells is high. Therefore, reducing the high temperatures of (PV) modules will contribute to increase the electrical efficiency of (PV) modules by extraction the thermal energy associated with the PV modules and achieve an appropriate conversion efficiency of (PV). The aim of the study in this paper is to recognize the performance of hybrid (PV/T) systems in different places, conditions, module designs which can be used in household applications, hotels, etc. Aiming to supply of electricity and thermal energy. The study indicates to use of cooling technique (water or air) to cooling (PV) modules will contribute to a large extent to strengthen the work of solar cells and the efficiency of (PV/T) system as well. And the rate return of the system of electricity and thermal energy will increase, especially when the hybrid photovoltaic/thermal (PV/T) solar systems were properly designed and the conversion rate of absorbed solar radiation for (PV) modules will increase as well.

Keywords

Photovoltaic, Thermal energy, PV efficiency, Solar radiation, Combisystem.

Introduction

Hybrid photovoltaic/thermal system experiencing rapid growth which provides simultaneously both electrical and thermal energy making it interesting for many applications [1], For that many researches has been conducted in developing and improving the performance of the system by increasing its efficiency, use (water or air) as a technique to cooling

solar cells the temperature reaches high levels and the negative effects on the work of the solar cells will appear [2]. This system contributes to reduction of environmental problems by reduce CO₂ emissions are needed in houses and buildings and concentrate on use renewable energy that should be more actively [3], the amount of energy that produce from hybrid PV/T system depend on the photovoltaic which convert only a small part of the absorbed solar radiation into electricity and type of solar cells use, where the greater part of solar radiation converted into heat and that lead to increasing their temperature and decreasing their electrical efficiency [4], Hybrid PV/T system produces electricity and heat (air or water preheating), that will contribute to improve efficiency of PV(/T) modules by extracting the heat loose by using (air or water) as a removal fluid and take this advantage for using in many applications [5]. Several study have been done about using air or water PV/T systems some of research found that use water systems seem desirable because of the nature of this fluid allowing better recovery of the heat [6], while other researches find that the results from an applied air type PV/T system gives a variety of results regarding the effect of design module and operational parameters on the performance of air type PV/T systems [7, 8], where can use the air to cool the surface temperature of the PV panel after pick up the surface heat which can use for household application, drying and other industrial purposes [9]. To ensure solar cell operate at low temperature and keep the PV module efficiency at a sufficient level, where used natural or forced (air or water) circulation as a simple method to remove heat from PV modules, but this method is less effective, especially if the ambient temperature is more than 20°C, to overcome that can be extracted the heat by circulating (air or water) through a heat exchanger that is mounted at the back

surface of the PV module. Where PV/T systems provide a higher energy output than standard PV modules and could be cost effective additional to that thermal unit is low [10-12]. These systems which working as solar active devices need requires to good oriented surfaces that towards the equator by suitable orientations on the surface must be exploitation for each square meter with orientation in order to achieve maximize the energy yield with keep the efficiency in suitable level [13]. Therefore, numerous researches done on the analytical and experimental studies of PVT systems in different places and conditions, intended to find out the methods that Contribute to increase the efficiency of these systems [14].

2. Behavior of hybrid photovoltaic/thermal system by using water

Modeling and simulation of hybrid PV–thermal solar system by use TRNSYS

The hybrid photovoltaic/thermal system which can provide at the same time both electricity, thermal energy and according to Cyprus conditions, it has worked both of “Soteris and Kalogirou” by used the

system it has been modeled using TRNSYS. Where the system consists of collection of series of PV panels included on a normal PV panel at the back of the heat exchanger fixed fins, a battery, an inverter, hot water storage for thermal system, pump through experiments daily, monthly and performance that done by the system. The results show that the average annual efficiency of the PV solar system was between 2.8% to 7.7%, thus increasing the mean annual efficiency of the system to 31.7%. And the best water flow rate of the system was 25 l/h. That would cover 49% of the hot water needs of a house [15]. A hybrid system which could be generating both electricity and hot water warming, it has been modeled number of cases in order to improve the water flow rate to collector. The outcome found that the electricity produced from the PV panel increases with the flow rate increases. Also, the outcomes show the primary value corresponds to 25 l/h, which mean low flow rate value for the system can be used in a thermosyphon module without depending to use a pump and which will improve the economic feasibility of the system [16].

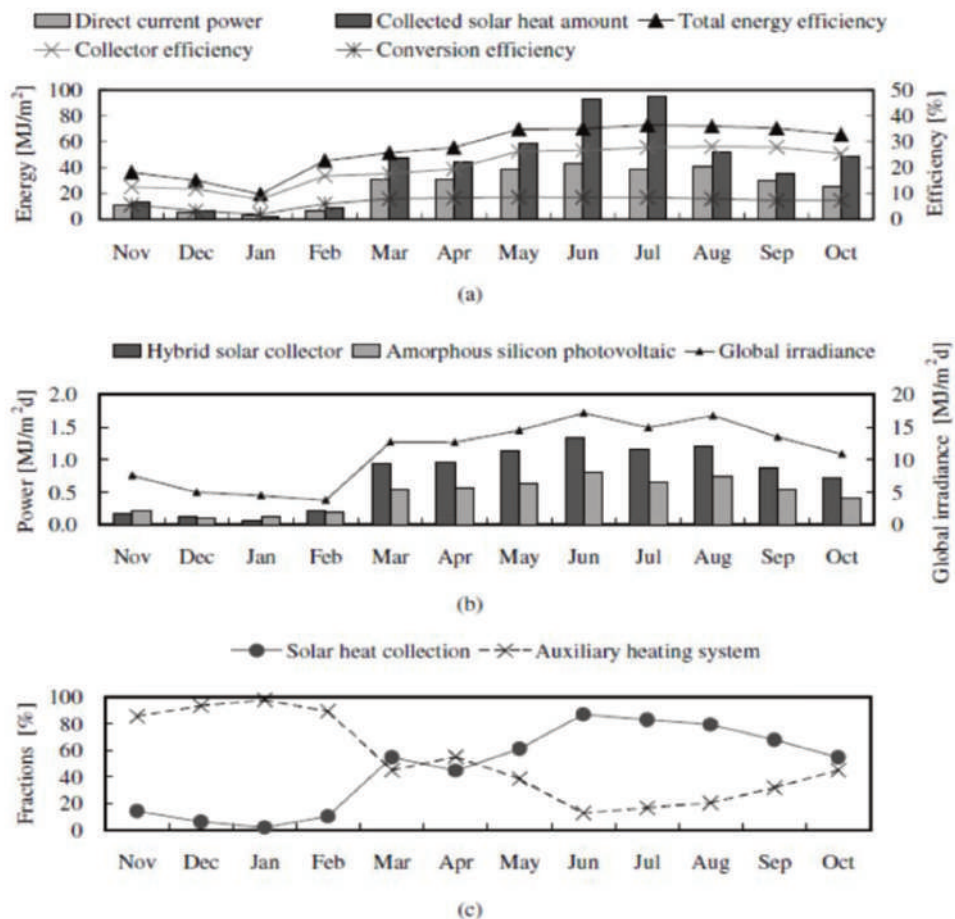


Figure 1. Field experimental results of the hybrid solar collector: (a) operating results of hybrid solar collector, (b) alternating current power generation, (c) heat fractions for domestic hot water supply [3]

Perform experiments on a hybrid PV/T solar collector

Conventional flat plate collector solar thermal with PV cells composite working in the absorption solar radiation for the output of both electrical and thermal energy, has removed the heat from PV cells that led to higher electrical efficiency of the photovoltaic and useful thermal energy extracted from one of the ends the ducts [17], as well as conducted tests and analyzes on performance the hybrid PV/T system which generation electricity and thermal both, this experiment done by constant temperature processing of marinade made. Where found that the conversion efficiency ranged from 10% to 13%, and collector efficiency was from 20 to 40 °C marinade than 40% heat and 50% and about 20% of successive [3]. Although there was reduced of collector efficiency, it has compared the efficiency of the hybrid solar collectors for this photovoltaic solar collectors, where were reads in the observational results of this study annual operation to assemble solar hybrid and the Figure 1a below show the maximum monthly amount of current energy 45.3 MJ / m² in June, and the minimum 2.8 MJ / m² in January, it means conversion efficiency groups.

Where stabilized about 25-28% with the exception in the winter season, it was stable at around 8-9%, only in the winter and the maximum value was 28.1% in august. In Figure 1b shows the difference monthly, current energy of the hybrid system and amorphous silicon photovoltaic per unit area of the panels 0.7 and 0.4 MJ / m² d, respectively, with the value of hybrid solar collector energy it was about 80%,A Where the efficiency decreased because snow due to thickness of snow in Figure 1c below shows the monthly and annual variation of provider of domestic hot water energy, where it was 13.1 GJ which was comparable to that value for the flat plate solar collector 46.3% [3].

Production electric and thermal energy of hybrid PV/T solar systems

Exploitation the amount of energy from hot water and electricity led to motivate many researchers to develop the performance of hybrid PV/T system in order to maintain the electrical efficiency of photovoltaic cells at the adequate level at high temperature, it is necessary for the operation of PV modules at low temperatures by using natural or forced air circulation simple and low-cost methods for transferring heat from the PV modules [18, 19]. The study was conducted at three sites in different regions of, Nicosia, Athens and Madison. As well as used in this study the prototype from polycrystalline

silicon (PC-Si) and amorphous silicon (a Si) and used to analysis the outcome a simulation TRNSYS. However, during the test found the production of electric power from the hybrid system is less than standard PV modules (maximum 38%) units Si PV gives increased total energy production compared to Si PV modules, Nevertheless, the contribution of solar energy to heat water rising in cold climates. Results showed and PC-Si cells produce more electricity (PEL) than identical a-Si cells, this due to higher efficiency of PC-Si cell. The a-Si cells produce more useful thermal energy at all three sites into Madison, Nicosia and Athens. The outcomes indicated that the electricity yield of solar system employing polycrystalline solar is more than that employ these amorphous, but the solar thermal contribution a little less. PV is a hybrid system produces about 38% of electric power and the domestic thermosyphonic system effective and largest system appropriate for residential construction or low office buildings [20].

Use direct solar floor for hybrid PV/T collectors to experiment Energy performance

The energy performance of water hybrid PV/T collectors where worked on this application both of Sorensen, Monroe, it has applied on combisystems of direct solar floor type. The target of this study was to take advantage of the hybrid solar collector to achieve maximize the contributions of solar energy to generate electricity and thermal profits useful. This application operates in the integration of photovoltaic (PV) modules in buildings allows one to view the multifunctional and then to trim back costs by replacing frame ingredients, used with this application amorphous cells or composed to improve the thermal output PV /T collector. To consider that hybrid PV/T solar water collectors as a one piece that including thermal absorption the heat exchanges and PV functions, by one day in summer (June) noticed the PV cell temperature there are evolving in their efficiency when the cell temperature increases, also in their efficiency which strongly dropped decreases from 7% to 4% [21]. As shown in Figure 2. On the same day the cell efficiency was stable around 8.4%, which represents a reduction of 28% and the annual efficiency of the conventional photovoltaic component was 9.4%. This is obviously due to the high temperature on the cover and the incident radiation on the PV cells decreased due to glass cover. It has found that without a glass cover the efficiency was 10%, this is 6% more in effect than a standard module because of the cooling effect [22]. Thus, it has gone from the traditional combisystem associated

control system which purports to extend the solar thermal energy output. As well as for heating water in homes by the water glycol flow in the back side of the PV modules. It has considered that at least one of the two hybrid solutions (with covered or not) is more efficient than the traditional one (PV + T), in order to

avoid the reduction of the age of solar hybrid assembly found two choices. The first one is obvious to imagine the collector is covered and the second is to study the PV modules which can be stable at high temperature [23].

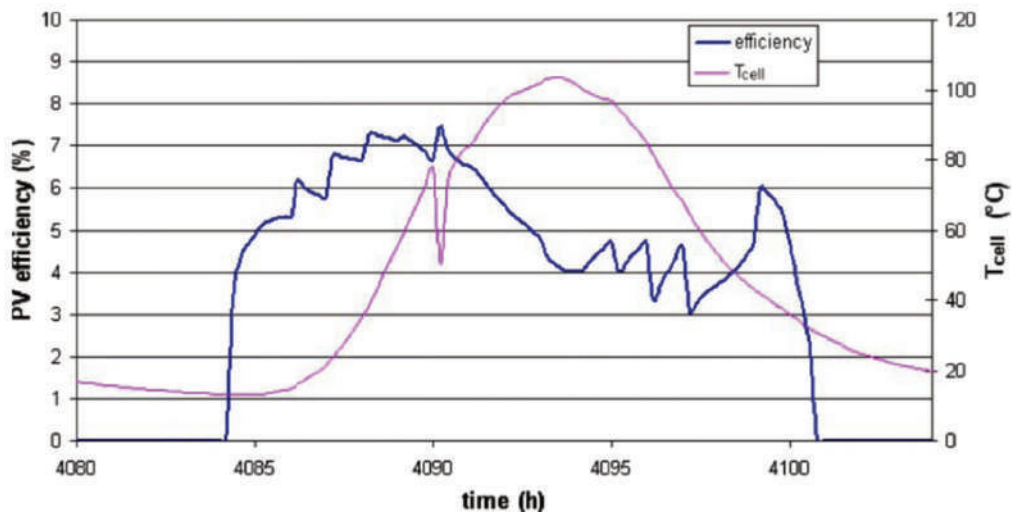


Figure 2. The PV cell temperature and efficiency evolutions [22]

Energy generation with a photovoltaic (PV/T) solar hybrid system

Many combinations of electricity generating solar systems and heat generating have been studied to cover the needs in large quantities to a residential house typical for a family without any fuel cost with average daily consumption of electric power for domestic about 7 kWh. Where the hybrid system consists of (PV) module and compound solar thermal collector energy are constructed and tested for energy collect, the study was conducted in Cyprus have comparatively high averages of exposure solar radiation throughout the year, hot summer days somewhat and for long periods and mild winters to some extent [24]. Depending on the type of solar cells with occupies an area of about 10 m², found that the amount of energy can be produced in electric with a 1600W (PV) system. Therefore large area solar modules will absorb large amounts of solar irradiation, so that will causes loss at the same time in heat units, it has examined experimentally some of hybrid system and found that when using of a booster diffuse reflector will contributed increased the performance of the system and gave giving possibilities for more active for practical applications take the benefit of absorbed solar energy which is not converted into electricity to utilized for thermal applications [25]. A result of this excessive heating of the modules will led to reduction of conversion unit's efficiency, for this reason some of this type does

not convert 80-95% of the energy collected to electricity to remove the extravagant heat. many systems have been designed to use it as an energy source for some other applications like household and industrial applications. As will found that the structure of the unit required some adjustment like to allow to distribute the medium cooling in order to the heat extraction when it is heat fluid transfer system either air or water and to enable watertight and corrosion free construction used water need a more overall amendments [26], The results obtained from these study PV modules absorb a significant sum of solar radiation that generates unwanted heat; however, this loss represents only 1% of the energy 7 kWh that is consumed by the typical family the proposed hybrid system produces thermal energy roughly 2.8 kWh per day. That led to total loss about 11.5% in electric power generation, because the different parts that are placed over the hybrid modules. The payback adjustment period was less than 2 years old, the low investment cost and pay back a relatively short period makes this hybrid system economically attractive, add to that, these hybrid systems that combine to produce electricity and hot water from one system in the same time [27].

Performance of a hybrid photovoltaic/thermal (PV/T) under active solar

A simple design of hybrid (PV/T) double-slope active solar still has been fined and its performance is

evaluated in field conditions, the solar energy productively still can be improved by increasing the temperature of the water in the solar energy is still one of the parameters, where it has designed, manufactured and evaluates the performance of a hybrid photovoltaic thermal system (double slope of the active solar still) and modifies the photovoltaic/thermal (PV/T) dual-slope active solar energy is still designed and fabricated to remote sites. And under field conditions in the natural circulation and forced mode (series and parallel), It had been experimented evaluating performance in order to improve the productivity of a dual slope solar energy solar still [28]. The water pump has been used between solar and photovoltaic (PV) integrated flat-panel collector for re-circulation of water during the

collectors and converted into solar still, from Figure 3 noted that the daily energy efficiency of 17.4% was gained for the parallel forced mode arrangement and higher than the series (16.4%) and of the natural circulation models (16.3%), still will produce a higher yield than the other configurations and obtained as 7.54 kg/day for each hour exergy efficiency is also found to be highest for the same shape and hit as high as 2.3%. The comparative yield obtained is about 1.4 times higher than that obtained for hybrid (PV/T) single slope, solar still, also found that the total cost of the fabricated still is about 14% less than hybrids (PV/T) single slope, solar still and the price will be further reduced substantially once production is held up on a commercial scale [29].

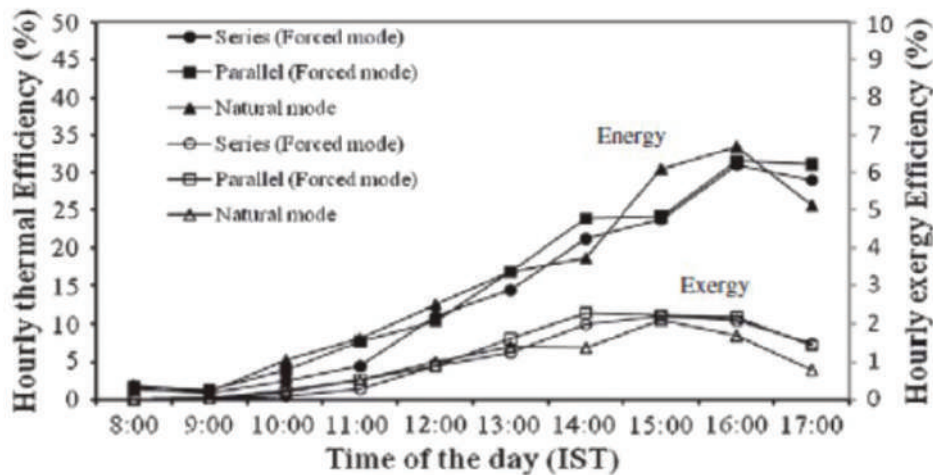


Figure 3. Hourly variation of thermal and exergy efficiencies of solar still during sunshine in different functional styles of hybrid double slope active solar still [29]

Application simulation of solar heating on hybrid photovoltaic/Thermal collectors (PVT)

To achieving the solar energy which can offer a suitable solution for the electricity and heat in solar panels and/or photovoltaic thermal panels because in this system of electricity production is specially priority for fields that do not have potential high solar energy, where totally recognize that the cell temperature affects on operate photovoltaic panels and efficiency which limits the growth of photovoltaic panels, Nevertheless, suggested one good solution to analyze the hybrid operation of PV/T integrated system that increase solar contributions for electricity and useful thermal profits [10]. Based on the energy and transfer of exergy analysis will use cooling cell panel as a resolution in the photovoltaic thermal (PV/T), where it is obtained on both electricity and warmth (air and water) as the heating

fluid in the PV/T collectors which can be used for heating purposes or in industrial applications, it is necessary for the performance of PV modules at low temperature will dilute the value of the gain heat and the efficiency of exergetic will be very small [30]. Used TRNSYS platform simulation PV/T system, cogeneration heating, established to look at the system performance of solar PV/T where in a typical day studied production of electrical energy from the collector PV/T, heat consumption, the exit temperatures of assistance the heat source and outlet temperatures from the heat storage tank as Figure 4 below shows the change graphs inlet and outlet temperature of PV/T collector work the fluid with solar radiation intensity the ambient temperatures in a typical day in the heating season. The average temperature outdoors was - 4.6 °C, and approach the highest solar radiation intensity 370 W/m², and the difference in the inlet and outlet temperature of the

working fluid inside collector PV/T increases with an increase in the intensity of solar radiation, the maximum difference in the inlet and outlet temperature appear in 12, which reaches 5.42 °C. After the flow of water through the collector the collector heat dissipation to the environment as it is able to earn more heat, in Figure (5) below shows the changes in heat consumption, outlet temperature assistant heat source, the outlet temperature of heat storage tank in the collector system along with changes in ambient temperatures in the outdoor, the startup assistant heat source is consistent with changes in ambient temperatures outdoors, temperature of the working fluid in the heat storage

tank to meet the demand of pregnancy, when the value of the highest solar radiation, heat storage tank will get more heat. The results of this study can be seen from the results of the simulation direction operating for the full year in the system to PV/T collector 32m² in size in the system can achieve annual energy production 4195 kWh, which means that the unit square meters of collector PV/T can output 131 kWh electricity annually, through the analysis of simulation results found the heating season that the solar part of the solar heating system is 31.7%, which is close to the design value of 30% [12].

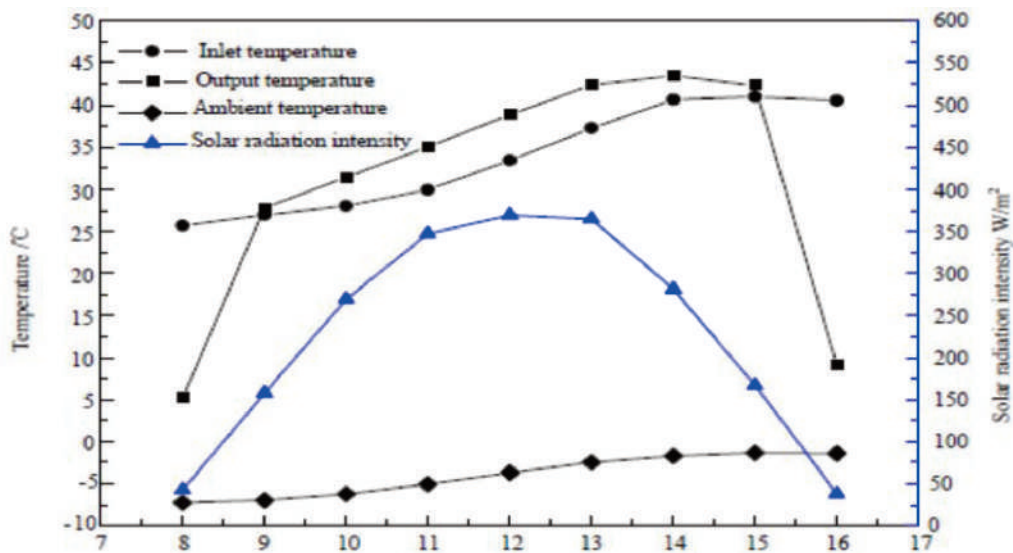


Figure 4. Graphs of the inlet and outlet temperature of PV/T collector working fluid with solar radiation intensity [12]

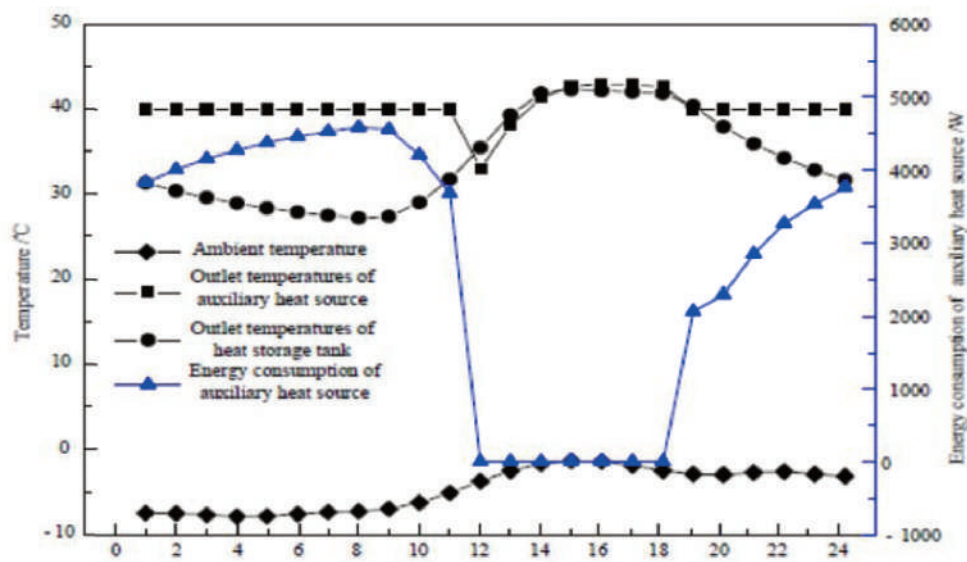


Figure 5. Graphs of heat consumption outlet temperatures of auxiliary heat source and outlet temperatures of the heat storage tank with outdoor ambient temperature [12]

3. Behavior of hybrid photovoltaic/thermal system by using water and air

Considerations about Design for flat-plate photovoltaic/thermal collectors

Several investigations have been conducted on flat plate PV/T collector in theory, as well as, the experience of development of cogeneration components such PV thermal (PV/T), which consists of a combination of photovoltaic (PV) cells and solar thermal energy. This is one of the causes behind the great total of research underway on the growth and integration of solar active devices in the building envelope, where the flat plate collectors PV/T can be split into various categories, for instance according to the nature of the heat transport medium (air or water) and there is an additional glass cover (covered and non-covered collectors) [13]. In this design have been integrated two main types of solar active devices to produce energy into the building thermal solar collectors to convert sunlight into usable heat and photovoltaic (PV) panels to convert solar radiation into electrical [19], found that relatively low conversion efficiency of photovoltaic cells (usually in the range 10-20%), and the cells have a high absorption of all the sun's rays, leading to most of the solar radiation absorbed by the PV cells in heat transfer will increase the cell temperature, therefore the reduced efficiency. For evaluation of solar

radiation absorbed by a c-Si solar cell and to evaluate the percentage of solar radiation converted into electricity performed measurements on commercial solar cells. It was a reflection of the spectrum and the spectral response of the cell was measured and is summarized in Figure 6 it absorbs about 90% of the radiation from the inside of the cell while only 15% is converted to generate electricity [10, 12]. Solar thermal energy absorption components can provide more effective solutions by beneficial capturing the heat produced in the PV cell and PV cell temperature PV/T collectors represented in case use of solar energy [31]. During Comparison between thermal hybrid systems in the building and the operating with the standard solar system and through simulations using TRNSYS, where tests showed the thermal efficiency is almost up as a good complex solar thermal and electricity efficient almost as high as the standard PV panel of the same quality and mode these active solar devices need a well-directed surface, usually towards the equator. Nevertheless, these surface areas on the surfaces or interfaces with limited suitable orientations, in order to maximize energy production, every square meter is available with suitable for solar applications orientation and should be used in the most effective way possible and that lead to an improvement in the thermal and electrical performance [32].

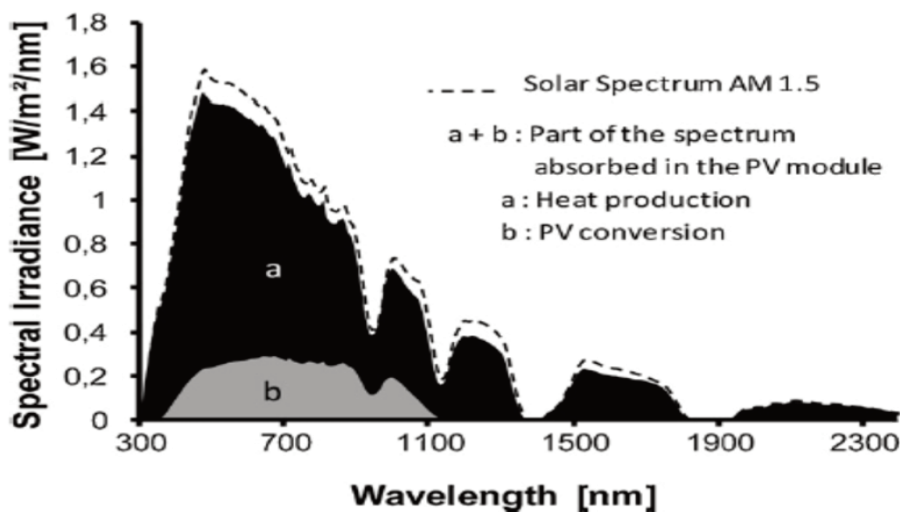


Figure 6. Spectral representation of the absorption, reflection and PV conversion of real c-Si solar cell [13]

Temporal analysis of PV/T solar system for generation of electricity & thermal (hot air/water) energy

To get electric and thermal energy simultaneously during use a appliance which has been developed and

new hybrid systems commercially as photovoltaic/thermal collectors, the system has been designed according to type and size of the solar cells which are identical with requirements of the environment, depends on the design of particular solar collectors, either water or air can be used as medium and works

as a carrier of heat it depend on the usage [10], this idea was based on two parts, the photovoltaic technology that derives from the solar cell technology and converted into electrical energy, and solar thermal technology, which is derived from the thermal collector and convert solar energy into thermal energy [33], where expected that lead to improve the performance with low cost of production and technology of the new energy future technological developments in the use of solar energy. The hybrid system (PV/T) designed to generate thermal and electricity simultaneously and utilization of a hybrid system can offset the need for an outside source of electric power it was experimental conducted in many cases.

1- (Double, pass PV/T collector with fins): As shown in Figure 7 this collection includes three main components: glass cover on the top, panel with photovoltaic cells and absorber at the bottom. The fins were fabricated using aluminum sheet to increase the ability to remove heat from PV cells and thus increase the efficiency and air was flowing through the upper part in the middle of glass cover and PV Panel and then going through the lower part below for PV panel.

2- (Single pass PV/T collector with V-groove absorber) in Figure 8 below shows the schematic diagram of this design, the PV plate is exposed to the sun, which later absorbs the heat and gain electricity simultaneously. By doing this, more heat can be transferred to the air and the PV plate becomes cooler without altering the shape of any Commercial PV module Based on the previous design, the efficiency of the electricity is reduced more than 50% when the PV plate is covered by the glass.

3 - (Double, pass PV/T collector with fin and CPC): As shown in Figure 9 below the parabolic concentrator (CPC) was added to increase the efficiency of the collector. The air flow as the same way as the collector with fins, but the solar irradiance increased using CPC. Fins attach underneath the PV cell help to remove the heat from a PV panel.

4 - (PV/T collector with rectangular tunnel absorber): As shown in Figure 10, the PV/T collector with rectangular tunnel absorber has the same functions and targets as other collectors, which is, to increase its efficiency. The main difference in this collection is the shape of the absorber with is in a rectangular design.

5- (Water based PV/T collector): The water based PV/T collectors are one of the research that being studied at the solar energy research institute. The principle of water based PV/T is similar to the air based collector where cold water is practiced as a medium to soak up heat from the sunlight which is

later can be used for low heat temperature processes [34]. Some various designs of PV/T collector based on water and air, every design had its own specific way of converting solar energy to electricity and thermal energy simultaneously, where preserve PV module in the current market showed enough potential in application, but these PV modules can only provide electrical energy by changing the preserve PV module with some specific modification, can thus produce electrical energy and caloric energy with the new blueprint of this PV/T. It is well known that using a hybrid system can eliminate the need for an external source of electrical energy, new technology developments in solar energy utilization are expected to result in the improvement of the photovoltaic performance with lower production cost. This will increase the demand and viability of commercial applications [35].

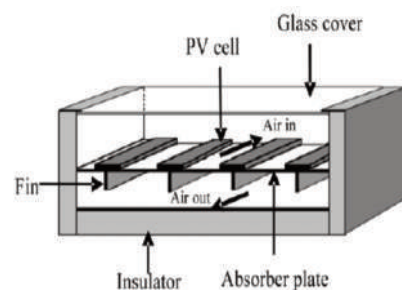


Figure 7. The schematic diagram of double pass PV/T collector with fins [33].

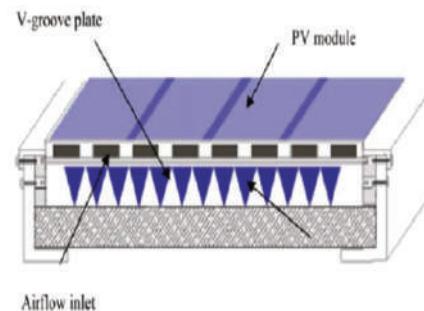


Figure 8. Schematic diagram of the PV/T collector with V groove absorber collector [33].

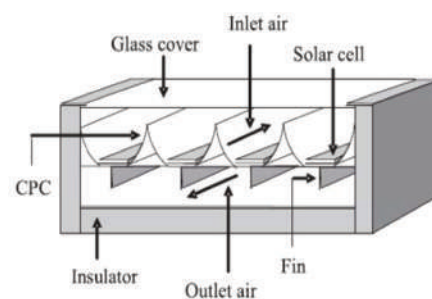


Figure 9. Schematic diagram of double pass PV/T [33].

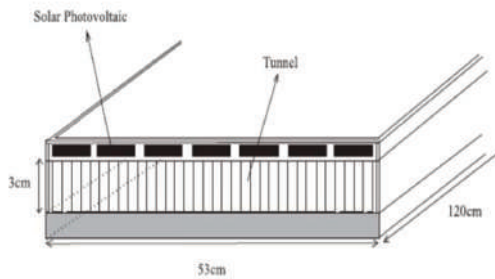


Figure 10. Schematic diagram of the PV/T collector with rectangular tunnel absorber [33].

Experimental yield of different combined hybrid PV-thermal designs

Have been working many test orders to improve the overall efficiency of solar energy devices by taking advantage of the heat discharged from the PV module system and use in other fields, in other hand increase the efficiency by absorbing the high temperatures from PV cell and achieve a higher energy conversion ratio of the absorbed solar radiation. [36], in addition the research has been conducted in PV/T associated with heating and cooling facilities and the thermal energy from the water-type PV/T collector systems, which can be used in buildings, and a solar collector for domestic hot water and space heating [37], which is similar in manufacturing to conventional thermal solar energy collector, Which can be achieved by circulating cooler fluid, water or air, by along the underside of the PV module PV/T collectors can be

classified according to the type of working fluid used (water, air or both). Most studies that examine the performance include estimates of the different types of panel absorption, such as sheet and tube, completely wet and the channel box types, analysis of several different types of collectors PV/T (sheet and tube, channel, free-flowing dual absorption), as shown in Figure 11 [38]. The experimental results indicated that the overall gain heat from the collector is 9.7 kWh, while the average thermal and electrical efficiency of the system is 30% and 17% respectively. It was also shown that the heating energy of the house can be reduced by 47%, and the heat gained from the integrated roof PV/T system by the water used for heating in the heating system, this means that the energy required in the building can be reduced dramatically by 47% at a temperature of water heating from 40°C heats. Therefore, it can be concluded that this system can reduce the energy required for igniting the building by nearly half by heating water and heating at low temperatures. Related to electrical efficiency and the highest level of performance, with an efficiency exceed 16.5% when the heating system with BIPVT (Building Integration photovoltaic/thermal) collector was working, has happened because the relatively low temperatures of liquid which had been circulated. So, the system very suitable to increase the energy performance of buildings also confirmed that the water temperature of the thermal storage tank [39].

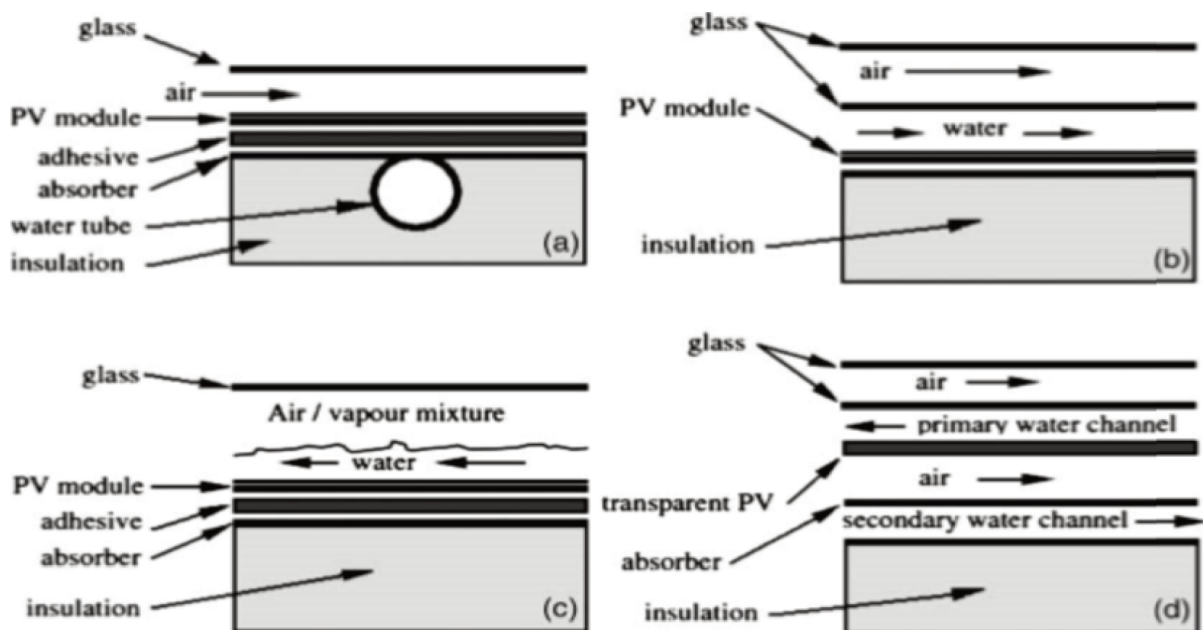


Figure 11. Types of PVT Collectors: Sheet-and-Tube (a), Channel (b), Free-Flow (c) and Dual-Absorber (d) [39]

4. Conclusion

Performance evaluation of (PV/T) hybrid systems for a lot of experiments were various where the amount of falling solar radiation, design, orientation and selection type solar cell, all of that plays essential role in the amount of energy produced. Where found during this study receive more direct exposure to solar radiation that will effect on the work of (PV) modules by increase temperature and drop the efficiency of solar cells. Therefore, use hybrid photovoltaic/thermal (PV/T) collector with mediums such as (water or air) will contribute to raising system efficiency during the absorption of excess heat from solar cells, and avoid the high temperatures absorbed by (PV) modules by the piping that fixed in the face back of the panel and take the advantage of heat which absorbed for household applications or heating purposes. That led to increase the rate return of the system of electricity and thermal energy, where contribute to a large extent to strengthen the work of solar cells, system efficiency and the conversion rate of absorbed solar radiation for (PV) modules will increase as well, especially when the hybrid photovoltaic/thermal (PV/T) solar systems were properly designed.

Acknowledgments

The author wishes to thank the support of the Southern Technical University for providing facilities for this paper. The researcher is grateful to have the support from (Hayder A. Alrazen and Qudama Al-Yasiri).

References

- [1] **Krauter S., Hanitsch R.:** 1994. Actual optical and thermal performance of PV–thermal modules. In Proceedings of the First Conference on Photovoltaic Energy Conversion, Hawaii pp. 734-37.
- [2] **Al-ktrane M. H. R., Schrempf N.:** 2016. Hybrid solar system (photovoltaic/thermal) utilization for household application. *Hungarian Agricultural Engineering*, Vol. 30, pp. 54-61.
<http://dx.doi.org/10.17676/HAE.2016.30.54>
- [3] **Saitoh H., Hamada Y., Kubota H., Nakamura M., Ochifuji K., Yokoyama S., Nagano K.:** 2003. Field experiments and analyses on a hybrid solar collector. *Applied Thermal Engineering*, Vol. 23, No. 16, pp. 2089–2105.
[http://dx.doi.org/10.1016/S1359-4311\(03\)00166-2](http://dx.doi.org/10.1016/S1359-4311(03)00166-2)
- [4] **Elazari A.:** 1998. Multi Solar System Solar multi module for electrical and hot water supply for residentially building/ In Proc. 2nd World Conf. on Photovoltaic Solar Energy Conversion. pp. 2430-2423.
- [5] **Mei L.:** 2003: Thermal modeling of a building with an integrated ventilated PV façade. *Energy and buildings*, Vol. 35, No. 6, pp. 605-617.
[http://dx.doi.org/10.1016/S0378-7788\(02\)00168-8](http://dx.doi.org/10.1016/S0378-7788(02)00168-8)
- [6] **Fraisse G., Souyri B.:** 2003. Rapport Programme Energie CNRS: “Compte rendu scientifique: conception d’un capteur PV/T – eau. Rapport premie`re anne`e. PRI 6.2. Inte`gration de capteurs hybrides photovoltaïques thermiques au ba`ti, pp. 56.
- [7] **Loferski J. J., Ahmad J. M., Pandey A.:** 1988. Performance of photovoltaic cells incorporated into unique hybrid photovoltaic/thermal panels of a 2.8 kW residential solar energy conversion system/In Proceedings of 1988 annual meeting. American Solar Energy Society. Cambridge, USA, pp. 427–32.
- [8] **Garg H. P., Adhikari R. S.:** 1997. Conventional hybrid photovoltaic/thermal (PV/T) air heating collectors. steady-state simulation. *Renewable Energy*, Vol. 11, No. 3, pp. 363–85.
[http://dx.doi.org/10.1016/S0960-1481\(97\)00007-4](http://dx.doi.org/10.1016/S0960-1481(97)00007-4)
- [9] **Charalambous P. G., Maidment G. G., Kalogirou S. A., Yiakoumetti K.:** 2007. Photovoltaic Thermal (PV/T) collectors: A review. *Applied Thermal Engineering*, Vol. 27, No. 2-3, pp. 275-286.
<http://dx.doi.org/10.1016/j.applthermaleng.2006.06.007>
- [10] **Florschuetz L. W.:** 1979. Extension of the Hottel–Whillier model to the analysis of combined photovoltaic/thermal flat plate collectors. *Solar Energy*, Vol. 22, No. 4, pp. 361–6.
[http://dx.doi.org/10.1016/0038-092X\(79\)90190-7](http://dx.doi.org/10.1016/0038-092X(79)90190-7)
- [11] **Raghuraman P.:** 1981. Analytical predictions of liquid and air photovoltaic/thermal, flat-plate collector performance. *Journal of Solar Energy Engineering*, Vol. 103, No. 4, pp. 291–298.
<http://dx.doi.org/10.1115/1.3266256>
- [12] **Cox C. H. III., Raghuraman P.:** 1985. Design considerations for flat-plate photovoltaic/thermal collectors. *Solar Energy*, Vol. 35, No. 3, pp. 227–241.
[http://dx.doi.org/10.1016/0038-092X\(85\)90102-1](http://dx.doi.org/10.1016/0038-092X(85)90102-1)
- [13] **Dupeyrat P., Ménézob C., Fortuinc S.:** 2012. Study of the thermal and electrical performances of PVT solar hot water system. *Energy and Buildings*. Vol. 68, Part C, pp. 751-755.
<http://dx.doi.org/10.1016/j.enbuild.2012.09.032>
- [14] **Vries D. W.:** 1998. Design of a Photovoltaic/Thermal Combi-panel. PhD thesis. Eindhoven University of Technology. Netherlands.
- [15] **Kalogirou S. A.:** 2001. Use of TRNSYS for modeling and simulation of a hybrid pv–thermal solar system in Cyprus. *Renewable Energy*, Vol. 23, No. 2, pp. 247–260.
[http://dx.doi.org/10.1016/S0960-1481\(00\)00176-2](http://dx.doi.org/10.1016/S0960-1481(00)00176-2)

- [16] **Imre L., Bitai A., Bohonyey F., Hecker G., Palfy M.:** 1993. PV–thermal combined building elements. Proceedings of ISES Solar World Congress, pp. 80-277.
- [17] **Bosanac M., Sørensen B., Katic I., Sørensen H., Nielsen B., Jamal Badran J.:** 2003. Photovoltaic/Thermal Solar Collectors and Their Potential in Denmark. EFP project 1713/00-0014, Final Report, pp. 114.
- [18] **Hendrie SD.:** 1979. Evaluation of combined photovoltaic/thermal collectors. In Proceedings of the international conference ISES, Vol. 3, Atlanta, Georgia, USA, pp. 1865–1869.
- [19] **Kern E. C. Jr., Russel M. C.:** 1978. Combined photovoltaic and thermal hybrid collector systems. In Proceedings of the 13th IEEE photovoltaic specialists. Washington DC, USA, 1978, pp. 1153–1157.
- [20] **Kalogirou S. A., Tripanagnostopoulos Y.:** 2006. Hybrid PV/T solar systems for domestic hot water and electricity production. *Energy Conversion and Management*, Vol. 47, No. 18-19, pp. 368–3382. <http://dx.doi.org/10.1016/j.enconman.2006.01.012>
- [21] **Sorensen H., Munro D.:** 2000. Hybrid PV/thermal collectors. In The EN World Solar Electric Buildings Conference. Sydney, 2000, pp. 1-7.
- [22] **Fraisse G., Menezo C., Johannes K.:** 2007. Energy performance of water hybrid PV/T collectors applied to combisystems of Direct Solar Floor type. *Solar Energy*, Vol. 81, No. 11, pp. 1426–1438. <http://dx.doi.org/10.1016/j.solener.2006.11.017>
- [23] **Affolter P., Ross D., Toggweiler P., Haller A.:** 2000. New generation of hybrid solar PV/T collectors/ Final Report DIS 56360/16868, pp. 55.
- [24] **Soteris K.:** 2003. The potential of solar industrial process heat applications. *Applied Energy*, Vol. 76, No. 4, pp. 337–361. [http://dx.doi.org/10.1016/S0306-2619\(02\)00176-9](http://dx.doi.org/10.1016/S0306-2619(02)00176-9)
- [25] **Bergene T., Lovvik M. O.:** 1995. Model calculations on a flat-plate solar heat collector with integrated solar cells. *Solar Energy*, Vol. 55, No. 6, pp. 453–462. [http://dx.doi.org/10.1016/0038-092X\(95\)00072-Y](http://dx.doi.org/10.1016/0038-092X(95)00072-Y)
- [26] **Erdil E., Ilkan M., Egelioglu F.:** 2008. An experimental study of energy generation with a photovoltaic (PV) – solar thermal hybrid system. *Energy*, Vol. 33, No. 8, pp. 1241–1245. <http://dx.doi.org/10.1016/j.energy.2008.03.005>
- [27] **Klugmann E.:** 2000. Influence of temperature on conversion efficiency of a solar module working in photovoltaic PV/T-integrated system/ photovoltaic solar energy conference. Glasgow, UK, pp. 1–5.
- [28] **Kumar S., Tiwari A.:** 2010. Design, fabrication and performance of a hybrid photovoltaic/thermal (PV/T) active solar still. *Energy Conversion and Management*, Vol. 51, No. 6, pp. 1219–1229. <http://dx.doi.org/10.1016/j.enconman.2009.12.033>
- [29] **Singh G., Kumar S., Tiwari G. N.:** 2011. Design, fabrication and performance evaluation of a hybrid photovoltaic thermal (PVT) double slope active solar still. *Desalination*, Vol. 277, No. 1-3, pp. 399–406. <http://dx.doi.org/10.1016/j.desal.2011.04.064>
- [30] **Chow T. T.:** 2010. A review on photovoltaic/thermal hybrid solar technology. *Applied Energy*, Vol. 87, No. 2, pp. 365–379. <http://dx.doi.org/10.1016/j.apenergy.2009.06.037>
- [31] **Prakash J.:** 1994. Transient analysis of a photovoltaic-thermal solar collector for co-generation of electricity and hot air/water. *Energy Conversion Management*, Vol. 35, No. 11, pp. 967-972. [http://dx.doi.org/10.1016/0196-8904\(94\)90027-2](http://dx.doi.org/10.1016/0196-8904(94)90027-2)
- [32] **Ruslan M. H., Othman M. Y., Spain K., Majid Z. A. A., Him W. A.:** 2008. Development of photovoltaic-thermal (PV/T) water based system. *World of Renewable Energy*, Glasgow, pp. 352–365.
- [33] **Othman M. Y., Ibrahim A., Jin G. L., Ruslan M. H., Sopian K.:** 2013. Photovoltaic-thermal (PV/T) technology – The future energy technology. *Renewable Energy*, Vol. 49, pp. 171-174. <http://dx.doi.org/10.1016/j.renene.2012.01.038>
- [34] **Kalogirou S. A., Tripanagnostopoulos Y.:** 2007. Industrial application of PV/T solar energy systems. *Applied Thermal Engineering*, Vol. 27, No. 8-9, pp. 1259-1270. <http://dx.doi.org/10.1016/j.applthermaleng.2006.11.003>
- [35] **Liang R., Zhang J., Zhou C.:** 2015. Dynamic Simulation of a Novel Solar Heating System Based on Hybrid Photovoltaic/Thermal Collectors (PVT). *Procedia Engineering*, Vol. 121, pp. 675 – 683. <http://dx.doi.org/10.1016/j.proeng.2015.09.001>
- [36] **Institute for Building Energy Conservation.:** 1992. The Course of Low Energy Houses and Buildings. Japanese. IBEC, Vol. 67, pp. 68–75.
- [37] **Hokkaido.:** 1998. Government Financial Assistance for Energy Conservation.
- [38] **Zondag H. A., de Vries D. W., van Helden W. G. J., van Zolingen R. J. C., van Steenhoven A. A.:** 2003. The yield of different combined PV-thermal collector designs. *Solar Energy*, Vol. 74, No. 3, pp. 253-269. [http://dx.doi.org/10.1016/S0038-092X\(03\)00121-X](http://dx.doi.org/10.1016/S0038-092X(03)00121-X)
- [39] **Kim J. H., Kim J. T.:** 2016. Performance Analysis of Roof-Integrated Water-Type PVT Heating System. *International Journal of Smart Home*, Vol. 10, No. 3, pp. 301-314. <http://dx.doi.org/10.14257/ijsh.2016.10.3.29>



EXAMINATION OF THE HUNGARIAN AGRICULTURAL MACHINERY MANUFACTURERS' PRODUCT PLANNING, QUALITY MANAGEMENT TECHNIQUES AND PRODUCTION COORDINATION

Author(s):

A. Goda – V. Medina – L. Zsidai

Affiliation:

Faculty of Mechanical Engineering, Szent István University

Email address:

adrienn.goda@gek.szie.hu, medaina.viktor@gek.szie.hu, laszlo.zsidai@gek.szie.hu

Abstract

The present research was conducted in July 2017. We get information about what kind of software is used in the areas we are investigating. It was examined, whether IT systems are used for enterprise resource planning. It was reviewed how the failure mode and effect analysis (FMEA), the rapid prototype modelling and the quality function deployment (QFD) are extended among the agricultural machinery manufacturers. We compare the results with the International Manufacturing Strategy Survey and an earlier survey conducted by us in the Hungarian cob cracker industry. The comparison of the agricultural machinery manufacturers, Hungarian and international companies' average shows us the areas we should develop

Keywords

product planning, quality management techniques, Hungarian agricultural machinery manufacture.

1. Introduction

The research is based on the questionnaire of the International Manufacturing Strategy Survey (IMSS) [1]. The IMSS was set up in 1992. The goal of the participant researchers was to have an overview about international production strategies, their introduction and their results in production and related areas (eg supply chain management, new product development etc.) [2]. The data collection was carried out internationally in Europe, America and Asia. The international data include the results of the 2009 IMSS research (562 company data). After the international research it was realized a Hungarian survey with a participation of 71 companies [1] [3].

2. International and Hungarian surveys

The surveys about the manufacturing strategy play an increasing role in the research of manufacturing management. We collected these surveys and summarized in the table 1. An overview about the researches is very important to be able to make proposals to develop the IMSS.

3. Methods

Next to the international and Hungarian IMSS we made a new research among Hungarian agricultural machine manufacturers. Within the framework of this survey 57 companies have been asked. In the survey the whole cob cracker adapter manufacturing sector was represented, which made us possible to compare the performance of this sector with the results of the other surveys (international, Hungarian and agricultural machinery sector) [12].

It is important for Hungarian agricultural machinery sector to meet the needs of the domestic agriculture. Domestic-built machines include, machines for tillage (plows, disc harrows, seedbed makers, cultivators, rollers), sprayers, harvester and thresher adapters, stalk crushers, tractor-loading machines and trailers, animal husbandry tools, handling, storage and farm machinery. These machines and tools can be used by small and big farms. The domestic agricultural supply offers a choice for all kind of farmers [13].

The aim of our quantitative research was to compare the cob harvesting adapters industry and the agricultural manufacturers with the results of the domestic and international IMSS. The questionnaire uses a measurement scale in some cases. The scale has values from 1 to 5. 1 represents the worst value,

3 is neutral, and the higher values are positive [14] [15].

When reporting the results, the term "industry", "machine manufacturers", "Hungarian" and "international" are used in the table header. In this case, the industry means the Hungarian cob cracker

industry, "machine manufacturers", the Hungarian agricultural machinery manufacturers, "Hungarian" referring to companies operating in Hungary, and the "international" reflects the corporate data collected in other countries. It was presented in all figures the average value of the sectors.

Table 1. International surveys about manufacturing strategy [4] [5] [6] [7] [8] [9] [10] [11]

SURVEY	SECTOR	SUBJECT
International manufacturing research group	Small machine tools	Efficiency, sales, forecast, manufacturing planning
International manufacturing strategy	Machine manufacturers	Business, strategies, manufacturing programs, manufacturing efficiency, plans for the future
International research of the production's future	America, Europe, Japan	Production strategy
World level manufacturing project	Electronics, vehicles, machines (America, Japan, Germany, Italy, UK)	Organisation factors, human resources, technology, infrastructure, quality management, partner relations, efficiency
Research of competitiveness	International	The whole process of the functioning (business, efficiency, relationships etc.)
Lean management	International	Introduction of the lean management
Other related research	International	Competitiveness of the countries

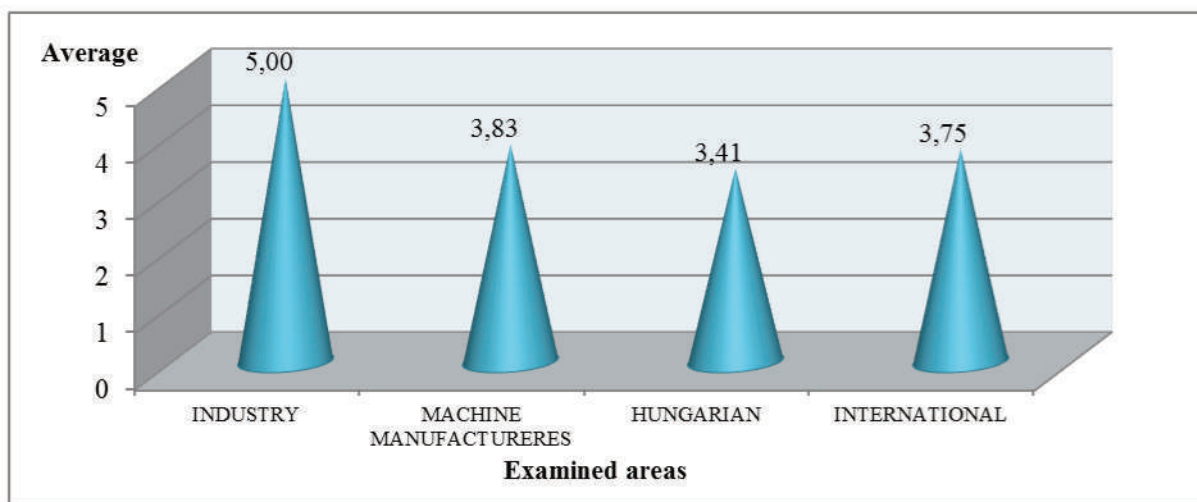


Figure 1. Usage of CAD/CAM software (scale 1-5, 1= not used, 5= frequently used)

4. Coordination of the product planning and manufacturing at the Hungarian agricultural machinery sector

The coordination of product planning and manufacturing was examined with seven questions. CAD / CAM software help engineers and other

design specialists in the cob cracker industry in their planning activities. The values are higher than the Hungarian and international average. This may be due to the fact that CAD software is nowadays the most basic design tool for engineers (engineers, builders, architects). As in the case of Hungarian agricultural machinery manufacturers, like the international one,

the more modern design programs (Inventor, SolidWorks, ProE, CATIA) are widespread (Figure 1). It can be assumed that there are several manufacturers among the examined companies,

which are multinational firms, where the parent company is a foreign owner and a larger amount is spent on upgrading software.

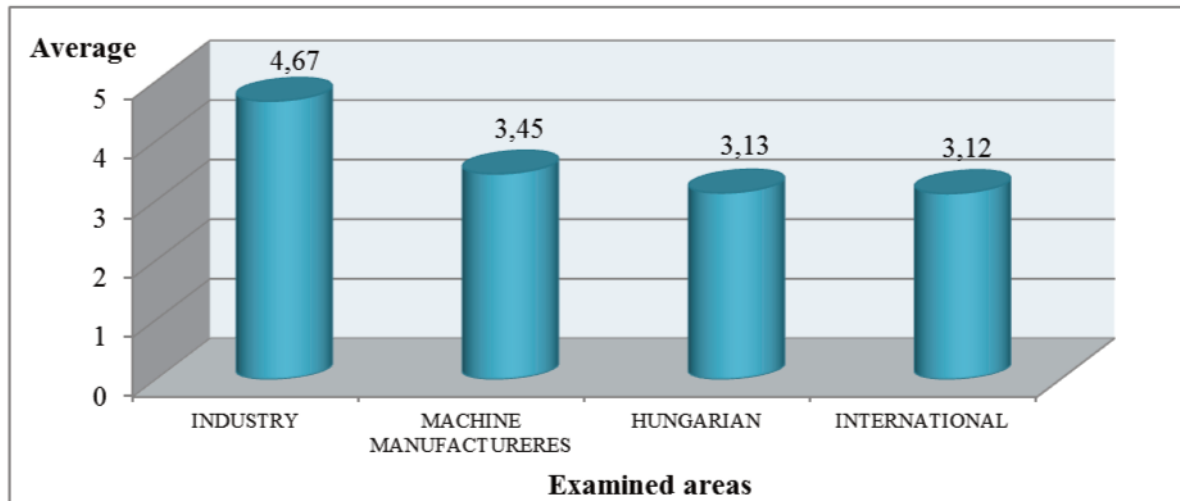


Figure 2. The role of planning (scale 1-5, 1= not used, 5= frequently used)

In the case of product planning and manufacturing coordination, we consider, it is important to study how the planning is being implemented. Machine manufacturers, with an average of 3.45, are on a similar level with the other investigated groups (manufacturers 3.45, Hungarian 3.13, international 3.12). The manufacturers of corn harvester adapters

have the highest value of 4.67 (Figure 2). It can be deduced from the results of the other examined areas round the middle vale that they don't focus so highly on the planning of production and assembly. In spite of this, the planning plays an important role in engineering.

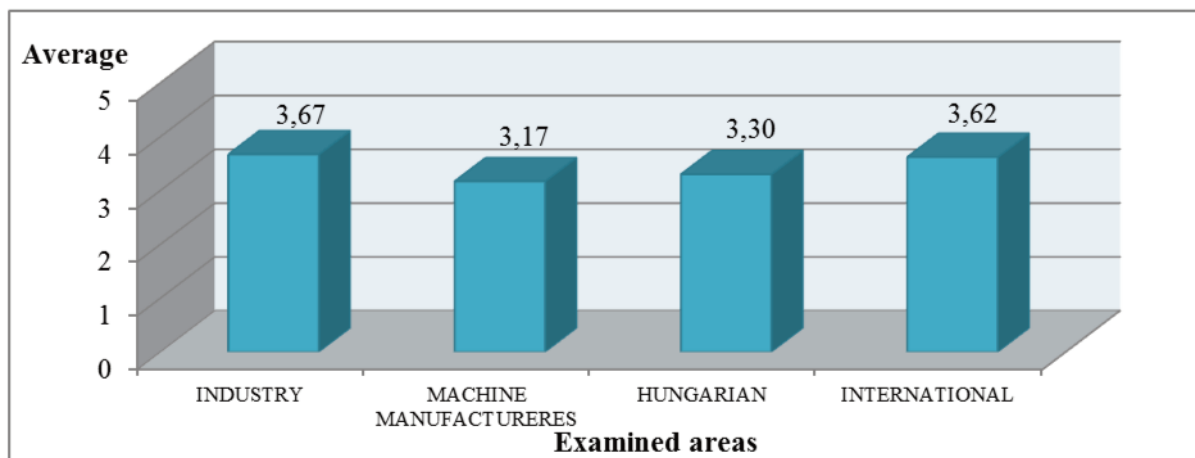


Figure 3. Usage of shared databases (scale 1-5, 1= not used, 5= frequently used)

When analysing the shared databases, it can be seen that the area of production of agricultural machinery (3,17) had the lowest value among the four areas. The Hungarian average did not differ significantly from the previously mentioned value (3,30). Figure 3

shows that the industry and international average are very close to each other. So, in all four areas, the average is higher than 3 that reflects the importance of reliable and long-term storage of data and the relatively quick retrieval of data.

We investigated the presence of corporate resource planning systems for agricultural machinery manufacturers. The results were compared to the averages of industry, Hungarian and international survey (Figure 4). In ERP systems, procurement, logistics, billing, shipping, financial, corporate governance, etc. processes can be integrated. All the operations can integrate that are part of a company's management, production and sales tasks. In the industry, 3.33; machine manufacturers 2.48; for Hungarian companies 2,68; international 3, 68 were the values. The background of the very low value of manufacturers, is that the questions were answered mainly by micro and forced enterprises.

In case of forced enterprises, the reason is often that they do not know the corporate governance system. In case of micro companies owner and the company manager coincide in almost every case. There are no different groups involved, the owners work with a

small number of employees. However, information is also a competitive advantage for them, so from the low value it can be seen that micro company / computing companies employ a small number of enterprise resource planning systems.

The low value of Hungarian companies means that most of the respondents are small and medium-sized companies, so introducing the ERP system is a big challenge for them. Based on the industry average, it can be said that the introduction, the software and systems are not a local decision, but rather the needs of foreign owners determine the process of the investment.

The FMEA (Failure Mode and Effect Analysis, for error, cause, and impact analysis) method can be used for product design and manufacturing process in parallel. In our study it becomes clear that the four areas use this method to a lesser extent (Figure 5).

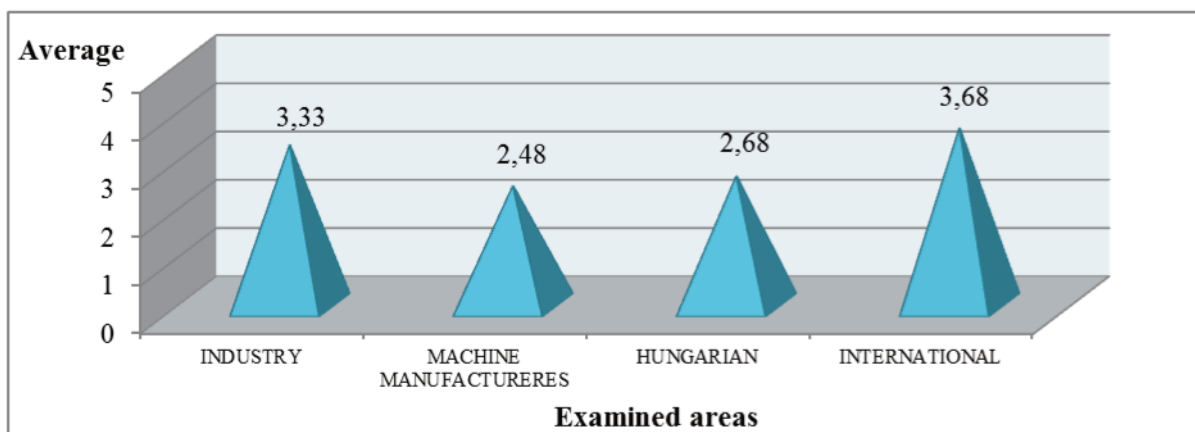


Figure 4. Enterprise resource planning (ERP) (scale 1-5, 1= not used, 5= frequently used)

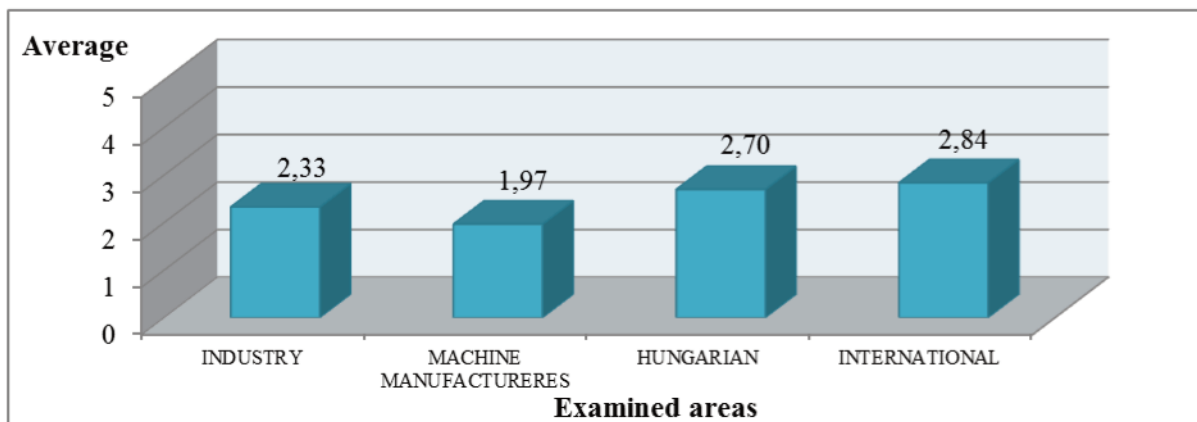


Figure 5. Failure Mode and Effect Analysis (FMEA) (scale 1-5, 1= not used, 5= frequently used)

It can be explained that FMEA has been slightly expanded due to its time requirement and that subjectivity is present in the risk assessment, therefore we cannot get sufficiently objective results in many times.

The benefits provided by the method would be advantageous, regardless of industry and size of the

company, for example, ranking mistakes based on estimated risks, dealing with future defects in a product, process, or system, this can be prevented so you can save costs.

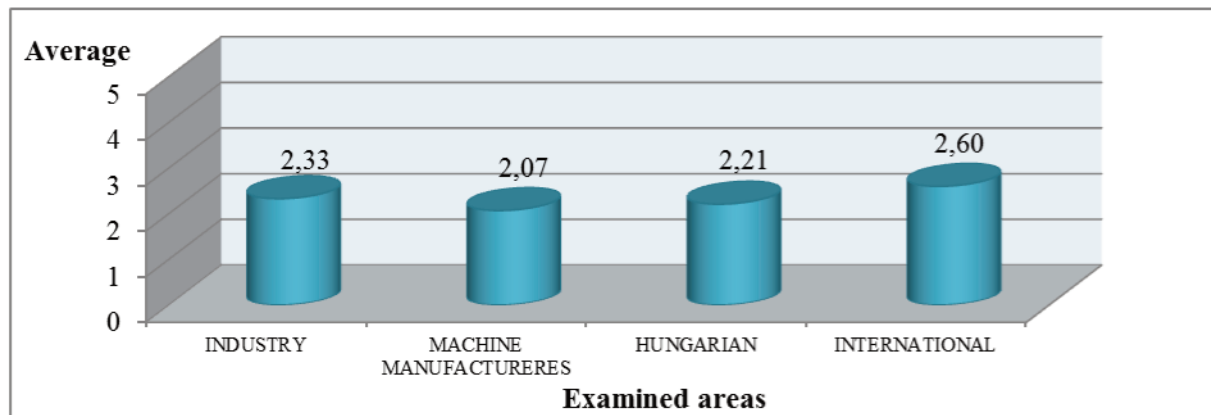


Figure 6. Rapid Prototyping (scale 1-5, 1= not used, 5= frequently used)

Fast prototype modelling was below middle value in all four areas. This is because maximum efficiency, high cost, too much work-saving and control cannot be solved for small-scale models of rapid prototype (RP) technologies (Figure 6). We would be desirable to put more emphasis on quick prototyping, because the insertion time of the pieces would decrease, design errors could be discovered, repaired and tested more easily.

The QFD model (Quality function deployment - “Quality House”) is a tool for quality systematic development that can be used for product design, construction and technology. Used to a small extent in the four areas under investigation (industry - 1.67, machine manufacturers - 1.66, Hungarian - 2.03, international - 2.65) (Figure 7). The reason for this is that the team needed to produce the QFD model is missing (due to lack of expertise). A leader needs for the team who leads a QFD project, motivates and educates the team members.

A QFD expert is needed in the team also. He is the one of them who develops his knowledge from conferences and literature, passes on it, controls the method and highlights the main issues. The members of the group must implement the QFD project, using their own experiences. By team-building and using the QFD method, customer requirements can be fulfilled and can reduce the loss costs that could hinder work.

5. Conclusion

We examined and compared four areas (Hungarian corn harvester adapting industry, Hungarian agricultural machinery manufacturers, other small and medium enterprises in Hungary together, and international companies with different production activities) in our qualitative research, bearing in mind the production technology.

Our research has resulted that the product design and production coordination (from a technological point of view) structured as follows by regions:

- corn harvester adaptation industry: 3.29
- Hungarian agricultural machinery manufacturers: 2.66
- other small and medium enterprises in Hungary together: 2.03
- companies carrying out different production activities in other countries: 2.65

In summary, in the field of agricultural machinery manufacturing, product design and production iare mainly based on CAD / CAM software and shared databases, its values are higher better than middle value.

The enterprise resource planning systems, FMEA, QFD and rapid prototyping have reached a weaker value. Therefore, in the future, more emphasis should be placed on these areas in order to improve quality and cost-efficiency. Calculating an average value of

all these areas we receive 2,66 in the field of the agricultural machinery manufacturers.

As a conclusion, it can be deduced that the manufacturers mainly spend for technological development if they are able to implement them with support. These tenders are available in limited numbers in this area. The agricultural manufacturers would have opportunity for technological development if they could save costs. For reducing costs we would like to propose some fields to develop.

We propose to use more frequently the prevention technics like FMEA or QFD.

The benefits of the FMEA model would be useful, regardless of the size of the company. The ranking of the errors based on the estimated risks, and dealing with errors which have not yet occurred makes possible the prevention and thus can save costs.

In the examined sector we see a great potential for applying the QFD model. With introduction of QFD model, the time and cost of development could be reduced by 30-50% and less technical changes would be needed during the manufacturing process. The savings originate from the decline of technical changes, the improved production quality and the decrease of losses.

Additionally, it would be expedient to place greater emphasis on rapid prototyping because the time of product's introduction into the manufacturing would decrease, the errors of planning could be discovered and repaired earlier, and the structure of the product could be tested. With these results, working time and cost-effectiveness would change in a positive direction.

References

- [1] **Matyusz Zs., Demeter K.:** 2011 A termelési stratégia és termelési gyakorlat kutatás részletes eredményei 2009-2010 [The detailed research results of production strategy and practice]. 145.sz. Műhelytanulmány, Budapest, pp. 21-23. HU ISSN 1786-3031.
- [2] **Demeter K., Matyusz Zs.:** 2009. A „külső tényezők és adottságok hatása a vállalatok teljesítményére az értékteremtés szűrőjén keresztül” projektzáró tanulmánya [„The impact of external factors and circumstances on corporate performance in the perspective of value creation” project closing study]. 54.sz Műhelytanulmány, pp. 19.
- [3] **Matyusz Zs., Demeter K.:** 2010. A termelési stratégia és termelési gyakorlat kutatás eredményei 2009-2010 [The research results of production strategy and practice 2009-2010]. 121. sz. Műhelytanulmány, Budapest, pp. 22.
- [4] **Flynn B., Schroeder R. G., Flynn E. J., Sakakibara S., Bates K. A.:** 1997. World- class manufacturing project: overview and selected results. *International Journal of Operations and Production Management*, Vol. 17., No. 7, pp. 671-685. <http://dx.doi.org/10.1108/01443579710175592>
- [5] **Holweg M.:** 2007. The geneology of lean production. *Journal of Operations Management*, Vol. 25, No. 2, pp. 420–437. <http://dx.doi.org/10.1016/j.jom.2006.04.001>
- [6] **Laugen B. T., Acur N., Boer, H., Frick J.:** 2005. Best manufacturing practices. What do the best-performing companies do? *International Journal of Operations & Production Management*, Vol. 25, No. 2, pp. 131–150. <http://dx.doi.org/10.1108/01443570510577001>
- [7] **Miller J. G., Roth A.:** 1994. A taxonomy of manufacturing strategies, *Management Science*, Vol. 40 No. 3, pp. 285-304. <http://dx.doi.org/10.1287/mnsc.40.3.285>
- [8] **Phillips L. W., Chang D. R., Buzzel R. D.:** 1983. Product quality, cost position and business performance: A test of some key hypotheses. *Journal of Marketing*, Vol. 47, No. 2, pp. 26-43.
- [9] **Schonberger R. J.** 2007. Japanese production management. *Journal of Operations Management*, Vol. 25, No. 2, pp. 403–419. <http://dx.doi.org/10.1016/j.jom.2006.04.003>
- [10] **Voss C. A.:** 1995. Alternative paradigms for manufacturing strategy. *International Journal of Operations & Production Management*, Vol. 15, No. 4, pp. 5–16. <http://dx.doi.org/10.1108/01443579510083587>
- [11] **Voss C. A.** 2005. Alternative paradigms for manufacturing strategy. *International Journal of Operations & Production Management*, Vol. 25, No. 12, pp. 1211–1222. <http://dx.doi.org/10.1108/01443570510633611>
- [12] **Somló J.:** 2002. Gépgyártástechnológia [Manufacturing engineering], 16. fejezet. Szerk: Horváth M., Markos S., Budapest: Műegyetemi Kiadó, pp. 145-173.o.
- [13] **Bellon E.:** 2009. A mezőgazdaságigép-gyártás jelenlegi helyzete és rövidtávú kilátásai [The current situation and short-term perspectives of agricultural mechanical engineering]. *Mezőgazdasági Technika [Agricultural Technology]*, pp. 12-14.
- [14] **Laugen B. T., Boer H.:** 2011. The International Manufacturing Strategy Survey, CINet Research Series, Serial Number: 2001-7. pp. 16-17. ISBN 978-90-77360-14-09
- [15] **Scipione P. A.:** 1999. A piackutatás gyakorlata [The practice of market research], Budapest, Springer-Hungária Kiadó, pp. 151-162.o. Abstract



CLASSIFICATION MODELS OF HUNGARIAN HONEY SAMPLES BASED ON ANALYTICAL AND PHYSICAL CHARACTERISTICS

Author(s):

T. Kaszab¹ – Zs. Bodor² – Z. Kovacs¹ – Cs. Benedek²

Affiliation:

¹Department of Physics and Control, Faculty of Food Science, Szent István University, Somlói út 14-16., Budapest, H-1118, Hungary

²Department of Dietetics and Nutrition, Faculty of Health Sciences, Semmelweis University, Vas u. 17., H-1088 Budapest, Hungary

Email address:

kaszab.timea@etk.szie.hu, zsanett.bodor93@gmail.com, zoltan.kovacs3@etk.szie.hu, benedek.csilla@se-etk.hu

Abstract

As one of the most often used natural sweeteners, honey has recently been reconsidered and more commonly used. Although Hungary is one of the main honey exporter countries, data referring to Hungarian honeys is very limited. Our aim was to investigate the analytical, physical and rheological properties of different honey samples and use these attributes to identify their geographical and botanical origin. Our results show the application of colorimetry, analytical and rheological measurements might be a promising combination of affordable methods for authentication of honey origin, however, further experiments are proposed to build up a robust database.

Keywords

honey, polyphenols, colorimetry, rheology, near-infrared spectroscopy

1. Introduction

The latest trends in nutrition shows towards the consumption of more natural and less processed food products, for instance honey. It is produced by honeybees (*Apis mellifera*) either from nectar, sap of plant parts or from the juicy material secreted by sucking insects. Honey is also a particularly valuable product because it is rich in nutritional components like vitamins, minerals, organic acids, proteins, and amino acids. Furthermore, every kind of honey or honeydew has a specific aroma, flavor and scent [1]. The quality of honey highly depends on its botanical

and geographical origin [2]. Physico-chemical and sensory properties of honey vary based on their origin [3][4]. Although Hungary is one of the main honey exporter countries, data referring to Hungarian honeys is very limited.

However, honey has been also target of food adulteration due to its emerging use and relatively high price. Methods for adulteration have a wide range from feeding bees with different kinds of sugar syrups to blending European honey with cheaper honey from different countries or with syrups like high fructose corn syrup (HFCS), beet syrup, or rice syrup [5]. Authorities and scientists apply different methods to detect adulteration, for example high-liquid chromatography (HPLC), gas chromatography/mass spectrometry (GC/MS), atomic emission spectroscopy (AES), nuclear magnetic resonance spectroscopy (NMR), etc. [5][6]. These methods are time-consuming and need very strict controlled operation criteria [7]. They also need high-cost instruments which are usually non-portable and need highly qualified, trained persons [8]. Therefore, there is an increasing need to develop rapid evaluation methods for identification of honey from different sources. Determination of parameters such as ash content, electrical conductivity, pH, color [9][10] and near infrared spectra [11][12] can be a good way to estimate the origin of honey and also for tracing quality [13][14]. Rheological properties of honey may also depend on the floral source [15]. The measurement of the total polyphenol content (TPC) is also a well-known method for the determination of floral or geographical origin of honey [9][16]. However, the determination of individual parameters does not always provide satisfactory accuracy for

origin identification or detection of adulteration. Therefore, simultaneous measurement of main physical and chemical parameters of honey, combined with chemometric methods could be more efficient.

Our aim was to investigate the analytical, physical and rheological properties of honeys and to use these attributes to identify their geographical and botanical origin using appropriate statistical methods.

2. Materials and Methods

Honey samples

In this study 29 honey samples were analysed with several methods explained in the Methods section (Figure 1). Most of the honey samples were collected directly from beekeepers.



Figure 1. Geographical origin of honeys

Honey samples are from different botanical origin such as acacia (10 samples), linden (6 samples), chestnut (5 samples) and polyfloral (8 samples). Samples were collected from different geographical regions, most of them are from different parts of Hungary. Some samples were collected from Transylvania and 1 honey from the market, being labelled as a blend of honeys from the European Union and outside this.

Methods

Main physico-chemical parameters like ash content, pH, electrical conductivity, refraction index and total soluble dry material content of honey samples were determined according to the methods recommended by the International Honey Commission [17].

Ash content

Three to seven grams of honey sample was measured to a porcelain jars and two drops of olive oil were given in each jar. Then the samples were pre-

combusted with a gas burner and put in the electric furnace at 600 °C until constant weight was reached.

pH determination

1.333 g honey sample was weighted in and dissolved in 10 ml carbon dioxide-free distilled water and measured with a pH meter.

Electrical conductivity

An amount of honey, equivalent to 20.0 g anhydrous honey, was dissolved in distilled water, then it was transferred quantitatively to a 10 ml volumetric flask and made up to volume with distilled water. The electrical conductivity of the solution was measured.

Refractometry

Honeys were also analyzed using an Abbé refractometer to read their refractive index which provides information about the dry matter content of the sample using the tables of the International Honey Commission [17].

Total polyphenol content (TPC)

1 g of honey sample was measured in a 10 ml volumetric flask and made up to volume with distilled water. Total polyphenol content was determined by the Folin–Ciocalteu colorimetric method using gallic acid as a standard: 1ml of the honey sample solution was put in a test tube and 7.5 ml distilled water was added. Then 0.5 ml of the Folin–Ciocalteu reagent was given to each tube and after 3 minutes 1 ml Na₂CO₃ solution was added. Absorbance was read on a Helios α-spectrophotometer at 750 nm, after a 30 minutes incubation period [18].

Color determination

Honey samples were measured with a Konica Minolta 410 colorimeter in the CIE L*a*b* color space. This color system is a three-dimensional coordinate system which means that it gives us information on the color properties in three dimensions: L* (light-dark), a* (green-red) and b* (blue-yellow).

Near infrared spectroscopy

The near infrared (NIR) spectra of the honey samples were collected with an Enterprise Telspec Food Sensor g1 scanner (Telspec Inc., Toronto, Ontario, Canada) in several sessions acquiring multiple spectra per sample in each session, with 2nm spectral step in the 950-1630 nm spectral interval. Reflectance

cuvette holder with 0.4 mm layer thickness was used during the data acquisition.

Rheology

RotoVisco1 rotational viscometer was applied to determine the shear stress of honey samples. The dynamical viscosity was calculated from the ratio of shear stress and shear velocity. Each sample was measured twice and the average values were evaluated. Each measurement includes three stages. The stages were as the follows: accelerated shear velocity up to 100 1/s during 100s; mixing at the maximum velocity during 100s; slowing velocity from the maximum to zero during 100s.

Statistical evaluation

The evaluation of the combined data of the analytical, physical and rheological parameters, as well as the NIR results were analyzed by linear discriminant analysis (LDA) [19]. LDA is one of the most frequently used of parametric classification procedures. In the LDA the classification scores depend on the descriptive scores linearly, where the groups are defined previously. The tasks of the model

maximize the ratio between-class variance and minimize the ratio of within-class variance. LDA supposes a prior knowledge of the group membership of each sample in a training set. The classification power of the model derived evaluate by using the original grouped cases or using cross-validation procedure. LDA models were built for the botanical and geographical origin identification of the honey samples, separately. LDA models were validated using one sample-out cross-validation and the models of NIR data were additionally tested by independent prediction. R-Project, Microsoft Excel and XLSTAT software were used for the data evaluation.

3. Results and discussion

Results of the evaluation of analytical, colorimetric and rheological measurements

The results of LDA model built for the classification of the different floral types of honey such as acacia, chestnut and polyfloral honeys using the data of rheological, colorimetric and analytical parameters (total polyphenol content, ash content, pH, electrical conductivity and refractive index) are shown in Figure 2 and Table 1.

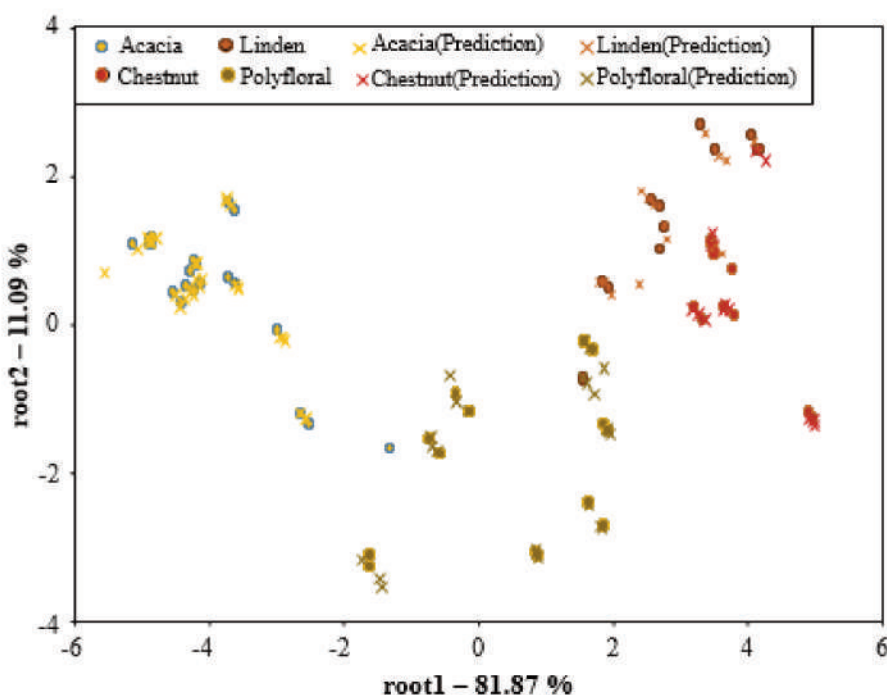


Figure 2. LDA score plots presenting the separation of the different floral groups of honey using rheological, colorimetric and analytical parameters (n=145)

The LDA model presented average recognition and prediction abilities of 89.29% and 90.48 %, respectively for the classification of acacia, chestnut, linden and polyfloral samples based on

their botanical origin as shown in more details in Table 1.

Classification models were also developed for the discrimination of the honey samples based on their

geographical origin by counties using the rheological, colorimetric and analytical parameters. Classification performance of the LDA model built for geographical origin identification provided average recognition and prediction abilities of 66.07 % and 79.76%, respectively, when data of all floral types were included.

Better results were obtained when separate models were built for the geographical origin identification of the individual honey types. In case of chestnut, polyfloral and linden honey types both recognition and prediction ability were found to be 100%. LDA model of acacia honey presented average recognition and prediction abilities of 100% and 80%, respectively (Table 2 and Figure 3).

Table 1. Confusion matrix of the LDA model built for the classification of the honey samples by their botanical origin using rheological, colorimetric and analytical parameters (n=145)

MODEL BUILDING (%)				
	Acacia	Chestnut	Linden	Polyfloral
Acacia	95.00	0.00	0.00	5.00
Chestnut	0.00	80.00	20.00	0.00
Linden	0.00	8.00	75.00	17
Polyfloral	0.00	0.00	0.00	100.00
MODEL VALIDATION (%)				
	Acacia	Chestnut	Linden	Polyfloral
Acacia	100.0	0.00	0.00	0.00
Chestnut	0.00	80.00	20.00	0.00
Linden	0.00	11.11	72.22	16.67
Polyfloral	0.00	0.00	0.00	100.00

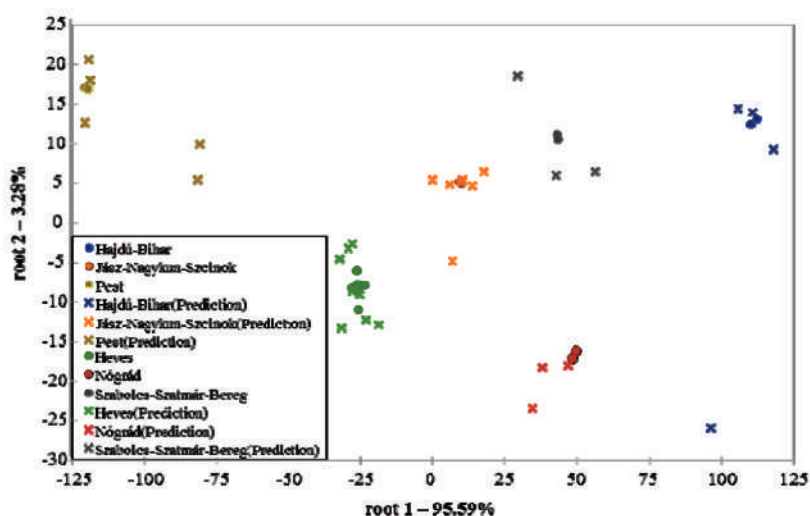


Figure 3. LDA score plots presenting the separation of the different geographical groups of acacia honey using rheological, colorimetric and analytical parameters (n=50)

Table 2. Confusion matrix of the LDA model built for geographical origin classification of acacia honey using rheological, colorimetric and analytical parameters (n=50)

ACACIA MODEL BUILDING (%)						
	Hajdú-Bihar	Heves	Jász-Nagykun-Szolnok	Nógrád	Pest	Szabolcs-Szatmár-Bereg
Hajdú-Bihar	100.00	0.00	0.00	0.00	0.00	0.00
Heves	0.00	100.00	0.00	0.00	0.00	0.00
Jász-Nagykun-Szolnok	0.00	0.00	100.00	10.00	0.00	0.00
Nógrád	0.00	0.00	0.00	100.00	0.00	0.00
Pest	0.00	0.00	0.00	0.00	100.00	0.00
Szabolcs-Szatmár-Bereg	0.00	0.00	0.00	0.00	0.00	100.00
ACACIA MODEL VALIDATION (%)						
	Hajdú-Bihar	Heves	Jász-Nagykun-Szolnok	Nógrád	Pest	Szabolcs-Szatmár-Bereg
Hajdú-Bihar	100.00	0.00	0.00	0.00	0.00	0.00
Heves	0.00	66.67	0.00	16.67	16.67	0.00
Jász-Nagykun-Szolnok	0.00	0.00	100.00	0.00	0.00	0.00
Nógrád	33.33	0.00	33.33	33.33	0.00	0.00
Pest	0.00	0.00	0.00	0.00	100.00	0.00
Szabolcs-Szatmár-Bereg	0.00	0.00	0.00	0.00	0.00	100.00

Results of the near infrared spectroscopy measurements

Results of LDA model built for the classification of the different honey samples based on their floral types such as linden, acacia, chestnut and polyfloral honeys based on their NIR spectra is presented in Figure 4. The average recognition and prediction abilities of the NIR based model were found to be 95.65 % and 92.61%, respectively.

Classification of the honey samples based on their geographical origin using the NIR spectroscopic data

provided average recognition and prediction abilities of 99.13 % and 95.65%, respectively, when data of all floral types was included.

Similarly to the results of the rheological, colorimetric and analytical parameters, better results and further improvement of the identification of the geographical origin were possible when separate models were built for the individual honey types. In case of all the tested honey types, i.e. linden, acacia, polyfloral and chestnut honey types both recognition and prediction ability were found 100%

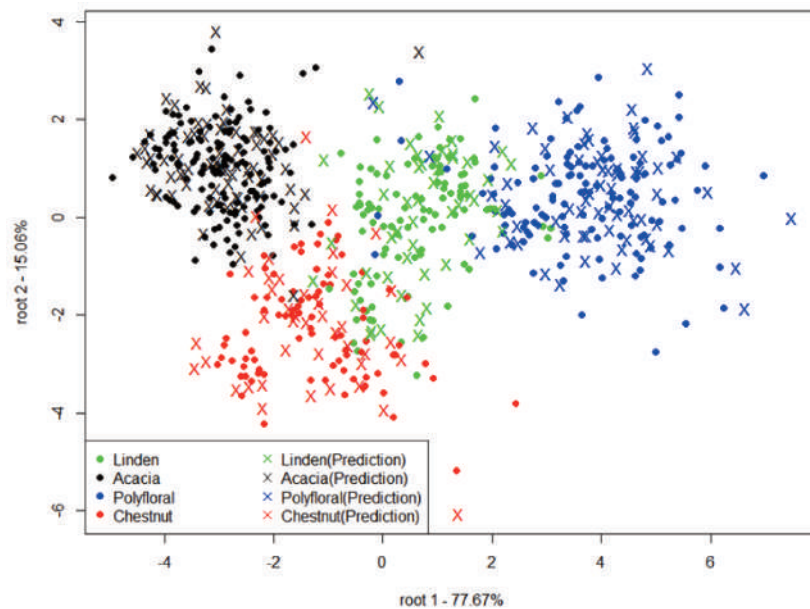


Figure 4. LDA score plots presenting the separation of the different floral groups of honey using data of near infrared spectroscopy in the range between 950 and 1630 nm (n=690)

4. Conclusion

Our results show that application of colorimetry, basic analytical and rheological measurements might be a promising combination of affordable methods for authentication of honey origin. Based on these first encouraging results, we propose further experiments to build up a robust database enlarging not only the geographical area, but also increasing the number of domestic honey samples. It also can be seen that these simple tools are also fairly reliable for the recognition of geographical origin identification if we build our models for individual honey types, this emphasizing the importance of characteristics determined by botanical origin over those influenced by the geographical origin.

According to our results, NIR spectroscopy applied on its own can also be an even more efficient method for honey classification based on botanical origin. A

special and very practical advantage of this latter is offered by non-destructive method needing no sample preparation and the portable instrument, qualifying thus this analysis suitable for field screenings. Also, NIR provided some impressive results for geographical origin determination all the tested honey types, reaching overall 100% recognition and prediction abilities. Based on these results, further building of a NIR database for honeys is fully justified and promising.

Acknowledgements

This paper was supported by the János Bolyai Research Scholarship of the Hungarian Academy of Sciences (Zoltan Kovacs). This paper was supported by the ÚNKP-17-2 (Zsanett Bodor) and ÚNKP-17-4 (Zoltan Kovacs) New National Excellence Program of the Ministry of Human Capacities. Authors are

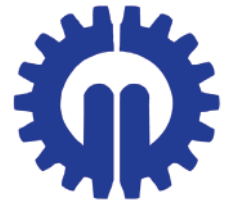
grateful to Telspec for providing technical support for the NIR analysis.



References

- [1] **Czipa N.:** 2010. Különböző eredetű mézek összehasonlító vizsgálata és a gyártmánykialakítás hatása a minőségre [Comparative study of honeys with different origin, the effect of production-forming on the quality]. Hankóczy Jenő Növénytermesztési, Kertészeti és Élelmiszertudományok Doktori Iskola [Jenkő Hankóczy Doctor's School of Plant Production, Horticulture and Food Sciences], pp. 143.
- [2] **Kiss T., Tóth G.:** 1987. A méhészeti termékek [Apiary products]. in A méhészet kézikönyve I. [The handbook of apiary], 1., A. Nikovitz A., Ed. 1987: Állattenyésztési és Takarmányozási Kutatóközpont. pp. 383–490.
- [3] **Anklam E.:** 1998. A review of the analytical methods to determine the geographical and botanical origin of honey. *Food Chemistry*, Vol. 63, No. 4. pp. 549–562.
[http://dx.doi.org/10.1016/S03088146\(98\)00057-0](http://dx.doi.org/10.1016/S03088146(98)00057-0)
- [4] **Da Silva P. M., Gauche C., Gonzaga L. V., Costa A. C. O., Fett R.:** 2016. Honey: Chemical composition, stability and authenticity. *Food Chemistry*, Vol. 196, pp. 309–323.
<http://dx.doi.org/10.1016/j.foodchem.2015.09.051>
- [5] **Zábrodská B., Vorlová L.:** 2014. Adulteration of honey and available methods for detection – a review. *Acta Veterinaria Brno*, Vol. 83, No. 10, pp. S85–S102.
<http://dx.doi.org/10.2754/avb201483S10S85>
- [6] **Mehryar L., Esmaili M.:** 2011. Honey & Honey Adulteration Detection: A Review. International Congress on Engineering and Food 11th, pp. 1–6.
- [7] **Amiry S., Esmaili M., Alizadeh M.:** 2017. Classification of adulterated honeys by multivariate analysis. *Food Chemistry*, Vol. 224, pp. 390–397.
<http://dx.doi.org/10.1016/j.foodchem.2016.12.025>
- [8] **Bougrini M., Tahri K., Saidi T., El Alami El Hassani N., Bouchikhi B., El Bari N.:** 2016. Classification of Honey According to Geographical and Botanical Origins and Detection of Its Adulteration Using Voltammetric Electronic Tongue. *Food Analytical Methods*, Vol. 9, No. 8, pp. 2161–2173.
<http://dx.doi.org/10.1007/s12161-015-0393-2>
- [9] **Can Z., Yildiz O., Sahin H., Akyuz Turumtay E., Silici S., Kolayli S.:** 2015. An investigation of Turkish honeys: Their physico-chemical properties, antioxidant capacities and phenolic profiles. *Food Chemistry*, Vol. 180, pp. 133–141.
<http://dx.doi.org/10.1016/j.foodchem.2015.02.024>
- [10] **Karabagias I. K., Vavoura M. V., Nikolaou C., Badeka A. V., Kontakos S., Kontominas M. G.:** 2014. Floral authentication of Greek unifloral honeys based on the combination of phenolic compounds, physicochemical parameters and chemometrics. *Food Research International*, Vol. 62, pp. 753–760.
<http://dx.doi.org/10.1016/j.foodres.2014.04.015>
- [11] **Gan Z., Yang Y., Li J., Wen X., Zhu M., Jiang Y., Ni Y.:** 2015. Using sensor and spectral analysis to classify botanical origin and determine adulteration of raw honey. *Journal of Food Engineering*, Vol. 178, pp. 151–158.
<http://dx.doi.org/10.1016/j.jfoodeng.2016.01.016>
- [12] **Bodor Zs., Koncz F. A., Rashed M. S., Kaszab T., Gillay Z., Benedek Cs., Kovacs Z.:** 2016. Application of near infrared spectroscopy and classical analytical methods for the evaluation of hungarian honey. in 1st International Conference on Biosystems and Food Engineering.
- [13] **Czipa N., Borbélyné Varga M., Győri Z.:** 2008. A méz minősítéséhez és nyomonkövethetőségéhez szükséges vizsgálatok [Essential examinations for honey qualification and traceability]. *Agrártudományi Közlemények [Acta Agraria Debreceniensis]*, Vol. 20, pp. 25–32.
- [14] **Cimpoiu C., Hosu A., Miclaus V., Puscas A.:** 2013. Determination of the floral origin of some Romanian honeys on the basis of physical and biochemical properties. *Spectrochimica Acta - Part A Molecular and Biomolecular Spectroscopy*, Vol. 100, pp. 149–154.
<http://dx.doi.org/10.1016/j.saa.2012.04.008>
- [15] **Belay A., Haki G. D., Birringer M., Borck H., Addi A., Baye K., Melaku S.:** 2017. Rheology and botanical origin of Ethiopian monofloral honey. *LWT - Food Science Technology*, Vol. 75, pp. 393–401,
<http://dx.doi.org/10.1016/j.lwt.2016.09.021>
- [16] **Alvarez-Suarez J. M., Tulipani S., Romandin S.i, Vidal A., Battino M.:** 2009. Methodological aspects about determination of phenolic compounds and in vitro evaluation of antioxidant capacity in the honey: a review. *Current Analytical Chemistry*, Vol. 5, No. 4, pp. 293–302.
<http://dx.doi.org/10.2174/157341109789077768>
- [17] **Bogdanov S.:** 2009. Harmonised Methods of the International Honey Commission. *International Honey Commission*, No. 5, pp. 1–63.
- [18] **Prior R. L., Wu X., Schaich K.:** 2005. Standardized methods for the determination of antioxidant capacity and phenolics in foods and dietary supplements. *Journal of Agricultural and Food Chemistry*, Vol. 53, No. 10, pp. 4290–4302.
<http://dx.doi.org/10.1021/jf0502698>

[19] **Berrueta L. A., Alonso-Salces R. M., Héberger K.:** 2007. Supervised pattern recognition in food analysis. *Journal of Chromatography A*, Vol. 1158, pp. 196–214. <http://dx.doi.org/10.1016/j.chroma.2007.05.024>



AXIAL FLOW TURBINE FOR SOLAR CHIMNEY

Author(s):

W. M.A Elmagid¹ – I. Keppler²

Affiliation:

¹Institute of Environmental Systems, Szent István University, Páter Károly street 1, Gödöllő, H-2103, Hungary

²Institute of Mechanics and Machinery, Szent István University, Páter Károly street 1, Gödöllő, H-2103, Hungary

Email address:

w.abdelmaged@Aswu.edu.eg, kepler.istvan@gek.szie.hu

Abstract

Producing sufficient amount of energy is critical issue over the entire world. A rather new method of harvesting renewable energy is taken into the focus of our research to cover the increase in electricity demand. The solar chimney power plant (SCPP) is one of some solutions to produce electrical energy by utilizing renewable source. The combination of solar energy and chimney effect is the renewable source that delivers the SCPP its energy. In this study, the redesign of an axial turbine for SCPP of Manzanares prototype is presented to simulate SCPP overall with using radiation model. Additionally, the investigation of flow inside the turbine is carried out by using the three dimensional CFD model. The CFD model solves Reynolds-averaged Navier–Stokes equations (RANS equation) using K- ϵ turbulent model. The solar radiation is calculated by using two different radiation models according to the physical state. P1 radiation model is applied in the fluid zone, and Monte Carlo model is applied in the solid zone. The comparison of the CFD results and previous experimental results show a good agreement, which validates our CFD model.

Keywords

Solar Chimney, Computational Fluid Dynamics, Turbine

1. Introduction

Utilization of renewable resources is dramatically essential for reducing fossil fuel effect on the human environment. Thus, the application of renewable energy has therefore been the goal of numerous researchers to improve the cost of energy production. To that end, many innovative concepts have been

proposed to capture more energy from the renewable energy sources such as solar, wind, and hydroelectric energy. The most promising paths towards the sustainable development are solar energy, especially in energy production.

One of the options that will help in global electricity production by using renewable energy resource is the solar chimney power plant (SCPP). The Solar Chimney Power Plant System (SCPPs) is a natural driving power generating system. It can convert solar energy first into thermal energy then into kinetic energy and finally into electrical power. The operation of a solar chimney power plant (SCPP) is based on a simple principle: when air is heated by the greenhouse effect under the transparent roof of a collector, buoyancy forces arise as a consequence of density variation, this less dense hot air rises up a chimney, which installed at the centre of the collector. At the base of the chimney, the air flows through a turbine to produce mechanical energy for driving a generator. It combines the concept of solar air collector and central updraft chimney to generate a solar induced convective flow which drives wind turbines to generate electricity. The SCPP consists of a greenhouse roof collector, wind turbine, and updraft chimney that is located at the centre of the greenhouse roof collector, as shown in Figure 1. The SCPPS has been proposed as a device to economically generate electricity from solar energy in commercial-scale in the future.

Cabanyes (1903) first proposed the solar chimney power technology concept. In 1978, Schlaich again presented the technology in a congress [1]. During the two-year period between 1981 and 1982, this technology has been verified by the successful construction and operation of the 50 kW Manzanares, Spain SCPP pioneer prototype [2]. This prototype has a 194.6 m high chimney, a radius of the collector is

122 m, and a vertical axis single-rotor turbine without inlet guide fans configuration installed at the base of the chimney. This prototype designed to operate with the peak power lying at about 50 kW for eight years, whereas in fact, the output measured was 36 kW [3].

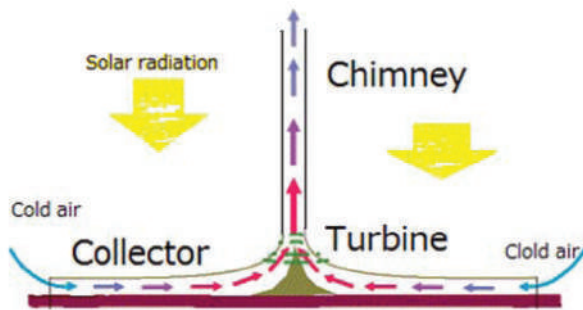


Figure 1. Schematic diagram of SCPP [4].

Since then, many prototypes of the SCPP had been built by experts in various countries. Australia intends to construct the largest SCPP in world at present with the generation capacity reaching up to 200MW in New South Wales of Australia. The chimney in the plant will be 1000m in height and the collector is 7 km in diameter, the system would cover a ground area of 38 km² [5]. Significant research effort has been put into the construction, simulation and operation of the solar chimney collector. An analytical model has been presented to study detailed performance for main plant elements (collector, chimney and wind turbine). Mullett [6] developed analysis for the SCPP, aimed particularly to calculate overall efficiency and performance. He concluded that the solar chimney is essentially a power generator of large scale. Overall efficiency is directly related to the height of the chimney and is shown to be about 1% for a height of 1000 m. This resultants is confirmed by Yan et al [7].

Experimental and numerical calculation method can be used to study the performance of the SCPPs. But the large scale system is hard to establish. Computational fluid dynamic (CFD) take an effective role in a solar chimney technology research. Subsequently, with the development of computer technology and CFD software techniques, both temperature and pressure distribution in the large system can easily be predicted by numerical calculation method [8]. Rafiuddin et al [9] study the optimization a geometry of the major components of the SCPP using a computational fluid dynamics (CFD) technique within software ANSYS-CFX to investigate and improve the flow characteristics inside the SCPP. Based on the CFX computational results, the best configuration was achieved using the chimney with a divergence angle of 2° and the

temperature inside the collector is higher for the lower opening resulting in a higher flow rate and power. Additional, other researchers is used FLUENT software to optimize the SCPP by changing the collector inlet opening and outlet diameter of the chimney, and concluded that the available power was virtually unresponsive to the variation of collector inlet opening, as [10].

Pasumarthi and Sherif [11] used experimental and mathematical model to study the effect of various parameters on the air temperature, air velocity, and power output of the solar chimney. Two experimental configuration were tried on the collector: increasing the collector base diameter and introducing an intermediate absorber. Enhancing the air temperature is resulted from the former modification, while the latter contributed to increasing the air temperature as well as the mass flow rate inside the chimney. Both enhancements helped to increase the overall chimney power output. Comparison of mathematical model results to published data of the solar chimney system built in Manzanares, Spain has been used to validate the calculated results. Also, an economic assessment of the system costs are presented in reference [12].

Pretorius and Kröger [13] have developed comprehensive models to solve the governing conservation and draught equations simultaneously, and Bernardes et al [14] presented same techniques to predict the SCPP performance. The results show that the height of chimney, the factor of pressure drop at the turbine, the diameter and the optical properties of the collector are important parameters for the design of solar chimneys. Gannon and Von Backström [15] adapted the standard gas turbine cycle to define a standard solar chimney cycle, and the adaption includes chimney friction, turbine system and exit kinetic energy losses in the analysis.

The objective of this study is to accurately analyze the SCPP system by using CFD simulation model, with fewer assumptions are used in the theoretical calculation, but more detailed descriptions of pressure and flow field could be obtained. A 3D approach for SCPP prototype is carried out by using ANSYS CFX v18 with axial vertical flow turbine. The turbine is designed of using free vortex and the matrix throughflow method. The 3D numerical simulation incorporating the radiation models and turbine models. Results from the mathematical model were compared with Manzanares experimental results for model validation. Based on the proposed numerical approach, the effects of solar radiation, pressure extracted at the turbine, and mass flow rate on the SCPP system performance were investigated in detail.

2. Description of Solar Chimney

A typical SCPP consists of three major components, namely, a solar collector, a chimney and wind turbines, as shown in Figure 1. In a SCPP, solar radiation collected by the solar collector and greenhouse effect, which heats up the ambient air entering the collector; then the hot air flows into the chimney through the collector exit, which is also the entrance of the chimney. In the chimney, the air density difference between the inside and outside of the chimney causes a large pressure difference between the system and the ambient air (chimney effect), which will drive the wind turbine installed at the chimney base to generate electricity (wind turbine effect). The SCPP has no adverse effect on the environment, needs no cooling water and has extremely low maintenance costs. Furthermore, the SCPP can operate even at nights since the soil under the collector works, as a natural heat storage system. These distinct advantages have made SCPP an attractive option for utilizing solar energy.

Principle of solar collector

The major component of a solar chimney power station is the solar collector. Solar energy collectors are special kind of heat transfer that transform solar radiation energy to internal energy of the ambient air (transport medium). The collector is the part of the chimney that produces hot air by the greenhouse effect. It has a roof made up of plastic film or glass plastic film. This covering admits the short wave solar radiation component and retains long wave radiation from the heated ground. Thus, the ground under the roof heats up and transfers its heat to the air flowing radially above it from the outside to the chimney. The height of the roof increases adjacent to the chimney base so that the air is driven to the chimney base with minimum friction loss. However, the structure of a collector change according to consideration of architectural and civil design [16].

Principle of updraft chimney

The chimney is the main characteristic of the solar chimney station. The tower, which acts like a large chimney, is located at the centre of the greenhouse canopy (collector). The tower utilize a temperature differential between the cool air at the top and the heated air at the bottom. The temperature difference create difference in density. This creates the chimney effect, which sucks air from the bottom of the tower out of the top. The chimney of the plant is extremely high and will need a stable base while still allowing

free flow of air through the turbine. It would also be advantageous to have the turbine as low as possible in the chimney to make its construction simpler.

Principle of air turbines

The turbine of the solar chimney is key component of the plant as it extracts the kinetic energy from the air and transmits it to the generator. It has significant influence on the plant as the turbine pressure drop and plant mass flow rate are coupled. The specifications for solar chimney turbines are in many aspects similar to those ones for large wind turbines. They both convert large amounts of energy in the airflow to electrical energy. However, there are also various important differences. The following characteristic are typical for solar chimney turbines in contrast to wind turbines.

The typical solar chimney turbine is of the axial flow type. It has characteristics between those of wind turbines and gas turbines: it has more blades than the typical two or three of wind turbines, but not as many as gas turbines. The rotor blades are adjustable, like those of wind turbines, but as in gas turbines, the flow is enclosed, and some of solar chimney turbine may have radial vanes of inflow inlet guide. The main function of the turbine is the efficient conversion of fluid power to shaft power. A secondary function of solar chimney turbines is flow and output power control by adjustment of its blade angles [17].

This Characteristic of solar chimney turbines leads the researchers to take different method during the design of the turbine. Gannon and Von Backström [17], Denantes and Bilgen [18], and Fluri and von Backström [19] used the free vortex design. The free vortex approach is used in an axial flow gas turbine stage annulus and is assumed to be fully cascaded aerofoil (two dimensions) when the flow parameters are functions of two space coordinates, which the radial effect on the flow is ignored. On the other hand, Y Zhou et al. [20] used Wilson design theory to design of the SCPP turbine. Wilson design is classical theory to design horizontal axis wind turbine.

3. Turbine Design of the SCPP

Solar chimney literature has little to say about factors affecting efficiency of the turbines, but merely assumes various fixed values of efficiency in the range 40-80%, according to Backström & Gannon, [17] and Mullett [6]. In this study, a new approach is present for redesign of the solar chimney turbine. The Matrix Throughflow Method (MTFM) usually design the axial flow turbine and fan. The MTFM is a two-dimensional analysis tool that is effective in the

design phase of turbine of SCPP. It simulates the machine as an axisymmetric duct with the blade rows represented by actuator discs or volumes. The MTFM considers the free vortex method assumed that all flow changes occurred within the blade row while in a real machine the velocity profiles change in the space ahead and behind the blades as well. Its main use in this analysis is to calculate the correct gas inlet and outlet angles to produce the correct amount of absorbed power from the fluid. In the next design step, profile shapes are designed based on these gas inflow and outflow angles. Using the MTFM method, the flow in the duct is also analysed to check and see that there are no adverse pressure gradients as the flow turns into the turbine as this could lead to separation at parts of the wall. This is achieved by using the interpolation method that allows values on a local orthogonal grid from the quasiorthogonal grid to be calculated using a simple linear interpolation method, by (Harms et al. [21]). This approach is used in an almost identical form in the application of the streamline through flow method (STFM) and detail of the implementation is given, which done in thesis presented by Gannon [22].

The Vista AFD under ANSYS Workbench v 18 is used to design the turbine of the SCPP. It is applied MTFM to design the axial fan. However, the design of the turbine is carried by entering the inlet flow condition as output of fan, and outlet flow condition is an inlet of fan. This condition is correct under free vortex design for 0.5 degree of reaction. Figure 2 shows the velocity triangle of free vortex at 0.5 degree of reaction in a turbine stage, where the blade angle is β , absolute flow angle is α , relative velocity is w , absolute velocity is c , and U is the blade speed. This condition allows reversing the turbo machine with same efficiency. The input aerodynamic parameter to Vista AFD is calculated from free model of the SCPP. The geometry parameter of the SCPP is also need to design the turbine, as shown in Table 1.

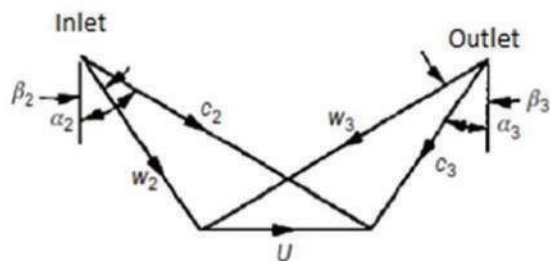


Figure 2. Velocity profile of half degree of reaction of the blade [23].

4. Simulation Model

A solar chimney power plant has many physics principles. The heating collector is work as air heater by solar energy, where all terms of heat transfer are applied to predict his performance. To analysis of chimney, the heat transfer is neglected but buoyancy force (fluid mechanics) is taken into account. The turbo machine theories should be applied to design and analyse the turbine.

Table 1. Boundary condition for Vista AFD

Input aerodynamic parameter	
Rotational speed (Ω)	100 rpm
Air Velocity (U_∞)	9 m/s
Inlet total pressure	92930 pa
Inlet total temperature	291.5 K
Total head rise	90 pa
Input geometry parameter	
Outer diameter	5 m
Hub\ tip rotor	0.15
Number of the blades	4

The Computational Fluid Dynamic (CFD) involves the numerical solution of the differential governing equations of fluid flows and heat transfer, with the help of computers. This technique has a wide range of engineering applications. In the field of solar energy research, this technique has become increasingly important and it is prominent for studying the SCPP.

ANSYS-CFX v18 was used for simulation purpose in this research project. ANSYS-CFX v18 uses unsteady Navier– Stokes equation in their conservation form to solve set of equations. The instantaneous equation of mass (continuity), momentum, and energy conservation are presented below:

Mass conservation:

$$\frac{\partial \rho}{\partial t} + \nabla \cdot (\rho \vec{v}) = 0$$

where ρ is density of the fluid, \vec{v} is the velocity vector, and t is time

Momentum conservation:

$$\frac{\partial (\rho \vec{v})}{\partial t} + \nabla \cdot (\rho \vec{v} \vec{v}) = -\nabla p + \nabla \cdot (\overline{\overline{\tau}}) + \rho \vec{g} + \vec{F}$$

where p is the static pressure, $\overline{\overline{\tau}}$ is the stress tensor, $\rho \vec{g}$ is the gravity force and \vec{F} are the other external body forces.

Energy conservation:

$$\rho \frac{De}{Dt} = \frac{\partial(\rho e)}{\partial t} + \nabla \cdot (\rho e \vec{v}) + \nabla \cdot (\vec{v} \cdot \tau) + \vec{v} \cdot S_m$$

where e is energy of the fluid, which write by total enthalpy $h + v^2/2$, the term $\nabla \cdot (\vec{v} \cdot \tau)$ represents the work due to viscous stresses and is called the viscous work term. This models the internal heating by viscosity in the fluid, and is negligible in most flows, and the term $\vec{v} \cdot S_m$ represents the work due to external momentum sources and is currently neglected.

In commercial codes, a friendly interface gives the user the possibility of easy setting the various options and analyzes the results. As an example, ANSYS CFX v18 that is used in present study. When approaching the study of fluid dynamics problems, the mathematical model is based on the fundamental mass, momentum and energy conservation principles. The Reynolds's Averaged Navier-Stokes (RANS) equations for the compressible fluid flow are included the equations of the conservation of mass and momentum. Therefore, the conservation laws are invoked in the following, in the vectorial notation and conservative form for unsteady, three-dimensional compressible flow [24].

For the prediction of solar chimney performance in this study, the $k-\epsilon$ turbulence models have been chosen which type of Two-equation models. Two-equation models have been the most popular models for a wide range of engineering analysis and research. These models provide independent transport equations for both the turbulence length scale, or some equivalent parameter, and the turbulent kinetic energy. With the specification of these two variables, two-equation models are complete; no additional information about the turbulence is necessary to use the model for a given flow scenario. While this is encouraging in that these models may appear to apply to a wide range of flows, it is instructive to understand the implicit assumptions made in formulating a two-equation model [25].

As mentioned, the SCPP unit consists of ground, cover collector, chimney and fluid zone. All component geometry is drawn as 3D using SOLIDWORKS, as shown in Figure 3 (light green is Cover collector, blue is Fluid zone and yellow is ground area). The ANSYS Design Modeler is used to enter CAD file, which is a part of ANSYS Workbench 18. It able to read CAD file and transfer data reading to grid generation program such as Meshing or turbo grid. However, ANSYS Meshing is used that suitable for SCPP geometry. This technique has many advantages, reading shape with high accuracy and save time and labor needing to enter data.

Grid generation converts the geometry into a format that can be understood by the CFD solver. It is often the most time consuming and tedious jobs in achieving the CFD solution. Grid generation is the most important before pre-processing step. It is very important to generate accurate grids for the solver to obtain correct results. The accuracy of the CFD solution depends on the quality of the grid used to perform the calculations. Figure 4 show the overall model grid.

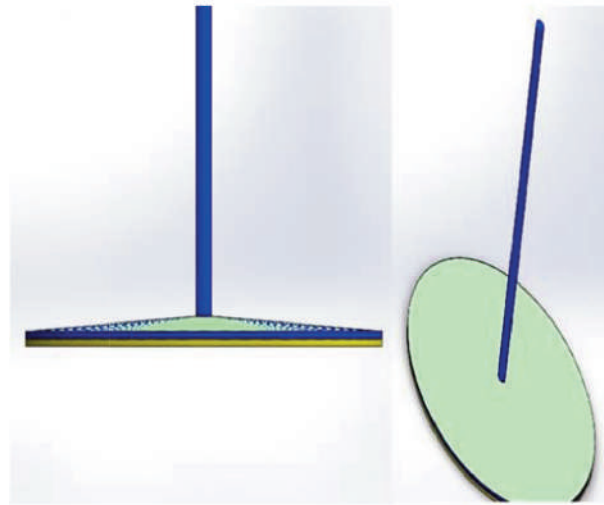


Figure 3. The 3D geometry of difference zone for the solar chimney unit.

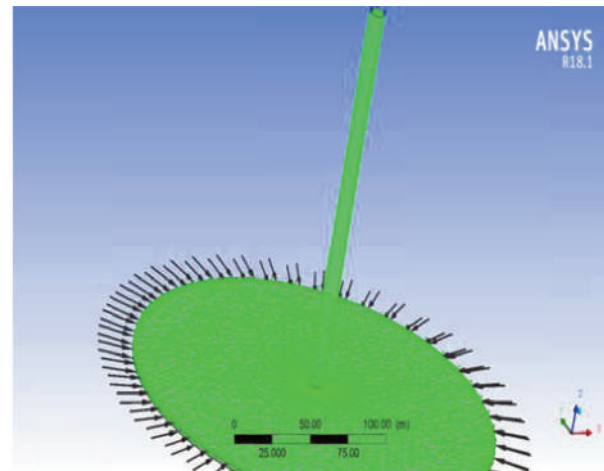


Figure 4. Grid of the solar chimney unit.

For generation turbine grid, turbo grid program is used that is specialized in turbo machine grid generation. One passage of flow is generated and the flow regions hub, shroud, inlet and outlet are defined. Figure 5 shows the turbo grid passage that used H/J/C/L-grid to make the flow region and O-grid in close to blade surface. This passage has rotating boundary condition.

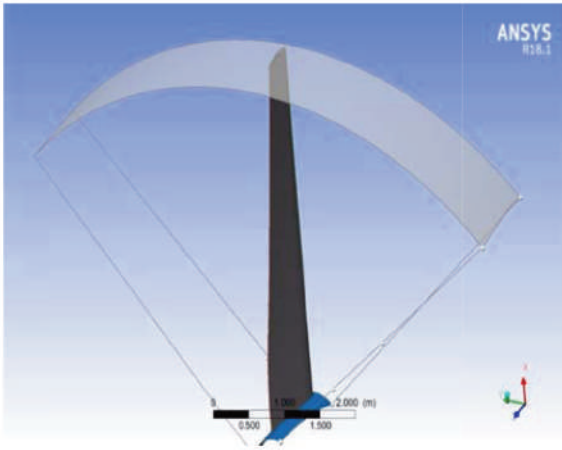


Figure 5. Turbo grid flow passage.

The interface between these two meshes is the GGI interface. The frozen rotor model is type of GGI interface, which available to use in ANSYS CFX v18. The two frozen rotor interfaces are used in this model. The first one is used between the passage inlet and side outlet from collector. The second interface is used between the outlet of passage and under surface of the chimney.

5. Results and Discussion

The axial turbine is designed by using the operation condition in the Table 1. Vista AFD software is carried out free vortex analysis to find a first approximation of the blade configuration. The next step of the analysis is to perform an axisymmetric simulation of the turbine. A Matrix Throughflow Method (MTFM) is used for this purpose, which able to handle the radial inflow and axial outflow that are found inside the solar chimney turbine. The airflow inflow and outflow angles from the turbine is then calculated by the MTFM approach. The values are slightly different from the free vortex prediction. From this calculation, the blade angle and chord distribution can be obtained for the most efficient design possible over the required operating range. Figure 6 show the 3D rotor geometry of the designed SSCP turbine. The BladeGen program under ANSYS Workbench v18 is used to present and modify the thickness distribution of the designed blade.

Beta angle is airflow angle of the designed blade, which is shown at leading and trailing edge along of the blade by Figure 7. In hub section generate (Range 0 to 0.5 of the blade length), the sharp change of the angle specifically at leading edge, the high twist angle of the blade. The blade with high twist angle has some difficult in his fabrications. Thus, more optimization will be required to reach the efficient performance and easy to fabrication.

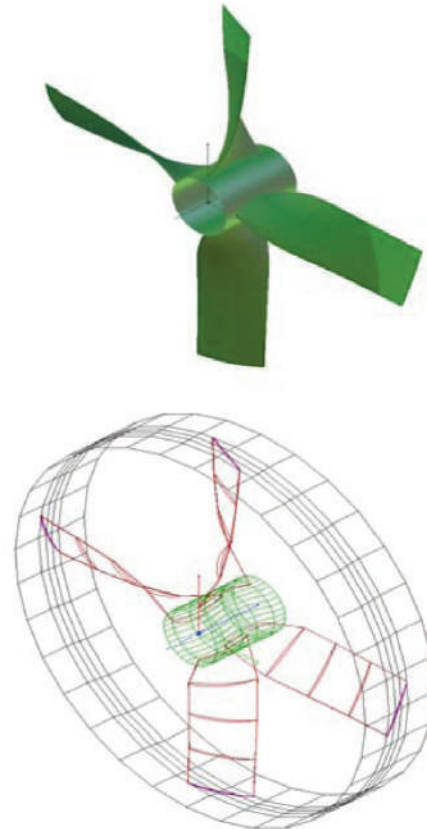


Figure 6. 3D axial turbine for the SSCP unit.

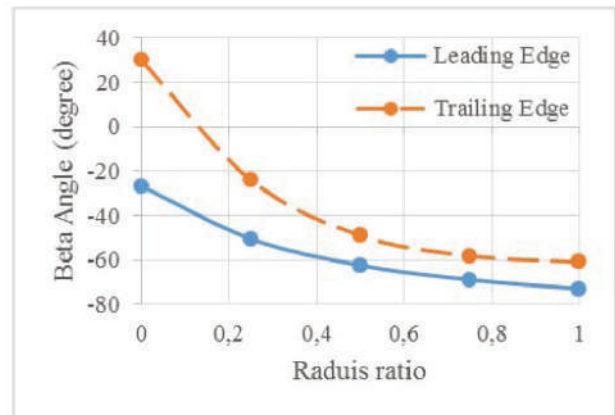


Figure 7. Beta angle at leading and trailing edge along the blade.

The blade thickness has serious influence in the turbine performance and toughness of the blade. NACA 0006 is selected to able the blade to perform well. Another factors are shape of NACA 0006 is easy to manufacture and the ratio of lift to drag coefficient in the work range of the SSCP turbine. The NACA 006 thinness is applied to the designed turbine by BladeGen software. Table 2 show the final chord distribution and twist angle of the design blade. The rotor is consisted from 4 blades that is described in Table 2.

Table 2. Designed blade configuration.

Span of the blade	Chord length (mm)	Twist Angle (degree)
0.00	1439.45	1.8
0.25	1442.91	-38.0
0.50	1441.65	-56.1
0.75	1452.01	-63.9
1.00	1470.66	-67.5

To validate the CFD model, calculated results are compared with the experimental results of the prototype from Manzanares, Spain. The measured data on September 2nd, 1982 are adopted from Reference (Haaf, 1984). The plant dimensions are given in Table 3. The comparisons between the calculation results and the experimental values are presented in Table 4. There is good agreement between measurement and calculation results, which are acceptable value.

Table 3. Geometrical dimensions of the pilot plant in Manzanares, Spain.

Mean roof radius	122 m
Average roof height	1.85 m
Tower height	194.6 m
Tower radius	5.08 m

Table 4. Comparison between measured data and mathematical model results.

	Measured	Calculated
Difference temperature at collector, °C	17.1	14.25
Upwind Velocity, m/s	9.045	9.11784
Power, P, kW	36	36.1552

The air velocity is calculated at different locations in the all domain of the SCPP unit. The upstream and downstream lines of the air velocity are calculated. As shown in Figure 8, the maximum velocity according at near close to the chimney entering, and uniform airflow in the collector region. The range of the velocity in the chimney is approximately 4 times the range of velocity in the collector. To capture more output power, the turbine should be located at high air velocity, which is achieved in near enter of the chimney.

Figure 8 illustrates contours of the pressure distribution at different zones of the chimney in a vertical intersection. The pressure around turbine has significant influence of the SCPP performance. Figure 9 shows that the pressure increases gradually as the air is flowing inside the chimney. It indicates also that the minimum static pressure is reached near the chimney base at the exit of the turbine due to extract the energy from the flow by the turbine.

The blade of an axial turbine flow depends on the airfoil theory. The pressure distribution around the airfoil surface controls in the lifting properties of the airfoil. Figure 10 show the pressure distribution at different lengths of the blade. As shown, the tip section of the blade has enough large pressure difference between the upper and lower surface. On other hands, the hub section has less pressure difference between its surfaces. Consequently, static pressure increases from root to tip. The degree of reaction control of the pressure distribution, which increases from root to tip according to free vortex assumption. However, the power production is constant a long of the blade. The energy production and degree of reaction is an agreement of the free vortex principle.

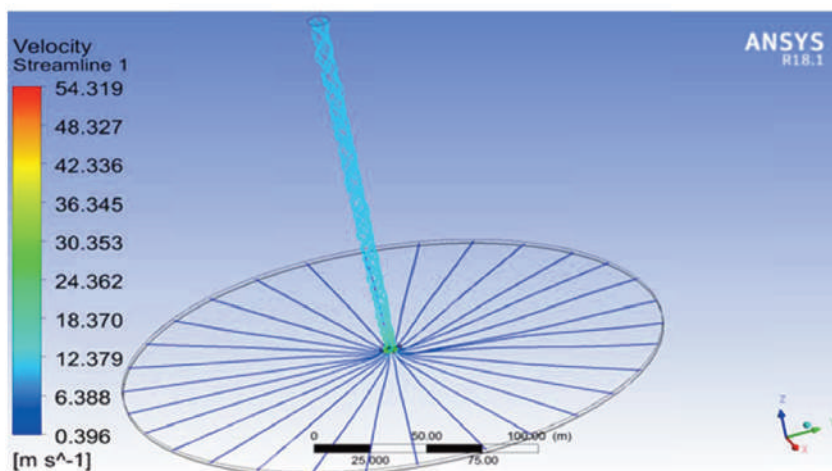


Figure 8. Streamline of air in SCPP model.

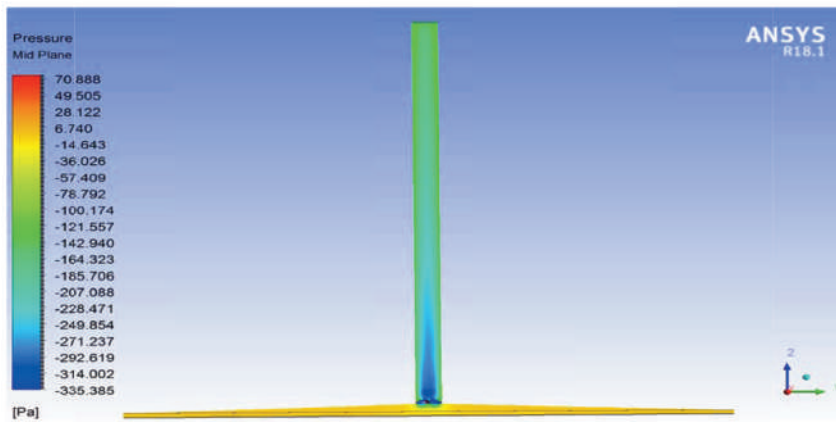


Figure 9. Contours of static pressure at different zones of the chimney.

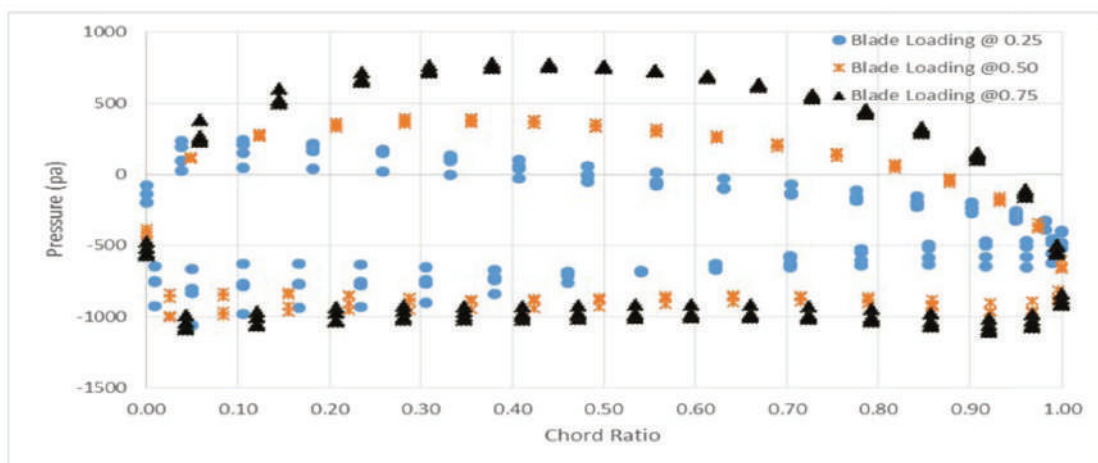


Figure 10. Pressure distribution at different length of the blade.

6. Conclusion

In this study, the main aims were: design and analysis of the axial flow turbine performance for solar chimney power plant. The advantage of free vortex design is used to calculate the geometric shape (chord distribution and twist angle) for the turbine blade. To simulate the turbine of the solar chimney, the standard $k-\epsilon$ turbulent and radiation model within ANSYS-CFX v18 is chosen, which predicts its performance. The comparison the CFD result and previous experimental data reveals a good agreement. The results have shown that free vortex theory and Matrix Throughflow Method have reasonable accuracy to obtain the good blade shape. The designed blade can be easily manufactured. However, the hub section needs more work in the fabrication phase. NACA 0006 airfoil is very close to thickness distribution calculation of MTFM. The characteristics of the NACA 0006 match the working condition of the SCPP. Thus, makes it is suitable to design the turbine for the SCPP.

The present study conclude the capability of CFD model, as a powerful research tool and engineering analysis method for analysis of complex thermal and aerodynamic system, such as the solar chimney power plant. The theoretical modeling approach can help to create an experimental study of a solar chimney plant to make it more effective and economical.

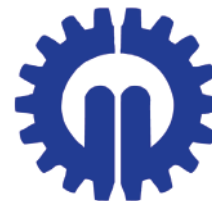
Acknowledgement:

"This work was supported by the Stipendium Hungaricum Programme and by the Mechanical Engineering Doctoral School, Szent István University, Gödöllő, Hungary."

References

- [1] Zhou X., Wang F., Ochieng R. M.: 2010. A Review of Solar Chimney Power Technology. *Renewable and Sustainable Energy Reviews*, Vol. 14, No. 8, pp. 2315-2338. <http://dx.doi.org/10.1016/j.rser.2010.04.018>

- [2] **Haaf W., Friedrich K., Mayr G., Schlaich J.:** 1983. Solar chimneys; Part I: Principle and construction of the pilot plant in Manzanares. *International Journal of Solar Energy*, Vol. 2, pp. 3–20. <http://dx.doi.org/10.1080/01425918308909911>
- [3] **Haaf W.:** 1984. Solar chimneys; Part II: Preliminary Test Results from the Manzanares Pilot Plant. *International Journal of Solar Energy*, Vol. 2, No. 2, pp. 141-161. <http://dx.doi.org/10.1080/01425918408909921>
- [4] **Mekhail T., Elmagid W. M., Fathy M., Bassily M., Harte R.:** 2016. Theoretical Investigation of Solar Chimney Power Plant Installed in Aswan City. In *International Symposium on Industrial Chimneys and Cooling Towers*, Rotterdam, Germany, October 5-8, 2016.
- [5] **Lu F., Zhang H., Yao X.:** 2006. Review of key technologies for solar chimney power generation, *East China Electric Power*, 2006.
- [6] **Mullett L. B.:** 1987. The Solar Chimney—overall efficiency, Design and performance. *International Journal of Ambient Energy*, Vol. 8, No. 1, pp. 35-40. <http://dx.doi.org/10.1080/01430750.1987.9675512>
- [7] **Yan M. Q., Sherif S. A., Kridli G. T., Lee S. S., Padki M. M.:** 1991. Thermo-fluid Analysis of Solar Chimneys. In *Industrial Applications of Fluid Mechanics*, Atlanta, GA, 1991.
- [8] **Huang H., Zhang H., Huang Y., Lu F.:** 2007. Simulation Calculation on Solar Chimney Power Plant System. In *International Conference on Power Engineering*, Hangzhou, China, 2007.
- [9] **Patel S. K., Prasad D., Ahmed R.:** 2014. Computational Studies on the Effect of Geometric Parameters on the Performance of a Solar Chimney Power Plant. *Energy Conversion and Management*, Vol. 77, pp. 424-431. <http://dx.doi.org/10.1016/j.enconman.2013.09.056>
- [10] **Vieira R. S., Garcia C., Junior I. C. A., Souza J. A., Rocha L. A. O., Isoldi L. A., dos Santos E. D.:** 2015. Numerical Study of The Influence of Geometric Parameters on The Available Power in a Solar Chimney. *Thermal Engineering*, Vol. 14, No. 1, pp. 103-109.
- [11] **Pasumarthi N., Sherif A. S.:** 1998. Experimental and Theoretical Performance of a Demonstration Solar Chimney Model-Part I: Mathematical Model Development. *International Journal of Energy Research*, Vol. 22, pp. 277-288. [http://dx.doi.org/10.1002/\(SICI\)1099114X\(19980310\)22:3<277::AID-ER380>3.0.CO;2R](http://dx.doi.org/10.1002/(SICI)1099114X(19980310)22:3<277::AID-ER380>3.0.CO;2R)
- [12] **Pasumarthi N., Sherif A. S.:** 1998. Experimental and Theoretical Performance of Demonstration Solar Chimney Model- part II: Experimental and Theoretical Results and Economic Analysis. *International Journal of Energy Research*, Vol. 22, pp. 443- 461. [http://dx.doi.org/10.1002/\(SICI\)1099114X\(199804\)22:5<443::AID-ER381>3.0.CO;2-V](http://dx.doi.org/10.1002/(SICI)1099114X(199804)22:5<443::AID-ER381>3.0.CO;2-V)
- [13] **Pretorius J., Kröger D.:** 2006. Solar chimney power plant performance. *Journal of Solar Energy Engineering*, Vol. 3, No. 128, p. 302–311. <http://dx.doi.org/10.1115/1.2210491>
- [14] **Bernardes M., Voss A., Weinrebe G.:** 2003. Thermal and technical analyses of solar chimneys. *Solar Energy*, Vol. 75, pp. 511–524. <http://dx.doi.org/10.1016/j.solener.2003.09.012>
- [15] **Gannon A., von Backström T.:** 2000. Solar chimney cycle analysis with system loss and solar collector performance. *Journal of Solar Energy Engineering*, vol. 122, p. 133–137. <http://dx.doi.org/10.1115/1.1314379>
- [16] **Dhahri A., Omri A.:** 2013. A Review of solar Chimney Power Generation Technology. *International Journal of Engineering and Advanced Technology (IJEAT)*, Vol. 2, No. 3, pp. 1-17.
- [17] **Gannon A. J., von Backström T.:** 2002. Solar Chimney Turbine Part 1 of 2: Design. In *2002 International Solar Energy Conference*, Reno, Nevada, USA, June 15-20, 2002.
- [18] **Denantes F., Bilgen E.:** 2006. Counter-Rotating Turbines for Solar Chimney. *Renewable Energy*, Vol. 31, pp. 1873–1891. <http://dx.doi.org/10.1016/j.renene.2005.09.018>
- [19] **Fluri T., von Backström T.:** 2008. Comparison of Modelling Approaches and Layouts for Solar Chimney Turbines. *Solar Energy*, Vol. 82, No. 3, pp. 239–246. <http://dx.doi.org/10.1016/j.solener.2007.07.006>
- [20] **Zhou Y., Gao B., Dong H. R., Hao K.:** 2016. Design for the Turbine of Solar Chimney Power Plant System with Vertical Collector. *IOP Conf. Series: Earth and Environmental Science*, Vol. 40, No 1. 012085. <http://dx.doi.org/10.1088/17551315/40/1/012085>
- [21] **Harms T., von Backström T., du Plessis J.:** 1996. Simplified Control Volume Finite-Element Method. *Numerical Heat Transfer*, Vol. B, No. 30, pp. 179-194. <http://dx.doi.org/10.1080/10407799608915078>
- [22] **Gannon A. J.:** 2002. Solar Chimney Turbine Performance. University of Stellenbosch (PhD Thesis), Matieland, South Africa, March 2002.
- [23] **Dixon B. S. L., Hall C. A.:** 2014. *Fluid Mechanics and Thermodynamics of turbomachinery (Seventh Edition)*, Oxford, UK: Elsevier Inc., pp. 556, 2014.
- [24] ANSYS CFX Introduction User Help.
- [25] **Celik I. B.:** 1999. *Introductory Turbulence Modeling,* Mechanical & Aerospace Engineering Dept. West Virginia University (Lectures Notes), Morgantown, Dec 1999.



PREDICTION OF MAIN ANALYTICAL AND PHYSICAL PARAMETERS OF HONEY WITH ELECTRONIC TONGUE

Author(s):

F. A. Koncz¹ – Zs. Bodor² – T. Kaszab¹ – I. Kertész¹ – J. L. Z. Zaukuu¹ – Cs. Benedek² – Z. Gillay¹ – Z. Kovacs¹

Affiliation:

¹Department of Physics and Control, Szent István University, Somlói út 14-16., Budapest, H-1118, Hungary

²Department of Dietetics and Nutrition, Faculty of Health Sciences, Semmelweis University, Vas u. 17., H-1088 Budapest, Hungary

Email address:

konczfanni54@gmail.com, kaszab.timea@etk.szie.hu, kertes.istvan@etk.szie.hu, zaukuu.john-lewis.zinia@hallgato.uni-szie.hu, benedek.csilla@se-etk.hu, gillay.zoltan@etk.szie.hu, kovacs.zoltan3@etk.szie.hu

Abstract

Honey is one of the most commonly adulterated product in the food market. The different types of adulterations affect the market negatively, therefore an effective honey evaluation method is required. The electronic tongue could be a new alternative tool for inspection. In this study 78 authentic Hungarian honey samples were analysed with electronic tongue. The main analytical and physical parameters of honey samples were also determined, with classical analytical methods. Multivariate regression models (PLSR, MLR, SVM) were built to predict the main physicochemical properties of honey based on the results of electronic tongue. Results showed that the merged data of electronic tongue and electrical conductivity provided the best models for the prediction of main physicochemical properties of honey.

Keywords

honey, taste perception, chemometric, antioxidant capacity, polyphenol content

1. Introduction

Honey is a multipurpose natural product with high nutritional value. It has a relatively high price, making it one of the most commonly adulterated products on the food market. Examples of honey adulteration include blending of honeys with sugar syrup, pollen filtration, heating. Food adulteration affects both customers and the beekeepers negatively. Current methods of honey inspection are

primarily based on rather expensive analysis instrumentation (e.g. NMR, LC-IRMS) and skilled operators [1]. Even these methods have their own limitations in terms of detection limit and detection of some types of adulterants. However, there is no efficient rapid technique available to determine the quality of honey, thus evaluation of new methods is strongly required and fully justified. Among the possible alternatives, different physical and analytical parameters, such as antioxidant capacity, polyphenols, ash content, electrical conductivity (EC), etc. have been largely investigated. [2]. Although these simple and fast methods are usually not satisfactory for the clear differentiation of different honeys and their blends, their combination with sensory analyses may offer promising pathways in authentication. The electronic tongue (ET) is a robust sensor based electronic device used to build fingerprints for food products based on their chemical patterns. It has several advantages such as, short analysis time and minimal sample preparation. There are various studies with promising results on honey investigation with ET, consequently it could be a new honey investigation tool. Major et al. (2011) [3] showed that ET combined with artificial neural networks (ANN) is a reliable tool for geographical discrimination of honey samples. In another study, voltametric and potentiometric ETs were compared to classify honey samples based on floral and geographical origin [4]. They utilized Principal Component Analysis (PCA) and Discriminant Analysis (DA) methods for this purpose and achieved 100% correct classification. According to Dias et al. (2015) [5], floral origin classification

using the ET yielded 92% and 100% correct classification for monofloral and polyfloral honeys, respectively. This was in combination with multiple linear regression (MLR), and the successful assessment of ratio of the main pollens in the samples ($R^2=0.92$) [5]. Thus, the ET proved to be more reliable than the Pollen analysis (melissopalynology), a common but very tedious method of honey origin determination. To clearly define honey quality however, there is a need to match these floral origin classifications with the main characteristics of the honey, especially in Hungary, where honeys have never been analyzed with the ET. From preliminary studies, ET measurements analyzed with different multivariate statistical methods (PCA and LDA) showed the applicability of ET for geographical and floral origin identification, giving the rise to use electronic tongue for determination of main analytical and physical parameters of honey samples. The objective of this work therefore, was to build models based on the results of ET for rapid prediction of main analytical and physical parameters of honey samples.

2. Materials and methods

Research design and sampling

Honey samples (78) were analyzed from different floral and geographical origins, focusing mainly on authentic Hungarian products. Most of the samples were collected directly from beekeepers and aseptically stored during the analysis, to ensure quality preservation. Commercial honeys, and samples collected from other countries were also analyzed, to compare them with Hungarian honeys. Standard methods were used to determine relevant parameters of the honey samples as described below.

Determination of the physico-chemical properties

Ash Content. Honey (3-7 g) was measured in a porcelain jar and two drops of olive oil were given to each jar. The samples were first pre-combusted on flame, then kept in an electric furnace at 600°C for four hours. After that the samples were put in a desiccator and the ash content was calculated [6].

Total polyphenol content and antioxidant capacities.

Honey (1 g) was measured into a beaker, dissolved in water, then integrally transferred to a 10 ml volumetric flask. The flask was made up to volume with distilled water. This stock solution was used for each antioxidant method.

Total Polyphenol Content (TPC).

The Total Polyphenol Content was determined by the Folin-Ciocalteu colorimetric method, which is based on the oxidation of phenolic compounds in honey. Briefly, 1ml of the honey stock solution was put in a test tube, then 7.5 ml distilled water was added, followed by 0.5 ml of the Folin–Ciocalteu reagent and - after 3 minutes - 1 ml Na_2CO_3 solution was also added. After 30 minutes of incubation at room temperature the solution was measured at 750 nm with a Helios α -spectrophotometer. Gallic acid was used as standard [7].

CUPRAC (Cupric Ion Reducing Antioxidant Capacity) assay.

The procedure based on reduction of Cu^{2+} ions was developed by Apak et al. (2007) [8]. For the measurements, 200 μl honey stock solution was mixed with 1 ml of CuCl_2 , 1 ml of NH_4 -acetate puffer solution ($\text{pH}=7.4$), and 0.9 ml distilled water. After 30 minutes of incubation, the samples were measured at 450 nm spectrophotometrically.

ABTS assay

The method is based on the spectrophotometrical monitoring at 734 nm of the scavenging of the $\text{ABTS}\cdot^+$ (2,2'-azino-bis (3-ethylbenzothiazoline-6-sulfonic acid) radical cation by the antioxidant compounds of the sample. 0.1 ml of the sample solution was put in a test tube and 3.9 ml ABTS reagent was given. Then it was incubated for 12 minutes in dark before the measurement. Trolox was used as standard [9].

Ferric Reducing Antioxidant Power (FRAP).

Honey stock solutions (500 μl) were mixed with previously prepared 7.5 ml FRAP reagent solution, according to literature. After an hour incubation at 37°C the solution was measured photometrically at 593 nm, using ascorbic acid as standard [10].

Measurement with electronic tongue

An α Stree electronic tongue (ET) (AlphaM.O.S., 2003) was used to determine the taste pattern of the honey samples after calibration and conditioning (according to the manufacturers direction). The instrument is able to recognize and analyze the compounds in liquid samples and includes an Ag/AgCl reference electrode, with seven potentiometric sensors developed for food analysis. For ET measurements 10 grams of honey sample was measured and diluted in a

100 ml volumetric flask with distilled water. The tests were done at room temperature.

Statistical analysis

Multivariate statistical methods were applied to evaluate the result of the ET measurements. Principle component analysis (PCA) [11] was used to describe multidimensional patterns of the ET dataset and to discover outliers. Quantitative models were built using partial least squares regression (PLSR) [12], multiple linear regression (MLR) [13] and support vector machine regression (SVM) [14] for the prediction of the physicochemical properties using the data of electronic tongue, pH and EC. The quantitative models were validated using one sample-out cross-validation and the models were evaluated by comparing the determination coefficients (R^2) and root mean square errors (RMSE) of calibration and cross-validation. The statistical analysis was performed with Matlab (v. Matlab 2016a 64-bit). Graphs made for the comparison of the different models were prepared using Microsoft Excel (Microsoft Corporation, USA).

3. Results and discussion

Results of the regression models built based on the results of electronic tongue

Results of the regression models built for the prediction of the tested physicochemical properties of the honey samples using the data of ET is summarized in Figure 1. Models calculated with the SVM method showed the worst results (Figure 1. a.). In spite of using SVM there was no model achieved for the prediction of ash content, PLSR and MLR however, showed the best accuracy for ash content determination followed by FRAP and ABTS (Figure 1. b, and c.). All the three methods showed the lowest R^2 for TPC and CUPRAC. Common problems such as drifts, non-idealities or interferences are often present in measurements with sensor based instruments such as electronic tongue especially in case of long term experiments [15]. In this study, mathematical drift correction was applied which resulted in slight improvements of the prediction models. Further improvement of the models were observed when fused data of EC, pH and ET were used.

Results of the regression models built based on the fused data of electronic tongue electrical conductivity and pH

Generally, models built based on the fused data of ET and EC resulted in significantly more accurate models (Figure 2) compared to those built based on the ET

results alone (Figure 1). The organic acids and mineral salts in honey are ionizable in solution with a property to conduct electric [16], affecting the electrical properties of the samples. The addition of the results of pH did not provide significantly better models probably because ET often shows high correlation with pH. Most noticeable improvement was found for the prediction of the ash content. This may be due to the linear relationship between ash and EC. Better accuracy was observed for all the tested physicochemical properties of the honey with all the three antioxidant methods, except for ABTS (Figure 2). There was no reliable model for the ash content with SVM. Irrespective of the high determination coefficient observed during the model building, the testing of the model failed using the one-sample-out cross-validation (Figure 2. a.).

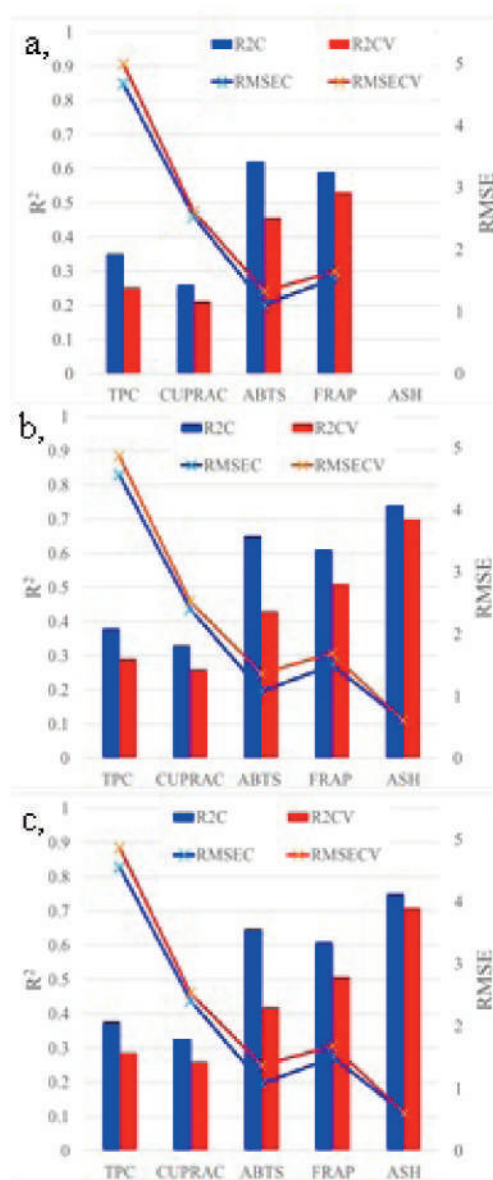


Figure 1. Performance summaries of a, SVM, b, PLSR, c, MLR calibration models and leave-one-

sample-out cross-validation fitted on the different physicochemical parameters of the honey samples using the data of electronic tongue (calibration: blue and cross-validation: red). R2=determination coefficient; RMSE=root mean square error; C=calibration; CV=one-sample-out cross-validation. RMSE values of CUPRAC and FRAP are divided by 10, ABTS is divided by 100, ASH is multiplied by 10 for better visualization.

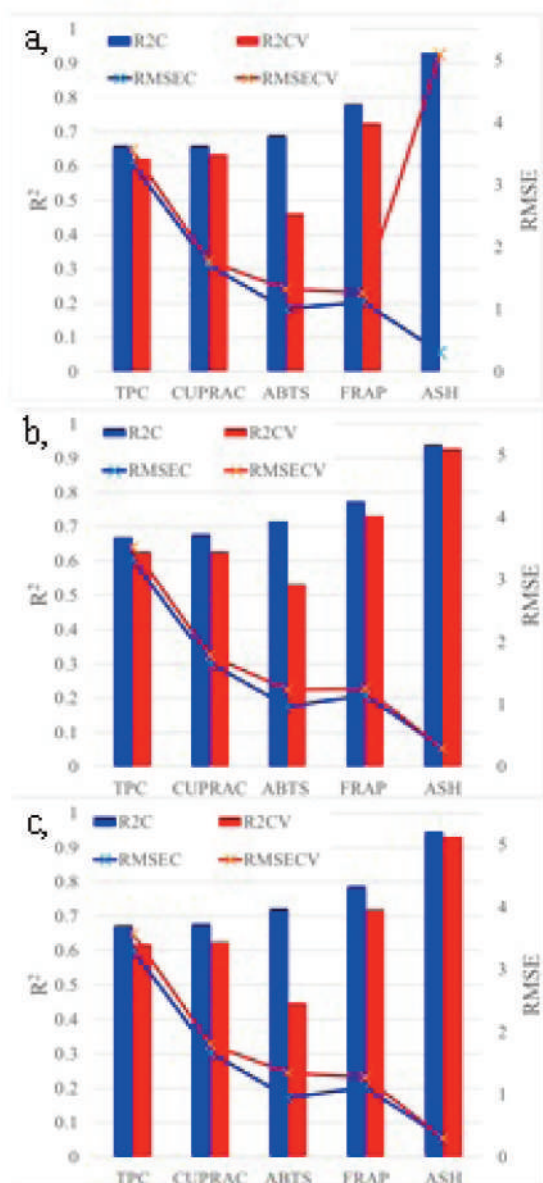


Figure 2. Performance summaries of a, SVM, b PLSR, c, MLR calibration models and leave-one-sample-out cross-validation fitted on the different physicochemical parameters of the honey samples using the fused data of electronic tongue (after drift correction) and EC (calibration: blue and cross-validation: red). R2=determination coefficient; RMSE=root mean square error; C=calibration; CV=one-sample-out cross-validation. RMSE values

of CUPRAC and FRAP are divided by 10, ABTS is divided by 100, ASH is multiplied by 10 for better visualization.

Although more accurate models could be built for the prediction of the tested parameters using the combined data of electronic tongue after drift correction and data of EC, the prediction of some parameters still did not achieve satisfactory accuracy. Furthermore, results of the regression models showed a different trend of the fitting of the predicted data points in the higher range compared to the lower one. Therefore, separate models were built for honey samples with high ash content (Table 1) and those having low ash content (Table 2).

Performance summary of the best models found for the prediction of the tested physico-chemical parameters of the honey samples with higher ash content is provided in Table 1. Better accuracy was reached when only the data of honey samples with higher ash content was used for modelling, compared to results found for all the samples (Figure 2).

Table 1. Performance summaries calibration models and leave-one-sample-out cross-validation of the best models fitted on the different physicochemical parameters of the honey samples containing high ash content (0.321%-0.918%) using the fused data of electronic tongue (after drift correction) and EC. R2=determination coefficient; RMSE=root mean square error; C=calibration; CV=one-sample-out cross-validation.

	TPC	CUPRAC	ABTS	FRAP	Ash content
Method	PLSR	PLSR	SVM	SVM	MLR
R2c	0.73	0.70	0.81	0.86	0.96
R2cv	0.68	0.64	0.73	0.82	0.94
RMSEC	3.53	17.86	113.18	10.39	0.03
RMSECV	3.82	19.51	135.95	11.82	0.03

Results of the models built based on the data of honey samples with lower ash content is summarized in Table 2 showing weaker results than those in Table 1, especially for ABTS. These results suggest that when honey samples with lower ash content is analyzed with ET we may reach the sensitivity level of the sensors involved in the experiment for the diluted honey samples

Table 2. Performance summaries calibration and CV models of the best models fitted on the different physicochemical parameters of the honey samples

containing low ash content (0.036-0.169%) using the fused data of electronic tongue (after drift correction) and EC. R²=determination coefficient; RMSE=root mean square error; C=calibration; CV=one-sample-out cross-validation

	TPC	CUPRAC	ABTS	FRAP	Ash content
Method	PLSR	PLSR	SVM	SVM	MLR
R ² c	0.63	0.70	0.46	0.64	0.90
R ² cv	0.56	0.66	0.27	0.56	0.86
RMSEC	2.81	15.29	91.04	11.5	0.02
RMSECV	3.1	16.17	105.84	12.69	0.02

The application of drift correction together with the data of EC resulted in significantly better accuracy models as showed above, therefore, the ability of ET has been tested in an ideal situation, i.e. data of one measurement day was used to build models. Figure 3 shows some selected results when data of one-day experiment is used for modelling. The results showed that, if there is no long-term experiment (i.e. reduced drift), fairly good results can be achieved. Full sized figures show the results of the models built using the fused data of ET and EC while the miniaturized figures show the results of the models built using only data of ET. In this case models built based on only the results of ET provided similar accuracy as the ones built based on the combined data of ET and EC.

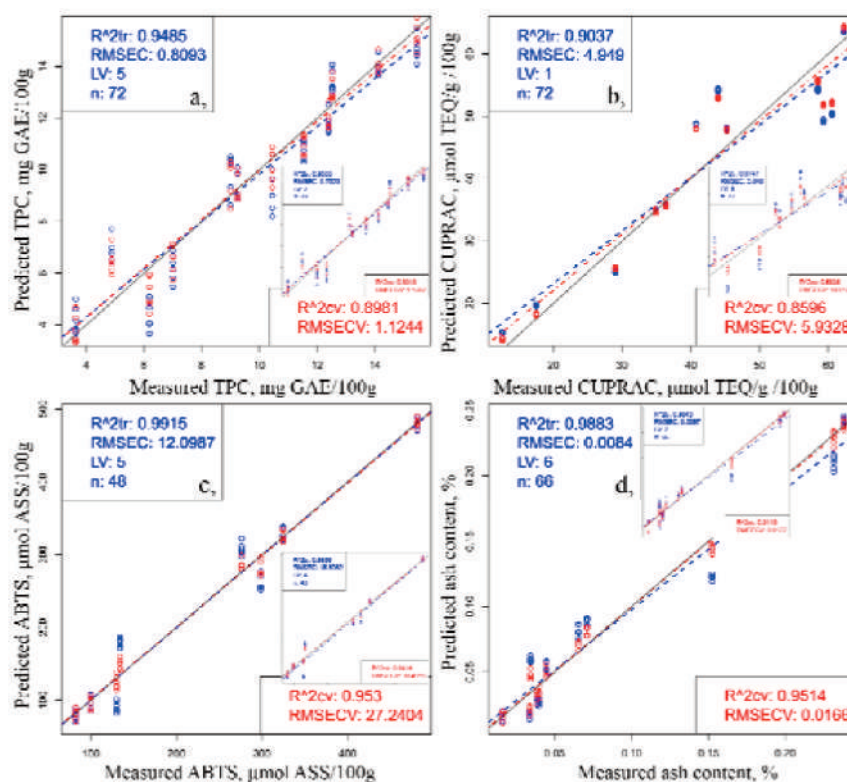


Figure 3. Selected PLSR models (based on data of only one-day measurement) on a, total polyphenol content b, Cupric Reducing Antioxidant Capacity c, ABTS d, ash content of the honey samples. Full sized figure shows the results of fused data of electronic tongue and EC. Miniaturized figure shows results of electronic tongue. Calibration (blue line and points), one-sample-out cross-validation (red line and points).

4. Conclusion

The objective of this work was to build models based on the results of electronic tongue for rapid prediction of main analytical and physical parameters of honey samples. The physicochemical properties of honey samples were determined with classical analytical methods.

Regression models were built to predict the tested analytical properties (total polyphenol content,

antioxidant capacity measured by different assays, ash content) of the honey samples, using the data of electronic tongue and SVM, PLSR, and MLR methods and leave-one-sample-out cross-validation. The models built based on the raw measurement results of electronic tongue showed weak prediction performance especially for ash content. Drift correction of the electronic tongue measurement results provided some increase in the accuracy of the models. However, significant improvement of the

prediction models were achieved when fusion of the data of electrical conductivity and electronic tongue was applied, especially for ash content determination. The most reliable solution was found by dividing the samples into two subgroups based on their high or low ash content, when models were more accurate for higher ash levels. Our results showed that application of electronic tongue as a fast, convenient method, with practically no environmental burden, might be a promising tool for predicting main analytical parameters of honey like total polyphenol content, antioxidant capacity and ash content. However, the improvement of long term stability of the electronic tongue results is indispensable for the field applications of this technique.

Acknowledgements

This paper was supported by the János Bolyai Research Scholarship of the Hungarian Academy of Sciences (Zoltan Kovacs). This paper was supported by the ÚNKP-17-2 (Fanni Adrienn Koncz and Zsanett Bodor) and ÚNKP-17-4 (Zoltan Kovacs) New National Excellence Program of the Ministry of Human Capacities.



EMBERI ERŐFORRÁSOK
MINISZTERIUMA

References

[1] Spiteri M., Jamin E., Thomas F., Rebours A., Lees M., Rogers K. M., Rutledge D. N.: 2015. Fast and global authenticity screening of honey using ¹H-NMR profiling. *Food Chemistry*, Vol. 189, pp. 60–66. <http://dx.doi.org/10.1016/j.foodchem.2014.11.099>

[2] Karabagias I. K., Badeka A. V., Kontakos S., Karabournioti S., Kontominas M. G.: 2014. Botanical discrimination of Greek unifloral honeys with physico-chemical and chemometric analyses. *Food Chemistry*, Vol. 165, pp. 181–190. <http://dx.doi.org/10.1016/j.foodchem.2014.05.033>

[3] Major N., Markovic K., Krpan M., Saric G., Hruskar M., Vahcic N.: 2011. Rapid honey characterization and botanical classification by an electronic tongue. *Talanta*, Vol. 85, No. 1, pp. 569–574. <http://dx.doi.org/10.1016/j.talanta.2011.04.025>

[4] Zhenbo J. W., Jun W. 2014. Tracing floral and geographical origins of honeys by potentiometric and voltammetric electronic tongue. *Computers and Electronics in Agriculture*, Vol. 108, No. C, pp. 112–122. <http://dx.doi.org/10.1016/j.compag.2014.07.014>

[5] Dias L. G., Veloso A. C. A., Sousa M.E.B.C., Estevinho L., Machado A.A.S.C., Peres A. M.: 2015. A novel approach for honey pollen profile assessment using an. *Analytica Chimica Acta*, Vol. 900, pp. 36–45. <http://dx.doi.org/10.1016/j.aca.2015.10.014>

[6] Bogdanov S., Martin P., Lullmann C.: 2002. Harmonised methods of the international honey commission. Swiss Bee Research Centre, FAM, Liebefeld.

[7] Singleton V. L., Rossi J. A.: 1965. Colorimetry of total phenolics with phosphomolybdic-phosphotungstic acid reagents. *American Journal of Enology and Viticulture*, Vol. 16, pp. 144–158.

[8] Apak R., Güçlü K., Demirata B., Ozyürek M., Celik S. E., Bektaşoğlu B., Ozyurt D.: 2007. Comparative evaluation of various total antioxidant capacity assays applied to phenolic compounds with the CUPRAC assay. *Molecules*, Vol. 12, No. 7, pp. 1496–1547.

[9] Re R., Pellegrini N., Proteggente A., Pannala A., Yang M., Rice-Evans C.: 1999. Antioxidant activity applying an improved ABTS radical cation decolourization assay. *Free Radical Biology and Medicine*, Vol. 26, No. 9–10, pp. 1231–1237.

[http://dx.doi.org/10.1016/S0891-5849\(98\)00315-3](http://dx.doi.org/10.1016/S0891-5849(98)00315-3)

[10] Benzie, I. F., Strain, J. J.: 1996. The ferric reducing ability of plasma (FRAP) as a measure of "antioxidant power": the FRAP assay. *Anal Biochem*, Vol. 239, No. 1, pp. 70–76.

<http://dx.doi.org/10.1006/abio.1996.0292>

[11] Cowe I. A., McNicol J. W.: 1985. The use of principal components in the analysis of near-infrared spectra. *Applied Spectroscopy*, Vol. 39, No. 2, pp. 257–266.

[12] Naes T., Isaksson T., Fearn T., Davies T.: 2002. A user friendly guide to multivariate calibration and classification. Chichester, UK: NIR Publications Official methods of analysis Proximate Analysis and Calculations Ash Determination (Ash) - item 51. Association of Analytical Communities, Gaithersburg, MD, 17th edition, 2006. Reference data: Method 942.05; MIN; ASH

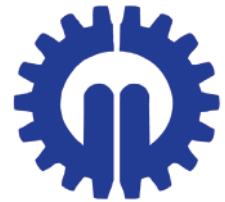
[13] Chatterjee S., A. S. Hadi.: 1986. Influential Observations, High Leverage Points, and Outliers in Linear Regression. *Statistical Science*, Vol. 1, No. 3, pp. 379–393.

[14] Vapnik V.: 1995. *The Nature of Statistical Learning Theory*. Springer, New York, pp. 314.

[15] De Marco R., Mackey D.J., Zirino A.: 1997. Response of the jalpaite membrane copper(II) ion-selective electrode in marine waters. *Electroanalysis*, Vol. 9, No. 4, pp. 330–334.

<http://dx.doi.org/10.1002/elan.1140090414>

[16] Kropf U., Jamnik M., Bertoneclj J., Golob T.: 2007. Linear Regression Model of the Ash Mass Fraction and Electrical Conductivity for Slovenian Honey. *Food Technology and Biotechnology*, Vol. 46, No. 3, 335–340.



A NEW SHAKER HEAD DESIGN FOR REDUCING BARK INJURIES ON FRUIT TREES

Author(s):

Z. Láng

Affiliation:

Technical Department, Szent István University, H-1118 Budapest, Villányi street 31

Email address:

lang.zoltan@kertk.szie.hu

Abstract

To reduce bark damaging moments on the fruit tree trunk, a new shaker head arrangement is proposed. By applying two identical complete shaker units symmetrically on both sides of the trunk, the resulting shaking force will be normal to it and uniform in any direction. To prove the assumption, a theoretical model was set up and a laboratory model was built and tested. The theoretical model made the calculation of pure centrifugal forces of the eccentric shaker masses possible. Besides the new shaker head arrangement, the laboratory model enabled the study of the performance of present shaker heads. Test results lived up to the expectations: In case of the new shaker arrangement, the acceleration pattern was nearly uniform in all directions, both in the free and “tree” shake mode. In case of the usual shaker arrangements, asymmetric acceleration distributions were measured, which, besides injuring the bark, may result in lower fruit detachment rate.

Keywords

fruit harvest; inertial shaker; shaker head; bark injury

1. Introduction

In the mechanical stone fruit harvesting practice, both uni- and multidirectional inertial shaker machines are used. The unidirectional shakers cause theoretically only normal force to the trunk. In the praxis however there are other effects, which may damage the bark. Maximum displacements were found by Affeld et al. [1] to be 2,5 times greater during start-up and shut-down, than at steady-state. Relative displacements between the shaker and the trunk were also excessive and can exceed tolerable bark strength limits.

According earlier experiments the effect of shaking direction influences the detachment rate [2]. By shaking the trees in multiple directions, nearly uniform acceleration acts on fruits in all directions. This results in higher detachment rate, compared to the uni-directional shaking. The phenomenon was also modelled and proved by FEM [3] [4].

Multidirectional shakers produce forces not only in normal, but in tangential directions. The tangential forces tend to separate the bark from the cambium layer, which can cause long-lasting damage to the tree. In practice in order to reduce bark injuries, lubrication is applied between the sling surfaces of the shaker head [5] [6].

In all cases, the shaker head is clamped to the trunk and is free to move, relative to the frame of the carrier machine. The present multidirectional shakers use a pair of counter-rotating eccentric masses to generate centrifugal forces changing in value and direction. The freedom of moving relative to the carrier is assured by the suspension of shaker head via 3 rubber isolators or chains (Figure 1).

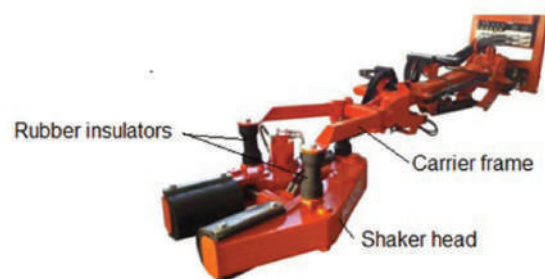


Figure 1. Tractor-mounted tree shaker by the company Agricola Noli, S.A.

One possible arrangement of eccentric rotating masses in the shaker head is stacking, where those are

rotating around the same axle. The dynamics of such shakers was studied by Snell and Birrell [7]. According to their findings beside normal forces, tri-axial torsion moments are raised on the tree trunk, which may damage the bark (Figure 2).

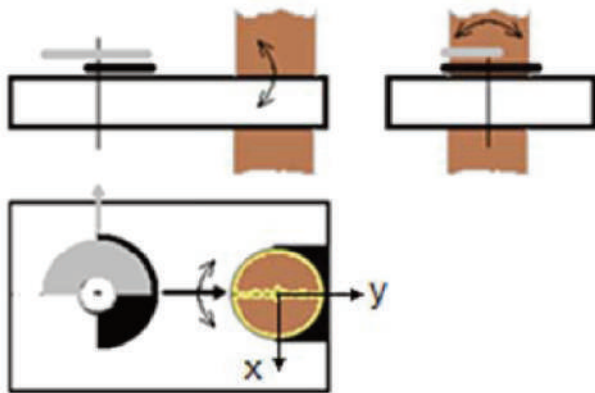


Figure 2. Typical stacked eccentric mass counter rotating system as it awakes tri-axial torsion moments on the trunk

In practice two other arrangements are also used as Figure 3 shows. To the left the eccentric masses are symmetrically placed on both sides, to the right on one side of the trunk. In both cases the energy-wheels rotate in the same plain, their centres of rotation and the centre line of the shaker head clamps are in line. Thanks to these designs two of those harming moments are excluded. The only remaining one is still harmful as it tends to turn off the bark of the trunk in the plane of the wheels (Figure 3).

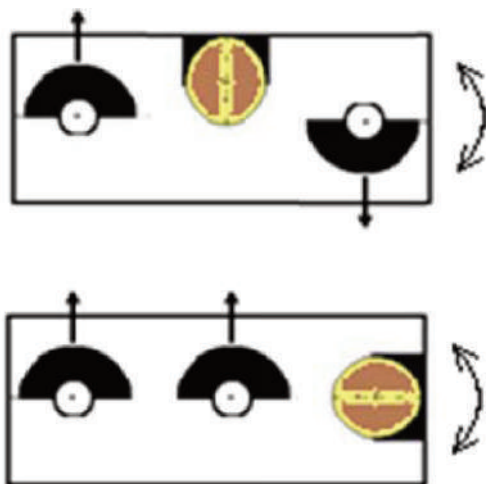


Figure 3. Shaker head with two rotating eccentric masses placed on both sides of the trunk and on one side in line with the tree trunk

Theoretically, by choosing different angular velocities and eccentric masses for the rotating

eccentric masses, a large scale of shaking forces or acceleration patterns can be achieved [8]. Horváth [9] studied and compared the shaking patterns in x-y plane of two uni- and one multidirectional shaker. As expected, the acceleration pattern of the unidirectional shakers was a narrow stripe, while the multidirectional shaker, working according to Figure 3 on the left, has shown a multidirectional pattern in tree shaking. Abdel-Fattah et al. [10] evaluated the shaking patterns of 21 commercial multidirectional shaker machines in x,y and z directions. They found that the displacement in the x and y direction differed significantly in all cases: on average 9.3 versus 4.4 mm respectively. The direction x is explained in Figure 2.

To avoid the third moment (Figure 3) the shaking force should act normally to the trunk axis in any shaking directions. Presuming vertical trunk position and symmetrical limb distribution, the shaking pattern would be symmetric and would not harm the bark of the tree in this case. Fodor [11] studied many technical solutions, which could fulfil these requirements. His final design enabled a pulsating force to rotate along curved rails around the centre of the trunk during shaking. Force pulsation was generated by two counter rotating eccentric masses. Unfortunately the construction would be complicated compared to the present shaking heads. There is no report of its realisation and field testing.

2. Materials and Methods

In this paper a new construction model is presented, which is able to fulfil the requirements of non-damaging shaking by a simple method. The principle of the idea is explained in Figure 3. If two identical and parallel forces $F/2$ are acting on a symmetrical body as shown in Figure 4, their effect is summed up in the midpoint, independent of the direction of forces, without causing any moment around it. Let's now place the tree trunk in the midpoint.

Following from the above, two identical and synchronised shaking unit can generate a force pulsating and changing directions on the tree trunk without generating harmful moments.

In order to prove the idea, a small laboratory model was designed and constructed. The arrangement of the model is shown in Figure 5. The shaking unit included a pair of two synchronised counter-rotating eccentric masses, the catching part and the drive.

The eccentric masses were of different size and had the form of half rings. This way they were able to rotate in the same plane without resulting in undesired moments. The rings were driven by chains from an external point by an electric drilling machine through

a flexible axe. This arrangement made possible the clamping of trunks with different diameters. As Figure 4 shows, the internal and external rings were rotating in opposite directions and at different speeds. The shaking unit was suspended from an external frame by tree cables (see in Figure 4 to the right). These made possible for the shaker to move independently from the frame. The tree trunk was

replaced by a polyethylene tube of 25 mm external diameter in “tree” shaking mode. When applied, the lower part of the plastic tube was strongly fixed to bottom of the external frame, the upper part to the shaking head. That’s why the acceleration of the tube at its fixing point to the shaker was regarded to the same as of the shaker itself.

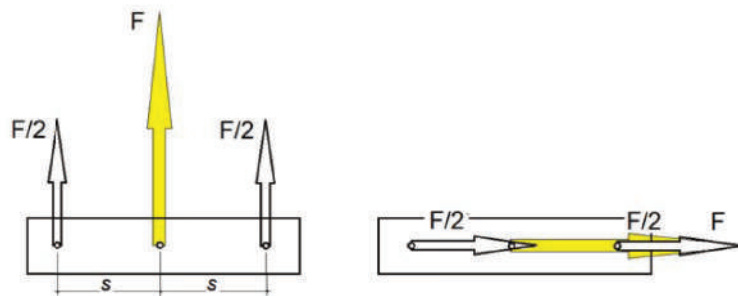


Figure 4. Two parallel and identical shaking forces don't result turning moment

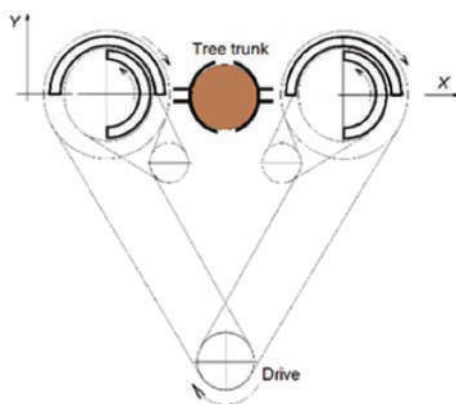


Figure 5. The design of the model and its realization (on the photo one of the diving chains is removed)

Figure 6 shows the dynamic model for both sides of the shaker head. The equations (1-4) of centrifugal forces for each side (according to Figure 5) are:

$$F_x = F_1 \cdot \cos \varphi_1 + F_2 \cdot \cos \varphi_2 \quad (1)$$

$$F_y = F_1 \cdot \sin \varphi_1 + F_2 \cdot \sin \varphi_2 \quad (2)$$

where

$$F_1 = m_1 \cdot s_1 \cdot \omega_1^2 \quad (3)$$

$$F_2 = m_2 \cdot s_2 \cdot \omega_2^2 \quad (4)$$

The values s_1 and s_2 are the distances between the centre of rotation and the centre of gravity of the half rings, m_1 and m_2 are the masses of rotating rings, ω_1 and ω_2 are their angular velocities.

The equations (5-6) for those distances are

$$S_1 = \frac{2 (R_e^3 - R_i^3) \sin \alpha_1}{3 (R_e^2 - R_i^2) \alpha_1} \quad (5)$$

and

$$S_2 = \frac{2 (r_e^3 - r_i^3) \sin \alpha_2}{3 (r_e^2 - r_i^2) \alpha_2} \quad (6)$$

where the indexes i and e mean internal and external, α_1 and α_2 are the half central angles of the rings (see Figure 6 in right) In this case $\alpha_1 = \alpha_2 = 90^\circ$

Ortiz-Canavate [8] declared that the shaking pattern of a double-eccentric-mass shaker depends on the ratios $m_1 \cdot s_1 / m_2 \cdot s_2$ and ω_1 / ω_2 .

On the model design the aim was to achieve a star shape shaking pattern. With the appropriate choice of

eccentric masses and geometrical sizes, the ratio for $m_1 \cdot s_1 / m_2 \cdot s_2$ resulted in 0.46, for $\omega_1 / \omega_2 = 1.22$ ($R_e =$

3.7 cm, $R_i = 3.2$ cm, $r_e = 2.8$ cm, $r_i = 2.1$ cm, $s_1 = 1.6$ cm, $s_2 = 2.2$ cm, $m_1 = 0.07$ kg, $m_2 = 0.108$ kg.)

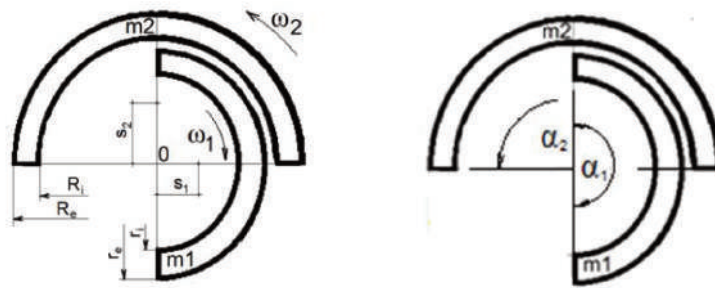


Figure 6. Geometry of the rotating rings

The shaking pattern for the system with $\omega_1=90$ 1/s, $\omega_2=73,8$ 1/s, $s_1 = 1.6$ cm, $s_2 = 2.2$ cm, and doubled m_1 and m_2 (due to the two shaker units) is shown in Figure 7. This pattern however is valid for a system composed of a pair of rotating masses. It doesn't include either the frame of the shaker and its drive or the effect of shaken tree.

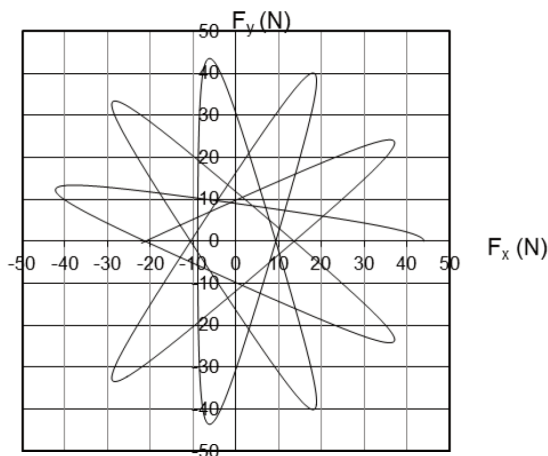


Figure 7. Calculated shaking force pattern with the data of two shaking units

To study the new and the conventional shaker head's behaviour laboratory tests were carried out in the following arrangements:

- 2.1 Both shaking units are driven, free shaking
- 2.2 Both shaking units are driven, "tree" shaking (left in Figure 5).
- 2.3 One shaking unit is driven only, free shaking
- 2.4 One shaking unit is driven only, "tree" shaking (right in Figure 5).
- 2.5 The rings are coupled on both side ($m_1 + m_2 = 0,178$ kg) and driven $\omega_1 / \omega_2 = -1.22$, free shaking
- 2.6 The rings are coupled on both side ($m_1 + m_2 = 0,178$ kg) and driven $\omega_1 / \omega_2 = -1.22$, "tree" shaking
- 2.7 The rings are coupled on both side ($m_1 + m_2 = 0,178$ kg) and driven $\omega_1 / \omega_2 = -1$, "tree" shaking

Accelerations in x-y-z direction were measured and registered by an accelerometer built in a mobile phone with the following specifications: Name: BMA254, vendor: Bosch Sensortec, version 1. Resolution: 0.019153614. Max. range: 39.2266. Power: 0.13 mW.

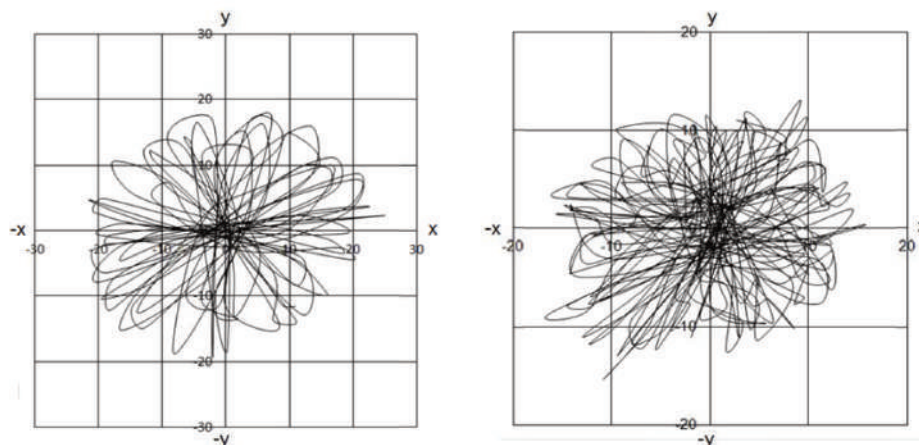


Figure 8. Accelerations measured in free (to the left) and in "tree" shaking arrangement of the model

The mobile phone was fixed to the shaking frame as Figure 8 shows. Fixing was made by placing the phone in an aluminium plate with flanges and framed by a thin robber stripe. It was presumed, that this way the natural frequency of the plate-phone system resulted in higher natural frequency than the applied shaking frequency. This latter was kept in the range of 14-18 Hz during all tests.

- 2.1 Both shaking units are driven, free shaking
- 2.2 Both shaking units are driven, "tree" shaking

To the left in Figure 8 the acceleration diagram of the proposed new shaker head arrangement is

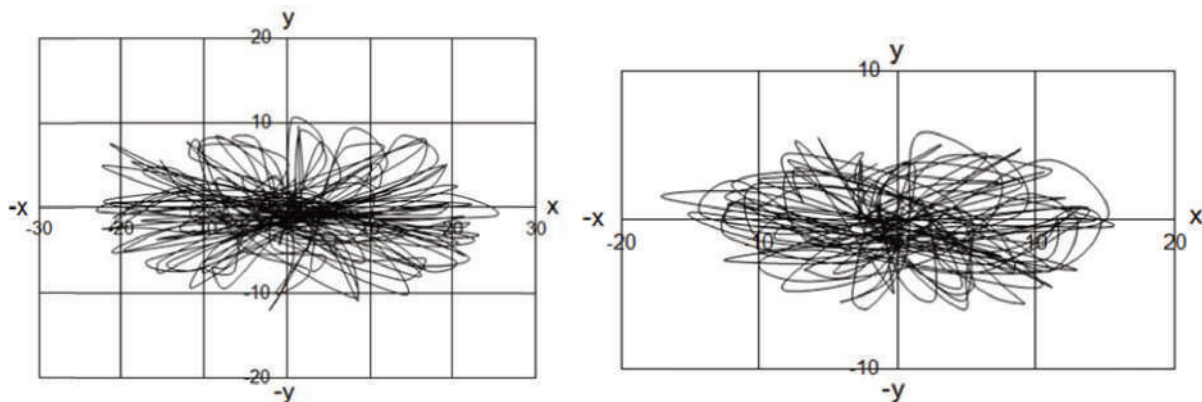


Figure 9. Acceleration pattern when shaking with one counter rotating system. To the left: free shaking, to the right: "tree" shaking

- 2.5 The rings are coupled on both side ($m_1 + m_2 = 0,178 \text{ kg}$) and driven $\omega_1 / \omega_2 = -1.22$, free shaking
- 2.6 The rings are coupled on both side ($m_1 + m_2 = 0,178 \text{ kg}$) and driven $\omega_1 / \omega_2 = -1.22$, "tree" shaking

This arrangement imitates the shaker in Figure 3 to the left. The eccentric rings on both side of the model

were coupled so that the internal and external ones overlapped each other. This way the rotating eccentric masses in both side resulted in 0,178 kg. Their speed ratio was $\omega_1 / \omega_2 = -1.22$. Tests were carried out in free and "tree" shaking mode. The acceleration patterns were similar to that what Horváth [9] has experienced (Figure 10).

presented at free shaking (without the plastic tube). To the right in Figure 8 the same shaker was connected to the plastic tube („tree" shaking).
 2.3 One shaking unit is driven only, free shaking
 2.4 One shaking unit is driven only, "tree" shaking

Figure 9 shows the acceleration patterns when one of the driving chains was removed. The photo in Figure 5 shows this setup: it complies with the stacked eccentric mass counter rotating system without its first two undesired moments (Figure 2). To the left, the pattern for free shaking is presented, to the right, "tree" shaking.

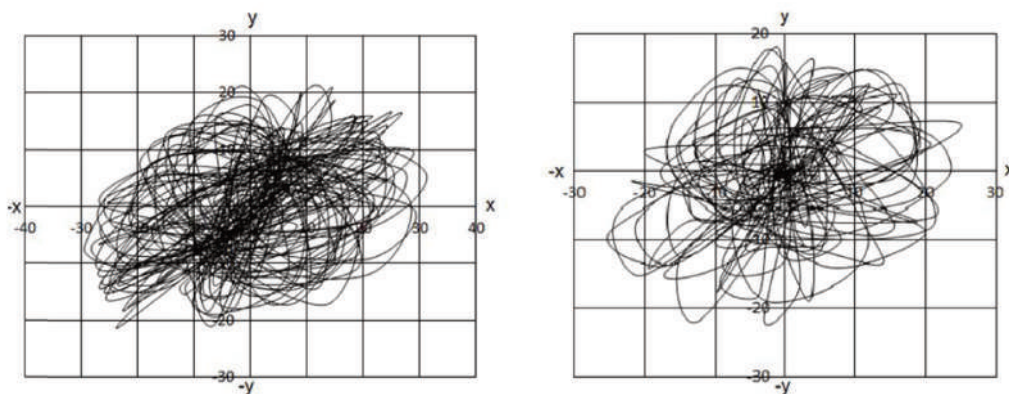
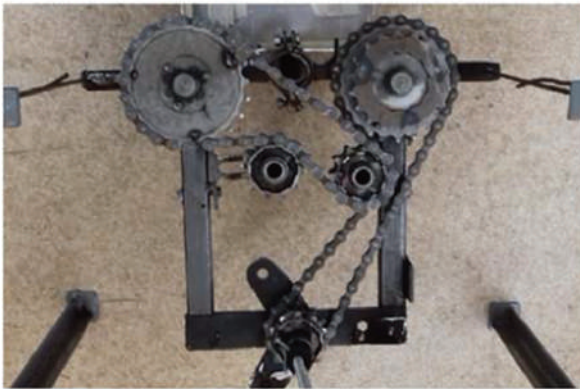


Figure 10. Acceleration pattern, when shaking with two counter rotating and uniform size eccentric masses. To the left: free shaking, to the right: "tree" shaking

2.7 Single eccentric mass is driven on both sides with $m_1 = m_2$, “tree” shaking

The setup on Figure 11 imitates the one-directional shakers with a pair of counter-rotating uniform size



masses [7] [9]. In the model the rings on both side are coupled, so $m_1 = m_2 = 0.178$ kg, the speed ratio: $= -1$.

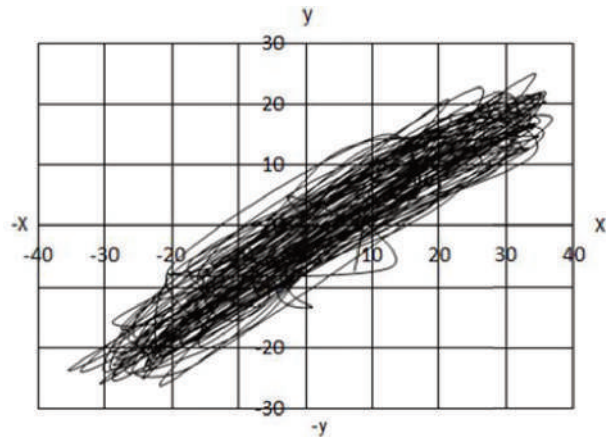


Figure 11. The setup when one eccentric mass is driven on each side with $m_1 = m_2$

Acceleration patten for one-directional shakers should be theoretically one single line both in free and “tree” shaking. Figure 11 shows instead a stripe of lines. This may be the consequence of inaccuracy in the mechanical system. The tilt angle of the stripe is the angle of the two rotating eccentric masses when in uniform position.

3. Results and Discussion

As expected, in the proposed arrangement the two identical and synchronised units worked in harmony: the resulting shaking pattern was nearly symmetric in both the free and “tree” shaking mode. The slight asymmetry can be explained by the asymmetric mass-distribution of the shaker head: as mentioned earlier, the new shaker arrangement works perfectly only when the shaking unit is symmetrical both in x, y and z direction (Figure 4).

Figures 10 and 11 coincide well with the test results of Horváth [9] as well as of Abdel-Fattah [10]. Concerning the direction of asymmetry in shaking patterns, in contrast to the shape in Figure 9, Abdel-Fattah et al. [10] measured larger accelerations in direction y than in x. This may be in conjunction with the different suspension geometries and centre of gravity positions of the model and real shaker machines.

Comparing the model results of the shakers in Figure 2 and left in Figure 3, the latter produced more equalised acceleration pattern (see Figures 9 and 10). However its torsion moment around the axis z is still harmful for the bark.

The advantage of the new shaker head arrangement is proven by the comparison of Figures 8, 9 and 10 both in free and “tree” shaking. The new concept enables the symmetric shaking of trees in any directions.

The model was also able to present the typical shaking pattern of one-directional shakers. The test results can be applied to the estimation of inertial masses in the model. The maximal calculated centrifugal force is $F_c = 44$ N (in Figure 7), which is generated by the two sets of shaker units. In case of the model, the maximal acceleration a_{max} at free shaking was measured to be approximately 20 ms^{-2} (Figure 8). According to Newton’s law (Equation 7) the inertia force:

$$F_i = m_t \cdot a_{max} \quad (7)$$

whereas m_t is the total mass of the shaker unit, a_{max} is its maximal acceleration. The inertia force is generated by the centrifugal force, hence Following from this, in free shaking the total mass, including the frame (Equation 8), drive and the eccentric masses is

$$m_t = F_c / a_{max} = 2,2 \text{ kg.} \quad (8)$$

The weighing of the shaking unit has led to similar result: $m_{t\text{measured}} = 2,13$ kg, which is near to the calculated value. By accomplishing the same calculation for the “tree” shaking mode, where $a_{max} = 13 \text{ ms}^{-2}$, the total mass, including now the “tree” as well resulted $m_{tt} = 3,38$ kg. In this case the

“tree” load in the system is the difference between m_{tt} and $3,38-2,2=1,18$ kg.

4. Conclusion

The presently used three different shaker head arrangements cause harmful moments to the tree trunk, which are eliminated on the most sophisticated products by lubrication between clamping head layers. The shaking pattern of the three type units is more or less asymmetric, which is disadvantageous from the point of view of fruit detachment. The new shaker concept, presented in this paper as a laboratory model, excludes all of those moments and generates a symmetric acceleration pattern. The shaking force is generated here by a pair of two synchronised counter-rotating eccentric masses which result in uniform size acceleration in any direction. The eccentric masses in the model are of half-ring shape, rotating around the same axle. This arrangement excludes all the disadvantages of stacked eccentric mass units by not generating any harmful moments.

The two pair of rotating eccentric masses could be replaced by two linear pulsators, turning around their own vertical axis. Calculations with the model data coincided well with the laboratory test results, which prove the conformity of the model for designing full-sized shaking machines. The calculated and measured total mass of the shaker system coincided well, which is another prove of the right modelling. Further research is planned to detect the reason of asymmetry in shaking patterns of conventional harvester machines.

Acknowledgement

Special thanks are due to the staff of the Technical Departments' Laboratory for their valuable contribution.

References

[1] **Affeld H. A. Jr, Brown G. K., Gerrish J. B.:** 1989. A new shaker for fruit and nut trees. *Journal of Agricultural Engineering Research*, Vol. 44, pp. 53-66. [http://dx.doi.org/10.1016/S0021-8634\(89\)80070-8](http://dx.doi.org/10.1016/S0021-8634(89)80070-8)

[2] **Garman C. F., Diener R. G., Stafford J. R.:** 1972. Effect of shaker type and direction of shake on apple detachment. *Journal of Agricultural Engineering Research*, Vol. 17, No. 2, pp. 195-205. [http://dx.doi.org/10.1016/S0021-8634\(72\)80008-8](http://dx.doi.org/10.1016/S0021-8634(72)80008-8)

[3] **Láng Z., Csorba L.:** 2015. Finite Element Modelling of Central Leader and Vase Shape Cherry Trees. *Progress in Agricultural Engineering Sciences*, Vol. 11, pp. 71-78.

<http://dx.doi.org/10.1556/446.11.2015.6>

[4] **Fenyvesi L., Csatár A., Fenyvesi D.:** 2015. Modeling of vibratory harvest with finite element method for trellis plantations. *Proceedings of the Institution of Mechanical Engineers, Part C: Journal of Mechanical Engineering Science*, Vol. 230, No. 9. <http://dx.doi.org/10.1177/0954406215576559>

[5] **Timm E. J., Brown G. K.:** 1985. Minimizing shear force transmission in trunk shaker clamp pads. *ASAE Paper No. 861563*. St. Joseph, Mich.: ASAE

[6] **Timm E. J., Brown G. K., Segerlind L. J., Van Ee G. R.:** 1988. Slip-Belt and Lubrication Systems for Trunk Shakers. *Transactions of the ASAE*, Vol. 31, No. 1, pp. 40-47.

<http://dx.doi.org/10.13031/2013.30662>

[7] **Snell L. D., Birrell S. J.:** 2015. Coupled moment analysis of stacked counter-rotating eccentric-mass tree shaker energy-wheel system. *Biosystem Engineering*, Vol. 136, pp. 92-101.

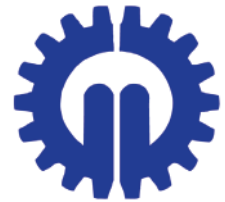
<http://dx.doi.org/10.1016/j.biosystemseng.2015.04.008>

[8] **Ortiz-Canavate J.:** 1969. Design of multi-directional trunk – shaker. *M. Eng. Thesis., Univ. Calif. Davis*.

[9] **Horváth E.:** 1996. A hazánkban üzemelő gyümölcsfa-tözsrázók mozgáspályájának vizsgálata [Acceleration pattern testing of trunk-shakers working in Hungary]. *Járművek, Építőipari és Mezőgazdasági Gépek [Vehicles, Construction and Agricultural Machines]*, Vol. 43, No. 5, pp. 175-183.

[10] **Abdel-Fattah H. M., Shackel K. A., Slaughter D.:** 2003. Substantial vertical tree displacements during almond shaker harvesting. *Applied Engineering in Agriculture*, Vol. 19, No. 2, pp. 145-150.

[11] **Fodor Á.:** 2015. Gyümölcsfa tözsrázó gépegység tervezése [Design of a trunk shaker for fruit trees]. *Technical University of Budapest*, 88 p.



THE FEASIBILITY OF MODELLING ROCKS IN ENGINEERING APPLICATIONS WITH THE USE OF DISCRETE ELEMENT METHOD

Author(s):

Á. Orosz – K. Tamás – J. P. Rádics

Affiliation:

Department of Machine and Product Design, Budapest University of Technology and Economics
Műegyetem rkp. 3., Budapest, H-1111, Hungary

Email address:

orosz.aakos@gmail.com, tamas.kornel@gt3.bme.hu, radics.janos@gt3.bme.hu

Abstract

This paper represents the motivation behind modelling rocks and the technique. Several possible agricultural engineering and other applications are introduced. The need for tracing each grain makes the discrete element method (DEM) ideal for the task. There are several types of rock aggregates, which need different models and parameter sets. Grains were represented with clumps and crushed rocks were approximated with convex polyhedral particles. The behaviours of the models were tested in simulations.

Keywords

discrete element modelling, gravel, crushed rock, clump, polyhedron

1. Introduction

Numerical computational simulations provide an excellent way to examine the behaviour of complex processes. A proper model can provide data, which are hardly accessible with measurements or would have high cost requirement. The simulation also gives a way to examine the effect of process parameters on the behaviour of the material independently.

There are many cases where engineering structures interact with rock aggregates. The modelling of these processes creates the opportunity to test the machines virtually, creating the possibility to improve the design, decrease the necessary manufactured prototype variants, and thus reduce development cost and time.

Several examples can be found for stone-tool interaction in the field of agricultural engineering. The modelling possibilities of soil-tillage interaction

was already examined [1, 2], which can be extended to study the effect of rocky soil on the cultivation tools. Rock crushers are often used to reclaim fields and also rock pickers for collecting stones. Internal parts of forage and combine harvesters can be damaged by rocks getting into the machine. In combine harvesters, there is a stone trap to avoid rock reaching sensitive parts, which indicates that this issue cannot be neglected.

A proper rock model also can be used in other fields, for example railway ballast conditioning, mining and roadwork.

The first phase of creating a rock-tool interaction model is defining a proper rock model. The finite element method (FEM) describes bodies by dividing them into elements and creating the so-called finite element mesh. These elements have prescribed number of common nodes, with defined number of degrees of freedom. In case of contacting bodies, the proper definition of every contact surface is needed. This makes very difficult and time-consuming to model aggregates with considerable amount of grains, therefore the discrete element method (DEM) was applied instead, as it was developed to model granular media.

DEM involves particles (elements) with independent motional and rotational degrees of freedom and arising forces between them [3, 4], so it creates the possibility to model and trace the grains independently. The displacements of the particles are computed via numerical integration, relying on the principle laws of dynamics. The time between two successive iteration steps is called the timestep.

The definition of the technique makes it ideal for modelling the mechanical behaviour of granular media e.g. soil [5], rock aggregates, fractured solid

stones [6] different seeds [7, 8], crops [9] and even buildings made of blocks [10]. The main challenge in the creation of a DEM model is that it needs calibration [11] for each material model.

The oldest and simplest element shape in DEM is the sphere, however more complex particles are used in our research, which can simulate the sliding of grains and interlocking effect between rocks more realistically.

2. Properties of rock aggregates

Different types of rock aggregates are distinguished based on the material, size and shape of the grains. Widely used construction materials are e.g. andesite, limestone, dolomite, quartzite and basalt. The desired gradation of a yielded aggregate is obtained by sorting it with different sizes of sieves. The properties of the aggregate are highly influenced by its origin. The naturally formed (river) gravels (Figure 1. a) have smooth surface with round edges and corners unlike manufactured crushed rocks (Figure 1.b) which have rough surface and sharp edges and corners. The grain shape theoretically can be classified as equant, flat, elongated or flat-elongated relying on the ratio of the length, width and height dimensions. However, only equant and flat classes are used in practice due to economic reasons and the features of separation processes. These dimensions are defined by the size of the imaginary bounding cuboid around the grain. This introduction to the different aggregates and grains shows that there is a wide variety of properties, that must be taken into account during the creation process of their numerical model, especially in defining the particle shape.

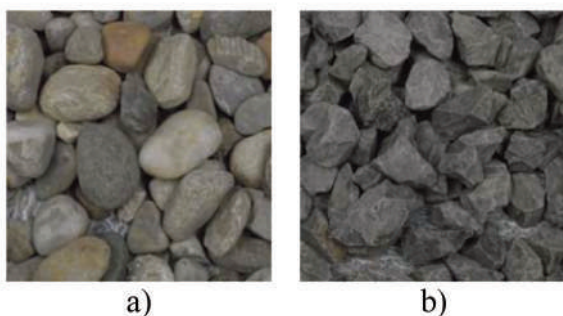


Figure 1. Aggregates made of a) gravels and b) crushed rocks

3. Definition of particle shapes

The gravel and crushed stone aggregates were modelled with different approaches in our research. The smooth gravels are approximated with clumps, which are particles made up by spheres with rigid connection between them. The elements that

represent equant (Figure 2. a) and flat (Figure 2. b) gravels, have spheres with different size ratio and constellation.

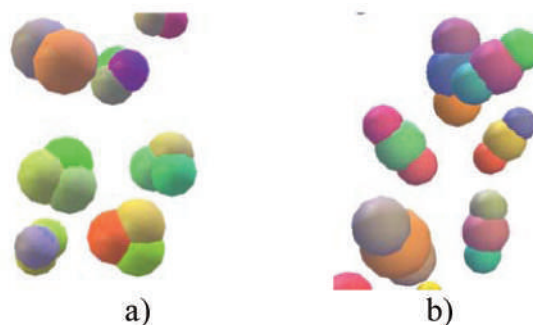


Figure 2. a) Equant and b) flat clump particles

Crushed rocks were approximated by randomly generated [12] convex polyhedra, with predefined size and shape index, which allows the creation of equant (Figure 3. a) and flat (Figure 3. b) particles. Polyhedra can simulate the significant interlocking between grains effectively, and effect of rough surface can be modelled with a properly set coefficient of friction.

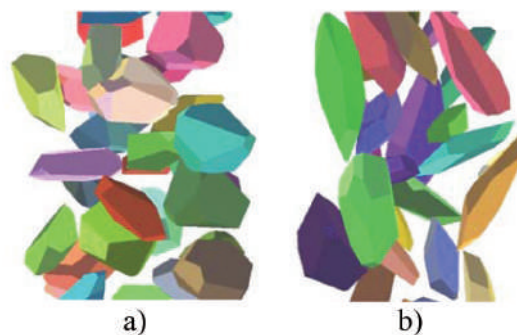


Figure 3. a) Equant and b) flat polyhedral particles

4. Interaction laws of arising forces

The interaction (constitutional) law computes the arising forces between the particles. Two of them was chosen from the many existing laws, one for the clump elements and one for polyhedra. The definitions of laws belonging to the corresponding particle types necessarily differ, but the aim was to find such ones that have the same base in some point.

Following from the behaviour of the rock aggregates, forces only need to be risen, when the particles come into contact, so the models have to be cohesionless. For clumps, the model of Cundall and Strack [13] was chosen and the law of J. Eliáš [14] was used for polyhedral particles. Both are implemented in Yade DEM software [15]. The particles are ideally rigid in both models, and their stiffness is represented by definition of the interaction law.

Clumps

The model of Cundall and Strack [13] is originally applied to spheres, but it can be also adapted to clumps. In the clump model, two kinds of forces arise between the particles during contact: normal (repulsive) and shear forces. The magnitude of the normal force (F_n) is linearly proportional (Equation 1) to the compression (u_n) of the imaginary linear spring between particles with normal stiffness k_n (Figure 4.).

$$F_n = k_n u_n \quad (1)$$

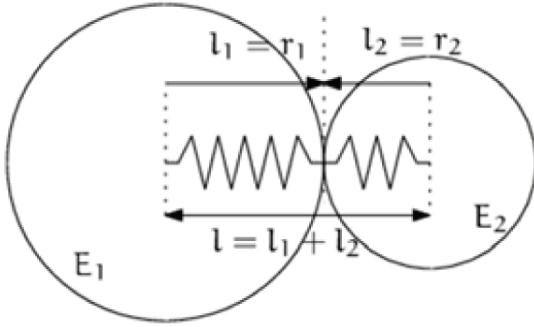


Figure 4. Visualization of normal force definition [15]

The shear force (F_s) is linearly proportional to the displacement (u_s) from the relative rotation and translation of the elements (Equation 2), and its maximum value (F_s^{max}) is regulated by the Coulomb friction law (Equation 3).

$$F_s = k_s u_s \quad (2)$$

$$F_s^{\text{max}} = F_n \tan(\varphi) \quad (3)$$

where:

F_s	shear force	[N]
F_s^{max}	maximum shear force	[N]
F_n	normal force	[N]
k_s	normal stiffness	[N/m]
u_s	relative displacement	[m]
φ	inter-particle friction angle	[rad]

Polyhedra

The polyhedral interaction law has several similarities to the clump law, as it only differs in the definition of normal force. The magnitude of normal force (F_{nv}) is linearly proportional to the size of the V_c intersecting volume (Equation 4). The same law is visualized by Figure 5. in profile. Because of the volumetric behaviour of the definition, the so-called volumetric normal stiffness (k_{nv}) is used as the proportional factor between the normal force and mutual volume, with the unit N/m^3 .

$$F_{nv} = k_{nv} V_c \quad (4)$$

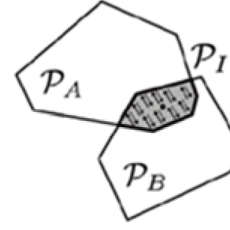


Figure 5. Visualization of normal force definition [14]

The computational method of the shear force is the same as seen in case of the clump constitutive law (Equation 2 and 3).

Damping

The applied interaction laws do not involve any kind of damping, which is essential to dissipate kinetic energies and to reach equilibrium state. Considering that, a so-called global damping [16] was applied in both models. Equation 5 refers to each particle separately. F_{dw} is a numerical, artificial, non-viscous damping, which decreases the forces that cause velocity increases and vice versa, with a damping coefficient factor which is between 0 and 1. Global damping has a restriction that it can only provide reliable results in quasi-static simulations.

$$\frac{(\Delta F)_{dw}}{F_w} = -\lambda \cdot \text{sgn} F_w \left(\dot{u}_w^{i-1} + \frac{\ddot{u}_w^i \Delta t}{2} \right) \quad (5)$$

where:

F	force	[N]
u^{i-1}	velocity of particle in the previous timestep	[m/s]
\ddot{u}^i	acceleration of particle in the current timestep	[m/s ²]
w	index of dimension (x, y, z)	
ΔF_d	damping force	[N]
Δt	duration of a timestep	[s]
λ	damping coefficient (0-1)	[-]

5. Simulation test setup

The behaviour of the clump and polyhedral models were tested in a uniaxial compression simulation. The aggregate is placed in a cylinder (Figure 6. and 7.) and a top plate applied a normal force to the aggregate up to 600 kN with constant velocity, then unloading began. The normal force on the plate and its displacement was registered.

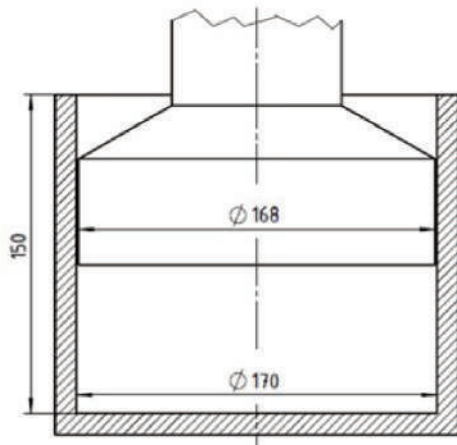


Figure 6. Sketch and dimensions of the test setup

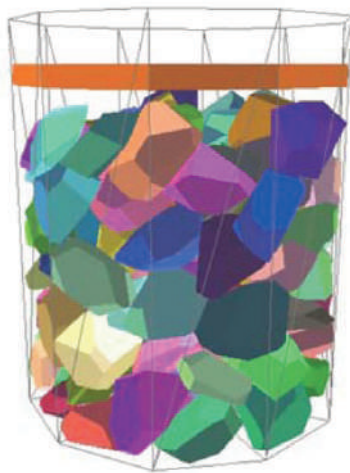


Figure 7. Initial state of the polyhedral pack before the pressing process

The applied micromechanical characteristics of the polyhedral model were:

	stones	plate + cylinder	
ρ	2600	7800	[kg/m ³]
k_{nv}	2·1013	2·1014	[N/m ³]
k_s	2·108	2·109	[N/m]
φ	0,6	0,4	[rad]

The parameters of the clump model were:

	gravels	plate + cylinder	
ρ	2600	7800	[kg/m ³]
k_n	3·1010	2,1·1011	[N/m]
k_s	3·106	2,1·107	[N/m]
φ	0,6	0,4	[rad]

Where ρ is the volumetric mass density. The value of the damping coefficient (λ) was 0,3 in every case.

6. Results

Figure 8. and 9. shows the results of compression simulations. Normal force, which was registered on the load plate, is shown in respect of the negative

displacement of the plate. Equant and flat aggregates were tested both in clump and polyhedral cases. The results in the case of clumps (Figure 8.) show little difference between the two particle shapes, although the flat grains can be compressed slightly better. However, there is a significant difference in case of polyhedra (Figure 9.). Studying the load curves of the polyhedral particles, peak forces can be observed. This behaviour is presumably due to the interlocking and stick slip of certain elements and it is assumed that it can be neglected.

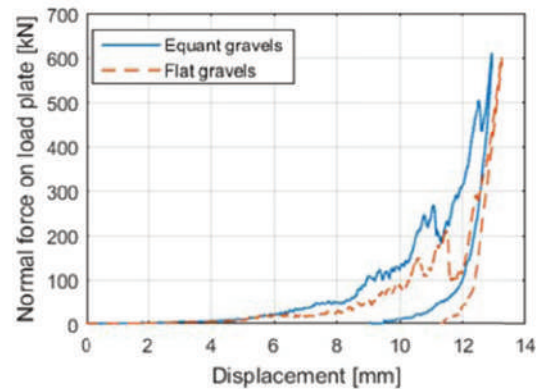


Figure 8. Load curve of the clump aggregates

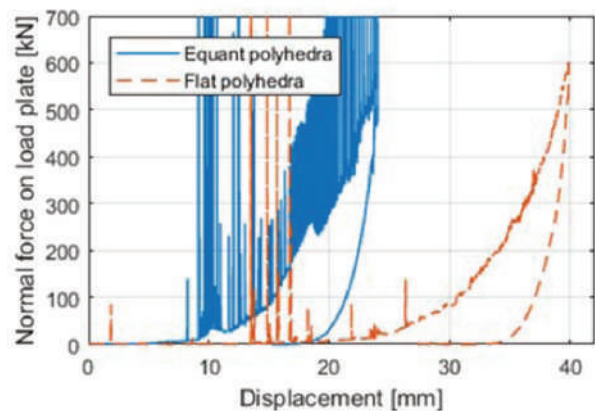


Figure 9. Load curve of the polyhedral aggregates

7. Conclusion

The paper discussed the motivation of the research on creating the numerical model of rocks and its the usability in the field of agricultural machinery engineering. The chosen tool was the discrete element method, which is suitable for modelling the distinct rock grains. Models for simulating gravels and crushed rocks with equal and flat shapes were introduced and studied.

In DEM models, the definition of particles and the law of interactions have to be defined. Our focus was on creating a model with a complex element shape, which is, in contrast with the simple sphere, able to model the interlocking and sliding between particles

accurately. The behaviour of the models, especially the effect of grain shape, was tested in the simulations of a uniaxial compressing test setup.

The evolution of the normal force acting on the top plate, in respect of the displacement of this plate, showed same characteristics in each test and fulfils the theoretical expectations. The load curves show the typical, highly nonlinear behaviour of rock aggregates. In the early phase of the process, the force raises slowly, as the result of the relatively high initial porosity of the aggregate. As interlocking and consolidation occurs, the aggregate becomes stiffer.

The particle shape, besides the application of the same constitutional law and parameters, have a noticeable effect on the compressibility of clump aggregates, and shows a significant influence in case of polyhedral bulk materials. This nature confirms the benefit of using complex element shapes in situations, where the influence of the grain shape on the behaviour on the whole aggregate cannot be neglected.

Acknowledgements

Supported by the ÚNKP-17-2-I New National Excellence Program of the Ministry of Human Capacities.

We would like to thank the support in questions related to geology and geotechnics to Miklós Gálos at the Department of Construction Materials and Technologies, Budapest University of Technology and Economics.

References

[1] **Keppler I., Hudoba Z., Oldal I., Csatar A., Fenyvesi L.:** 2015. Discrete element modeling of vibrating tillage tools. *Engineering Computations*, Vol. 32, pp. 308-328. <http://dx.doi.org/10.1108/EC-10-2013-0257>

[2] **Tamás K., Jóri I. J., Mouazen A. M.:** 2013. Modelling soil-sweep interaction with discrete element method. *Soil & Tillage Research*, Vol. 134, pp. 223-231. <http://dx.doi.org/10.1016/j.still.2013.09.001>

[3] **Cundall P. A., Hart D. H.:** 1992. Numerical modelling of discontinua, *Journal of Engineering Computations*. Vol. 9, No. 2, pp. 101-113. <http://dx.doi.org/10.1108/eb023851>

[4] **Bagi K.:** 2007. A diszkrét elemek módszere [The method of discrete elements]. BME Department of Structural Mechanics, Budapest, pp. 5-12. ISBN 978 963420 929 4

[5] **Kotroc K., Kerényi Gy.:** 2014. Modeling of the soil-rigid wheel interaction using discrete element method, *Poljoprivredna Tehnika [Agricultural*

Engineering], Vol. 39, No. 3, pp. 1-11.

[6] **Scholtès L., Donzé F. V.:** 2012. Modelling progressive failure in fractured rock masses using a 3D discrete element method. *International Journal of Rock Mechanics & Mining Sciences*, Vol. 52, pp. 18-30. <http://dx.doi.org/10.1016/j.ijrmms.2012.02.009>

[7] **Kovács Á., Kerényi Gy.:** 2017. Modeling of corn ears by discrete element method (DEM). *ECMS 2017: 31st European Conference on Modelling and Simulation Proceedings*, pp. 355-361. <http://dx.doi.org/10.7148/2017-0355>

[8] **Ghodki B. M., Goswami T. K.:** 2016. DEM simulation of flow of black pepper seeds in cryogenic grinding system. *Journal of Food Engineering*, Vol. 196, pp. 36-51. <http://dx.doi.org/10.1016/j.jfoodeng.2016.09.026>

[9] **Kovács Á., Kotroc K., Kerényi Gy.:** 2015. The adaptability of discrete element method (DEM) in agricultural machine design. *Hungarian Agricultural Engineering Vol. 27*, pp. 15-19. <http://dx.doi.org/10.17676/HAE.2015.27.14>

[10] **Simon J., Bagi K.:** 2016. Discrete element analysis of the minimum thickness of oval masonry domes. *International Journal of Architectural Heritage*, Vol. 10, No. 3, pp. 457-475. <https://doi.org/10.1080/15583058.2014.996921>

[11] **Keppler I., Kocsis L., Oldal I., Csatar A.:** 2011. Determination of the discrete element model parameters of granular materials. *Hungarian Agricultural Engineering*, Vol. 23, pp. 30-32.

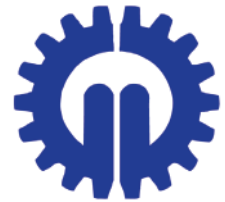
[12] **Asahina D., Bolander J. E.:** 2011. Voronoi-based discretizations for fracture analysis of particulate materials. *Powder Technology*, Vol. 213, pp. 92-99. <http://dx.doi.org/10.1016/j.powtec.2011.07.010>

[13] **Cundall P. A., Strack O. D. L.:** 1979. A discrete numerical model for granular assemblies. *Géotechnique*, Vol. 29, pp. 47-65. <http://dx.doi.org/10.1680/geot.1979.29.1.47>

[14] **Eliáš J.:** 2014. Simulation of railway ballast using crushable polyhedral particles. *Powder Technology*, Vol. 264, pp. 458-465. <http://dx.doi.org/10.1016/j.powtec.2014.05.052>

[15] **Šmilauer V. et al.:** 2015. *Yade Documentation 2nd ed.. The Yade Project*, pp. 526. <http://dx.doi.org/10.5281/zenodo.34073>

[16] **Chareyre B., Villard P.:** 2005. Dynamic Spar Elements and Discrete Element Methods in Two Dimensions for the Modeling of Soil-Inclusion Problems. *Journal of Engineering Mechanics*, Vol. 131, pp. 689-698. [https://doi.org/10.1061/\(ASCE\)0733-9399\(2005\)131:7\(689\)](https://doi.org/10.1061/(ASCE)0733-9399(2005)131:7(689))



NON-DESTRUCTIVE POSTHARVEST MATURITY EVALUATION OF GOLDEN DELICIOUS APPLE

Author(s):

V. Zsom-Muha¹ – L. Ember² – G. Hitka² – L. Baranyai¹ – L.L.P. Nguyen³ – D. Nagy¹, T. Zsom²

Affiliation:

¹Department of Physics and Control, Faculty of Food Science, Szent István University, Villányi út 29-43., Budapest, H-1118, Hungary

²Department of Postharvest Science and Sensory Evaluation, Faculty of Food Science, Szent István University, Villányi út 29-43., Budapest, H-1118, Hungary

³Department of Refrigeration and Livestock Products Technology, Faculty of Food Science, Szent István University, Villányi út 29-43., Budapest, H-1118, Hungary

Email address:

Zsomne.Muha.Viktoria@etk.szie.hu, Hitka.Geza@etk.szie.hu, Baranyai.Laszlo@etk.szie.hu, Nguyen.Le.Phuong.Lien@etk.szie.hu, Zsom.Tamas@etk.szie.hu

Abstract

The aim of our work was the non-invasive maturity determination of Golden Delicious apples during 35 days long cold (2°C) and shelf-life storage (20°C). Significant difference was found between cold and at 20°C stored samples in case of mass loss, acoustic stiffness coefficient, RGB color parameters and chlorophyll content related parameters (IAD, F0, FM, FV/FM). The DA-value and the chlorophyll fluorescence values did not show significant differences between the blushed and shaded sides of the samples.

All the applied non-invasive measuring methods were found to be suitable for the detection of postharvest maturation related quality changes of apple.

Keywords

DA-index®, chlorophyll fluorescence, acoustic stiffness, computer/machine vision system.

1. Introduction

Nowadays, the consumers' demand for fresh apples in excellent quality became more and more important. Apple is one of the main fruits available during all the year in Hungary for fresh consumption and postharvest storage. Concerning this, the objective quality determination of fresh apple samples is also an important task to solve. In order to store the apples for months it is essential to know the internal processes. Internal and

external quality features such as stiffness, taste and color are the most valuable parameters for the consumers.

The new non-destructive quality evaluating methods offer the possibility to supply precise information about the quality and its changes during the postharvest period. Abbott et al. [1] found the relationship between the resonance frequency of the apples and their firmness. Since then, more and more research groups carried out experiments using the acoustic method. More fruits' and vegetables' stiffness, such as pear [2], peach [3], tomato [4], carrot [5], were measured successfully by this technique.

The outlook is a very important parameter during quality evaluation and purchase. Computer aided machine vision system offers the possibility for size, shape and color analysis [6, 7].

The maturity related surface color change can be characterized by the logistic curve related color changes in case of many fruits and vegetables [8, 9].

Photosynthetically active chlorophyll content and postharvest quality related maturity changes can be determined by the use of chlorophyll fluorescence analysis [10, 11] and the measurement of DA-value (index of absorbance difference, IAD) by a DA-meter [3, 12, 13, 14, 15].

The aim of our work was the non-invasive maturity and quality determination of freshly harvested Golden Delicious apple samples during simulated postharvest cold and shelf-life storage.

2. Materials and methods

Mature green and fresh Golden delicious apple samples (*Malus domestica* cv. Golden delicious L.) were bought from an experienced grower in uniform maturity. According to uniform size, mass, shape and freedom from defects, 50 pieces were randomly divided into two groups. They were stored in temperature-controlled refrigerator at 2 ± 0.5 °C and at ambient temperature of 20 ± 1 °C for 35 days wrapped in thin LDPE (low-density polyethylene) bags.

Two measuring points on the blushed and shaded side were selected for the nondestructive measurements as surface color measurements carried out by a machine vision system, chlorophyll fluorescence analysis and DA-index® evaluation. In case of the optical methods the parameters were calculated as the average on the two sides measured values. Mass loss (% of fresh weight) was calculated based upon the measured weight data of each sample on every measuring day.

Surface color changes were determined by a specific self-developed machine vision system consisting homogeneous illumination provided by halogen lamps and a high-performance camera. Average red, green and blue color characteristics (and additionally the normalized values too) of the different sides of each sample were evaluated during the 35 day long cold and shelf-life storage period. The normalized R, B, and G values were calculated upon the intensity of R or B or G value divided by the sum of the R, B and G values.

Maturity related changes of photosynthetic activity, integrity and efficiency of photosystem II (PSII) were characterized by the measurement of chlorophyll fluorescence parameters. F_0 (dark fluorescence signal), F_m (maximum dark fluorescence signal) and F_v (variable fluorescence $F_v = F_m - F_0$) parameters at the above mentioned two points of each apple side were measured by a PAM WinControl-3 controlled MONI-PAM multi-channel chlorophyll fluorometer (Heinz Walz GmbH, Germany). The calculated index of F_v/F_m reflects the potential maximum photon yield of photochemistry, i.e. the maximum photochemical efficiency. It is a valuable tool to determine both photosynthetic capacity and stability in connection with chlorophyll degradation related postharvest maturation.

In order to characterize the change in fruit surface color or tissue related chlorophyll content, the DA index® was measured by a FRM01-F type Vis/NIR DA-meter® (Sintéleia s.r.l., Italy) on every two measurement points per side of each apple. Index of absorbance difference ($IAD = A_{670nm} - A_{720nm}$) is

calculated upon the absorbance difference between 670 nm (near the Chl-a absorption peak) and 720 nm (background of the spectrum). The DA index® (or IAD) is proportional to the amount of chlorophyll present in the fruit and varies from 0 to 5 (Ziosi et al. [15]). For the calculation of DA index®, back light luminosity value (BK), Red light value (RED) and IR light value (IR) were also measured automatically by the device.

Textural changes were measured by a purpose-built laboratory device using the acoustic impulse response technique. Samples were tapped lightly on the equator with a wooden stick. The apples' acoustic response was collected by microphone located under the cushioning sample holder. The microphone's output was recorded by a sound card in a PC-compatible computer. Custom Fast Fourier Transform software was used to analyze the recorded acoustic response. From the resulting frequency spectrum, the characteristic frequency was selected. The characteristic frequency and the sample mass were used to calculate the acoustic stiffness coefficient [5, 16] by the equation below (Equation 1), where f is the characteristic frequency of the sample (Hz), m is the sample mass (g) measured with a high precision balance:

$$S = f^2 * m * 10^{-6} \text{ [N/mm]} \quad (1)$$

Data were converted by means of routines in MS-Excel and were analyzed using the SPSS for Windows ver. 14. Statistical analysis was performed at 95 % significance level (in figures marked with 95 % CI).

3. Results and discussion

During the postharvest storage the firmness, the mass and the color changes of the apple samples were observed. Figure 1 shows the mass loss changes of the samples in the two different storage temperatures. It can be seen, that the mass loss of the 2°C stored apples was only 3% during the 35 days long storage period. Compared to that, the 20°C stored apple's mass loss was more than 10% with significant difference from the 4th day.

During the storage the mass loss and the firmness changed together. Figure 2 represents the changes of the acoustic stiffness coefficient. The trend is similar to that of mass loss changes versus time. Here also significant difference was found between the two groups from the 4th day.

In contrast to that, in case of the 20°C stored samples, the degree of the decrease in the acoustic stiffness coefficient after the 25th day was not as

significant compared to the mass loss changes. It is worth evaluating the relationship between the mass loss and the relative acoustic stiffness coefficient (Figure 3). Based on the observed changes, it can be concluded, that the acoustic stiffness coefficient is much more sensitive parameter compared to the mass loss (note the change of the relative acoustic stiffness: it was more than 80 %, and the mass loss changes was about 15 % during the 35 days).

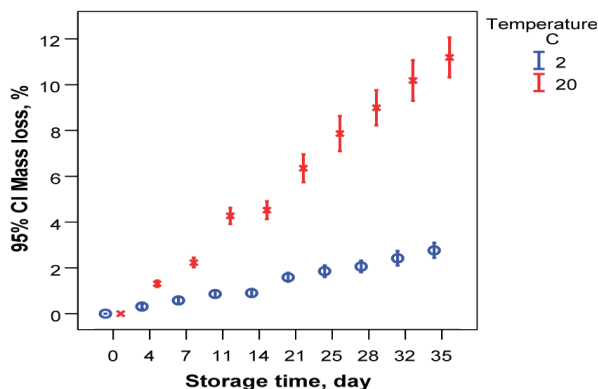


Figure 1. Mass loss changes of the apples stored at 2°C and 20°C.

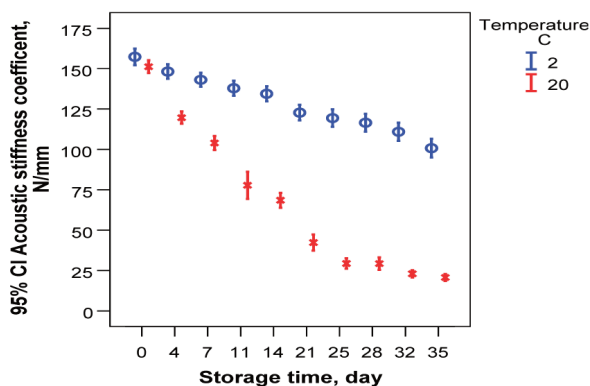


Figure 2. Acoustic stiffness changes of the apples stored at 2°C and 20°C.

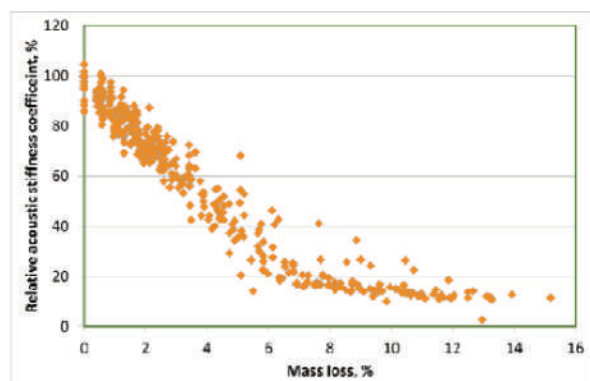


Figure 3. Relationship between mass loss and relative acoustic stiffness coefficient

The acoustic stiffness coefficient's change also clearly and objectively showed the significant difference between the cold and room temperature stored samples quality decrease (tissue softening) during postharvest. Until having reached about the 4 % of mass loss, the stiffness change intensity was almost the same as the mass loss change suggesting a linear relationship (Figure 3). After this point, the stiffness change is less intensive compared to the mass change.

Figures 4-6 show the changes of the normalized R, G, B color parameter of the samples, respectively. The dominant color component was found to be the red. During maturation, the red color parameter increased, while the green and the blue parameters decreased continuously, following a logistic like trend.

In case of all three parameters, significant difference was found between the two storage conditions. Regarding the normalized color parameters, the speed of the color changes was approximately two times higher and more intensive in case of the 20 °C stored apples compared to the 2 °C stored samples. The large-scale changes were observed on the same day (after the 11th day) in case of the two groups. During the storage, the initially green samples became yellow due to the postharvest maturation process.

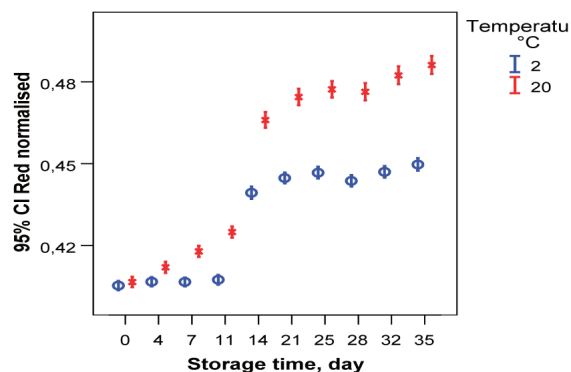


Figure 4. The changes of the normalized red color parameter of the samples

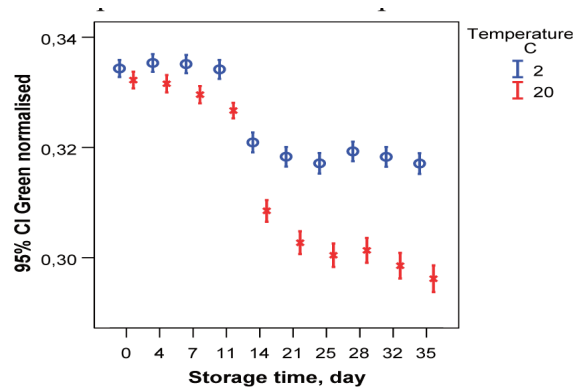


Figure 5. The changes of the normalized green color

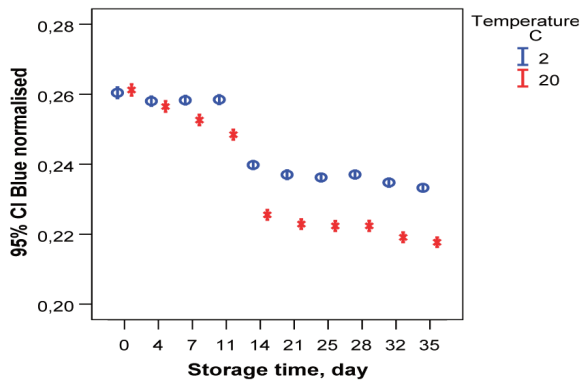


Figure 6. The changes of the normalized blue color

In Figure 7 the change in chlorophyll content related DA index[®] (IDA) values can be seen. It was about 1 at the beginning of the storage and decreased continuously during the measurement period. From the 4th day of storage, significant difference was observed between the two groups. The decrease was only about 0.2 DA value in case of 2°C sample and about 0.7 in case of 20°C stored apples. In case of 20°C stored apple it means that almost all the chlorophyll content decayed during this 35 days long storage period. It confirms that the initial green color of the samples changed to yellow. That change was also shown in case of the normalized color parameters (Figure 4-6).

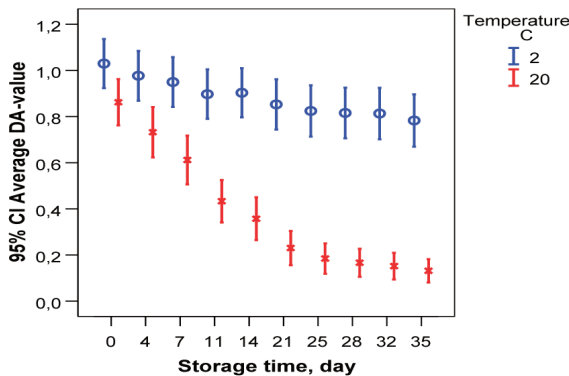


Figure 7. The changes of the DA index[®] during the storage

Compared to the initial values, the average IR value increased during the storage (Figure 8). From the 4th day of storage, in case of this parameter significant difference was found between the two groups stored at different storage conditions too. The IR parameter of the 20°C stored samples increased to almost twice as the initial.

The changes of the chlorophyll content related Fv parameter are shown in Figure 9. During the storage, the content of the photosynthetically active chlorophyll content decreased as it was already shown earlier by the DA index[®] values (Figure 7).

From the 4th storage day, significant difference was observed between the two groups. The Fv value decreased from 2500 to about 2000 relative value in case of 2°C stored apples and to about 250 in case of 20°C stored samples clearly representing the negative effect of higher storage temperature on postharvest maturity changes. After the 21st day, the rate of the decrease was almost negligible in case of the 20°C stored group.

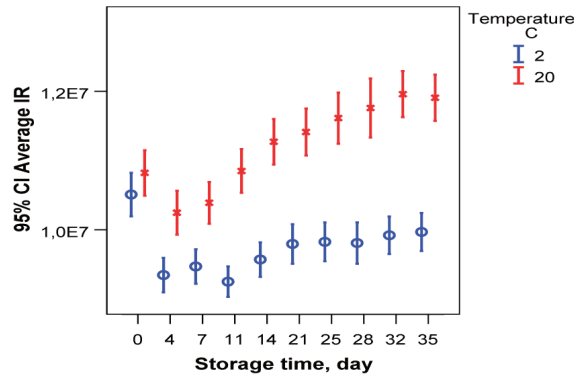


Figure 8. The changes of the IR-value during the storage

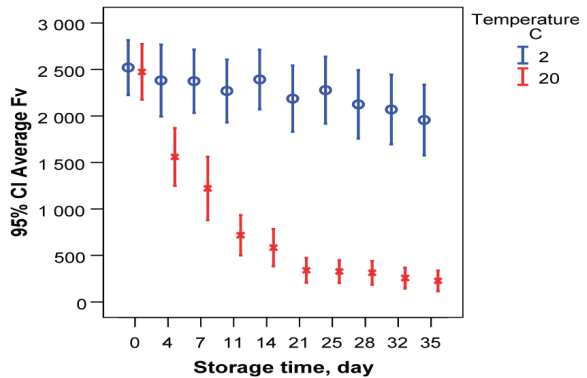


Figure 9. The changes of the Fv parameter during the storage

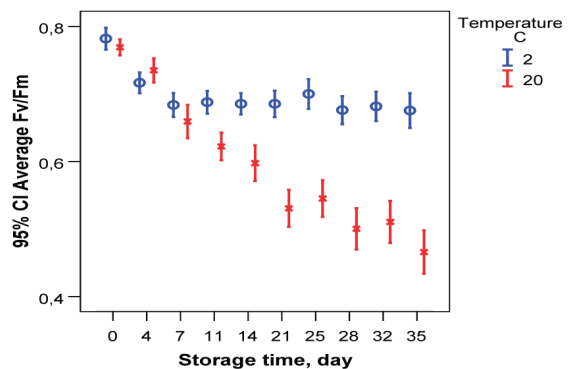


Figure 10. The changes of the Fv/Fm parameter during the storage

The Fv/Fm value decreased also (Figure 10), but in the first week there was no significant difference

between the groups, the way of decrease showed a similar trend. In contrast to that, after the 7th day significant difference occurred in the way of the two groups behavior. The change of the Fv/Fm value of 2°C samples was only 0.1, compared to the higher change of 0.3 in case of 20°C stored samples revealing a fast and rapid maturity change at improper storage conditions.

4. Conclusions

Non-destructive measurements such as chlorophyll fluorescence analysis, DA index® measurement, acoustic stiffness measurement and computer aided machine vision system-based surface color measurement were carried out during the test period of 35 days on the Golden delicious apple samples stored at 2°C and 20°C.

According to our results shown above, all the applied non-invasive quality measurement methods were found to be suitable for the detection and follow-up of postharvest maturation related quality changes of apples stored at different storage temperatures proving the positive effect of reduced temperature on apple quality.

As a main conclusion, it can be declared that by the use of the applied methods, significant differences were determined between at cold and ambient temperature stored samples quality from the 4th day of storage in case of textural changes such as mass loss, acoustic stiffness, surface color related DA index® values, and additionally from the 7th-11th day of storage in case of chlorophyll fluorescence related parameters.

Acknowledgements

The project is supported by the European Structural and Investment Funds (grant agreement no. VEKOP-2.3.3-15-2017-00022).

References

[1] **Abbott J. A., Bacherman G. S., Chiders R. F., Fitzgerald J. V., Matusik F. J.:** (1968). Sonic technique for Measuring Texture of Fruits and Vegetables. *Food Technol*, Vol. 22, pp. 635-646.
[2] **Jancsó P. T., Clijmans L., Nicolai B. M., de Baerdemaeker J.:** (2001). Investigation of the effect of shape on the acoustic response of ‘conference’ pears by finite element modelling. *Postharvest Biology and Technology*, Vol. 23, pp. 1-12.
[3] **Hale G., Lopresti J., Stefanelli D., Jones R., Bonora L.:** 2013. Using non-destructive methods to correlate chilling injury in nectarines with fruit

maturity. *Acta Horticulturae*, 1012: VII International Postharvest Symposium, pp. 83-89.

<http://dx.doi.org/10.17660/ActaHortic.2013.1012.4>

[4] **Vandewalle X., de Baerdemaeker J., Schrevels E.:** 1994. Non-destructive, On-plant Monitoring of the Firmness of Apples and Tomatoes. Cost 94 Post-Harvest Treatment of Fruit and Vegetables Workshop on “Quality Criteria”, April 19-21 (1994), Bled, Slovenia, pp. 1-8.

[5] **Zsom-Muha V., Felföldi J.:** 2007. Vibration Behaviour of Long Shape Vegetables. *Progress in Agricultural Engineering Sciences*, Vol. 3 pp. 21-46.

[6] **Brosnan T., Sun D. W.:** 2004. Improving quality inspection of food products by computer vision – a review. *Journal of Food Engineering*, Vol. 61, No. 1, pp. 3-16.

[http://dx.doi.org/10.1016/S0260-8774\(03\)00183-3](http://dx.doi.org/10.1016/S0260-8774(03)00183-3)

[7] **Pathare P. B., Opara U. L., Al-Said F. A. J.:** 2013. Colour measurement and analysis in fresh and processed foods: a review. *Food and Bioprocess Technology*, Vol. 6, No. 1, pp. 36-60.

<http://dx.doi.org/10.1007/s11947-012-0867-9>

[8] **Tijskens L. M. M., Evelo R. G.:** 1994. Modelling colour of tomatoes during postharvest storage. *Postharvest Biology and Technology* Vol. 4, No. 1-2, pp. 85-98.

[http://dx.doi.org/10.1016/09255214\(94\)90010-8](http://dx.doi.org/10.1016/09255214(94)90010-8)

[9] **Schouten R. E., Huijben, T. P. Tijskens L. M. M., van Kooten O.:** 2007. Modelling quality attributes of truss tomatoes: linking colour and firmness maturity. *Postharvest biology and technology*, Vol. 45, No. 3, pp. 298-306.

<http://dx.doi.org/10.1016/j.postharvbio.2007.03.011>

[10] **Bron U. I., Ribeiro R.V., Azzolini M., Jacomino A. P., Machadoc E. C.:** 2004. Chlorophyll fluorescence as a tool to evaluate the ripening of ‘Golden’ papaya fruit, *Postharvest Biology and Technology*, Vol. 33, No. 2, pp. 163-173.

<http://dx.doi.org/10.1016/j.postharvbio.2004.02.004>

[11] **Herppich W.B., Foerster J., Zeymer J., Geyer M., Schlüter O.:** 2012. Chlorophyll fluorescence imaging for non-destructively monitoring of changes in fresh and fresh-cut produce. In: C Nunes (ed.): *Proceedings of the International Conference Environmentally Friendly and Safe Technologies for Quality of Fruits and Vegetables*, Faro, Portugal, 14.-16.01.2009, pp. 45-51.

[12] **Costa G., Bonora E., Fiori G., Noferini M.:** 2011. Innovative Non-destructive device for fruit quality assessment. *Acta Horticulturae*. 913: VII International Symposium on Kiwifruit, pp. 575-581.

<http://dx.doi.org/10.17660/ActaHortic.2011.913.78>

[13] **Nyasordzi J., Friedman H., Schmilovitch Z., Ignat T., Weksler A., Rot I., Lurie S.:** 2013. Utilizing

the IAD index to determine internal quality attributes of apples at harvest and after storage. *Postharvest Biology and Technology*, Vol. 77, pp. 80–86.

<http://dx.doi.org/10.1016/j.postharvbio.2012.11.002>

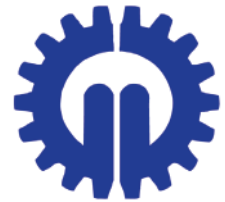
[14]Spadoni A., Cameldi I., Noferini M., Bonora E., Costa G., Mari M.: 2016. An innovative use of DA-meter for peach fruit postharvest management. *Scientia Horticulturae*, 201, pp. 140-144.

<http://dx.doi.org/10.1016/j.scienta.2016.01.041>

[15]Ziosi V., Noferini M., Fiori G., Tadiello A., Trainotti L., Casadoro G., Costa G.: 2008. A new index based on vis spectroscopy to characterize the progression of ripening in peach fruit. *Postharvest Biology and Technology*, Vol. 49 pp. 319–329.

<http://dx.doi.org/10.1016/j.postharvbio.2008.01.017>

[16]Felföldi J., Fekete A.: 2003. Detection of small scale mechanical changes by acoustic measuring system. *ASAE Annual Meeting Paper*, Las Vegas, No. 036097, pp. 1–8.



EFFECTS OF LENGTH ON MECHANICAL DURABILITY OF VARIOUS WOOD PELLETS

Author(s):

R.C Akdeniz¹ – O. Esmer²

Affiliation:

¹Ege University, Faculty of Agriculture, Department of Machinery and Technologies Engineering, Bornova/Izmir, 35100, Turkey

²Ege University, Graduate School of Natural and Applied Science Institute, Agricultural Machinery and Technologies Engineering, MSc, Bornova/Izmir, 35100, Turkey

Email address:

rcakdeniz87@gmail.com, ogulcanesmer@gmail.com

Abstract

In this study, an investigation was made of the effect of length on the mechanical durability of pellets made from Valonia Oak industrial waste, Calabrian Pine residue and sawdust at various mixture ratios of these materials. The pellets were classified into six length classes of $3.15 \text{ mm} < \text{PL} \leq 20 \text{ mm}$, $20 \text{ mm} < \text{PL} \leq 35 \text{ mm}$, $35 \text{ mm} < \text{PL} \leq 38 \text{ mm}$, $38 \text{ mm} < \text{PL} \leq 40 \text{ mm}$, $40 \text{ mm} < \text{PL} \leq 45 \text{ mm}$ and $45 \text{ mm} < \text{PL}$, and each length class was classified into four categories (C-I, C-II, C-III and C-IV) according to surface cracks. Mechanical durability test results showed that, in the 66.5-33.5% acorn-pine mixture ratio, only the $20 \text{ mm} < \text{PL} \leq 35 \text{ mm}$ -C-I pellets met the 97.5% mechanical durability limit of ENplus, but most of the other classes met the minimum PFI standard mechanical durability limit of 95%.

In the free fall tests, all length classes showed the same results for C-I pellets: these did not break into pieces easily, whereas C-IV pellets broke into pieces at the first fall. Also, their weight loss was greater than that of the other categories.

Keywords

wood pellet, forest residue, valonia waste, length, mechanical durability

1. Introduction

Turkey has approximately 22 342 000 ha of forest, of which 5 886 195 ha or 26.34% is oak, and 5 610 215 ha or 25.11% is Calabrian pine [1]. These tree species

are widely used in the timber industry, especially in furniture making [2]. Also, acorns are used as a raw material in the leather industry in the tanning process [3] and in the animal feed industry [4] [5].

It is estimated that the sawdust and other wastes from the processing of these and other tree species, together with the branches, shoots and other pruned materials have an energy value of 859 899 TOE according to BEPA data. The min-max oven-dry calorific values of oak and pine are 3972-4287 cal/gr and 4216-4531 cal/gr [6] respectively, so that these materials could be used as an important source in the production of heat energy.

Because of its dispersed state and various other physical characteristics, this biomass must undergo some pre-treatment in order to convert it into a productive form. Pelletizing technologies are widely applied in order to increase the energy density of biomass and to reduce the costs of storage and transport [7]. In order for pellets to be easily transported and to have a long shelf life, it is necessary to set up standard accepted mechanical durability values for pellets [8].

In this study, an investigation was made of the mechanical durability of pellets made at a factory producing valonia from acorns, using the waste from the valonia production process (Figure 1), [9] mixed at a proportion of 60-81% [3] with Calabrian pine forest residue and sawdust. These pellets are used to meet the heating needs of the factory itself and some are sold commercially. The effect of cracks on the pellet surface was also investigated, separating the pellets into length classes.



Figure 1. Valonia production process

2. Materials and Methods

Materials

Raw Materials

Pine forest residue, industrial waste from the acorn industry and sawdust waste from the furniture industry were used (Figure 2). The pine residue contained 10.14% moisture, the acorn waste 40.59%, and the sawdust 10,92%. The acorn waste was spread on the ground and dried naturally, reducing moisture content to a value of 28.56%.

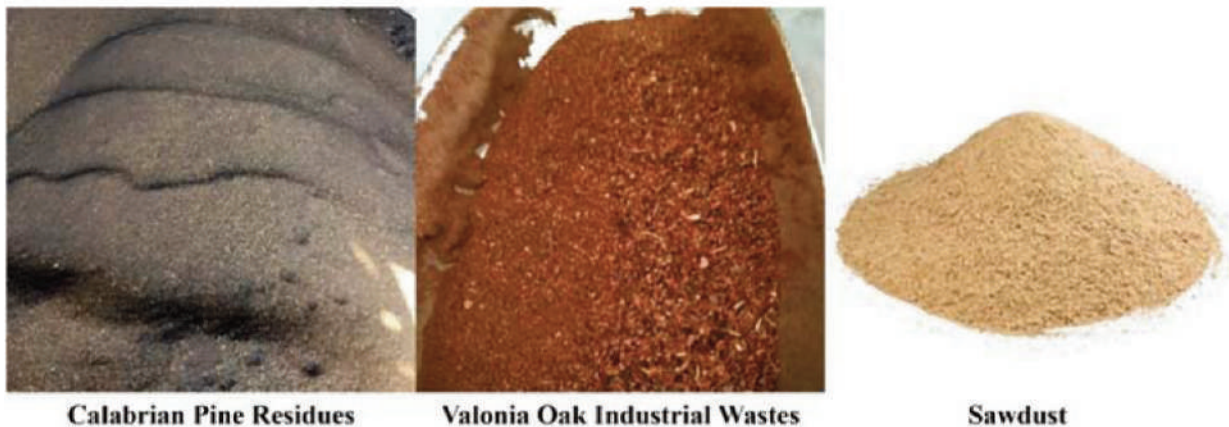


Figure 2. Raw Materials

Pellets

The pellets used in the study were from a biomass mixture consisting of 66.5-33.5% acorn-pine and 50-25-25% acorn-pine-sawdust. Granule size was

reduced in a hammer mill, and the pellets were produced in a disc-type pelletizing machine with a capacity of 1000 kg/h and holes of 8 mm diameter, and cooled naturally (Figure 3).



Figure 3. Pelletizing machine with 8 mm disc and pellets

Devices and Equipment

A drying oven (a) was used in moisture analysis of the pellets, digital calipers (b) with an accuracy of 0.001 to measure length and diameter, a scale (c) with an accuracy of 0.001 to measure weight, a durability tester (d) and sieves (e) to determine mechanical

durability, a steel plate (f) as the surface on which the pellets fell in free fall tests, a digital microscope (g) with a five megapixel sensor, adjustable polarizer, up to 200x magnification depending on working distance, and a resolution of 2592x1944 to photograph cracks. Sample containers (h) were used in all analyses (Figure 4).



Figure 4. Devices and Equipment

2.2. Methods

Moisture Analysis

Samples of at least 50 g were weighed with five iterations on a sensitive scale and dried in a drying oven at a temperature of 105°C for 24 hours. Moisture values were calculated on the basis of wet weight (MWb) by Equation 1, and on the basis of dry weight (MDb) by Equation 2 [10].

$$M_{Wb}(\%) = \frac{W_{fi} - W_f}{W_{dry\ sample} + W_{water}} \times 100 \quad (1)$$

$$M_{Db}(\%) = \frac{W_{fi} - W_f}{W_{dry\ sample}} \times 100 \quad (g) \quad (2)$$

W_{fi} = First Weight of Sample and Container (g)

W_f = Final Weight of Sample and Container (g)

$$W_{water} = W_{fi} - W_f \quad (g)$$

$$W_{dry\ sample} = W_{fi} - W_{container} - W_{water} \quad (g)$$

Distribution of Pellets by Size

Pellet lengths (PL) of each mixture were separated into six classes of 3.15 mm < PL ≤ 20 mm, 20 mm < PL ≤ 35 mm, 35 mm < PL ≤ 38 mm, 38 mm < PL ≤ 40 mm, 40 mm < PL ≤ 45 mm, 45 mm < PL, and percentage distributions of the length classes were calculated according to weight and number. The original length class designations were written in the text but were named in the tables as follows:

$$-3.15 \text{ mm} < \text{PL} \leq 20 \text{ mm} = \text{PL1}$$

$$-20 \text{ mm} < \text{PL} \leq 35 \text{ mm} = \text{PL2}$$

$$-35 \text{ mm} < \text{PL} \leq 38 = \text{PL3}$$

$$-38 \text{ mm} < \text{PL} \leq 40 \text{ mm} = \text{PL4}$$

$$-40 \text{ mm} < \text{PL} \leq 45 \text{ mm} = \text{PL5}$$

$$-45 \text{ mm} < \text{PL} = \text{PL6}$$

It was determined that in general, pellets produced on the market have a length of 3-4 times their diameter [11], and so the ideal length of pellets produced with an 8 mm disc would be 20 mm < PL ≤ 35 mm. Maximum pellet length is 38.1 mm according to the PFI standard [12] and 40 mm according to the ENplus standard [13]. The proportion of pellets accepted longer than the maximum pellet length is 1% for the two standards, while according to the ENplus standard [13], pellets longer than 45 mm are not accepted at all. Therefore, the length classes of 35 mm < PL ≤ 38 mm, 38 mm < PL ≤ 40 mm and 45 mm < PL were selected. Also, because pellets with a granule size of less than 3.15 mm are classed by the PFI [12] and ENplus [13] standards as dust, the proportion by weight of dust was calculated with the help of a 3.15 mm sieve.

Distribution of Length Classes by Crack Categories

The pellets were examined under four categories, C-I, C-II, C-III and C-IV, according to the cracks on their surfaces.

The categories were defined as follows:

-C-I: No visible cracks on the surface

- C-II: At most two cracks on the surface in the form of scratches or slightly deepened
- C-III: More than two surface cracks in the form of scratches, or deep
- C-IV: Shape changed by cracks; pellets about to break up (Figure 5).

Because pellets in the $3.15 \text{ mm} < \text{PL} \leq 20 \text{ mm}$ length group were too short, pellets in this group were not examined for division into crack categories.

The distribution of crack categories was calculated within each length class and as a percentage of all samples.



Figure 5. Crack Categories

Length – Diameter – Weight Measurements

The length (mm), diameter (mm) and weight (g) of 100 selected pellets was measured, and the maximum, minimum, mean and standard deviation were found.

Mechanical Durability by Length and Crack Categories

Test with a Pellet Durability Tester

The testing stages were as follows:

- Pellet sample were taken $500 \text{ g} \pm 10 \text{ g}$ in accordance with the ASAE S269.5 standard and weighed after removal of dust. This was recorded as the Pellet Sample Weight (PSW).
- The tester was operated for 10 minutes at $50 \pm 2 \text{ rpm}$.
- The samples were removed from the tester, and in accordance with the ASAE S269.5 standard [15], the broken pellet pieces and dust were separated from the sample using a 6 mm and 3,15 mm sieve, and weighed. Their weight was then recorded as the Pellet Final Weight (PFW).
- Pellet Durability (PD) was calculated using Equation 3, which showed the relationship between the variable PSW (the mass of the pellet pieces before tumbling) and the variable PFW (the mass of the pellet pieces after tumbling) [14].

$$(PD) = \frac{PSW(g)}{PFW(g)} \times 100 (\%) \quad (3)$$

Free Fall Tests

Pellets of each length class and crack category were allowed to fall freely from a height of 1.85 m, with

five iterations. The number of falls after which the pellet broke up was observed, and weight losses were calculated by weighing on a sensitive scale.

Photographs of Cracks

Photographs of the cracks taken with a digital microscope (Figure 4) were used to show the differences between the crack categories according to the surface cracks.

3. Results & Discussion

Results

Moisture Analysis

It was found that the average moisture on a wet and dry weight basis was 14.16% and 16.49% for 66.5-33.5% acorn-pine mixture ratio pellets, and 14.30% and 16.69% for 50-25-25% acorn-pine-sawdust mixture ratio pellets. The moisture of both samples was above the 10% maximum on a wet weight basis of the PFI [12] and ENplus [13] standards.

Distribution of Pellets by Size

Pellets of neither mixture accorded with the PFI standard, which states that the proportion of pellets exceeding the maximum pellet length of 38.1 mm should be 1% [12]. In the case of the acorn-pine mix, the total proportion of pellets longer than 38 mm was 13.55%, while for the acorn-pine-sawdust mix this figure was found to be 7.76%. According to the ENplus standard, the maximum pellet length is 40 mm, and at most 1% of pellets must be in the $40 \text{ mm} < \text{PL} \leq 45 \text{ mm}$ class [13]. The $45 \text{ mm} < \text{PL}$ class is

not accepted [13]. It was determined that the mixtures did not conform to these standards.

According to both standards, pieces smaller than 3.15 mm are counted as dust [12], [13]. The amount

of dust in both mixtures was below the maximum proportion of 1%.

Table 1. Distribution of Pellet Length Classes by Number and Weight

Pellet Type 1: 66.5-33.5% Acorn-Pine Mixture Ratio					
Length Class	No	%	Distribution in 100 pellets	Weight (g)	%
PL1	1676	39.21	39	1187.00	21.26
PL2	1799	42.09	42	2589.66	46.38
PL3	220	5.15	5	431.78	7.73
PL4	132	3.09	3	273.13	4.89
PL5	277	6.48	7	637.37	11.42
PL6	170	3.98	4	439.85	7.88
Total	4274	100.00	100	5558.79	99.56
			Fines (g)	24.78	0.44
			Total (g)	5583.57	100
Pellet Type 2: 50-25-25% Acorn-Pine-Sawdust Mixture Ratio					
Length Class	No	%	Distribution in 100 pellets	Weight (g)	%
PL1	2206	49.91	50	1474.23	31.11
PL2	1749	39.57	40	2209.56	46.63
PL3	122	2.76	3	223.14	4.71
PL4	64	1.45	1	126.85	2.68
PL5	141	3.19	3	307.39	6.49
PL6	138	3.12	3	353.72	7.47
Total	4420	100	100	4694.89	99.09
			Fines (g)	43.34	0.91
			Total (g)	4738.23	100

Table 2. Distribution of Each Length Class by Crack Categories

Length Class		Pellet Type 1					Pellet Type 2				
		Crack Categories				Total	Crack Categories				Total
		I	II	III	IV		I	II	III	IV	
PL2	No	614	921	257	7	1799	459	986	285	19	1749
	%	34.13	51.20	14.29	0.38	100	26.24	56.38	16.30	1.08	100
PL3	No	64	129	25	2	220	31	75	14	2	122
	%	29.09	58.64	11.36	0.91	100	25.41	61.48	11.48	1.63	100
PL4	No	24	83	22	3	132	15	41	7	1	64
	%	18.18	62.88	16.67	2.27	100	23.44	64.06	10.94	1.56	100
PL5	No	93	152	28	4	277	31	89	15	6	141
	%	33.58	54.87	10.11	1.44	100	21.99	63.12	10.64	4.26	100
PL6	No	68	75	24	3	170	44	83	11	0	138
	%	40.00	44.12	14.12	1.76	100	31.89	60.14	7.97	0.00	100
Note: The 3.15 mm < PL ≤ 20 (PL1) class was not separated into crack categories.											

Distribution of Length Classes by Crack Categories

Distribution of Each Length Class

Table 2 shows the numerical and percentage distributions of crack categories within each length class of pellet. It can be seen from this that in the length classes of both mixture types, there were more pellets in C-II than in the other crack categories. In

66.5-33.5% of acorn-pine-sawdust mixture ratio pellets, C-II, C-III and C-IV cracks were found most in the 38 mm < PL ≤ 40 mm class.

In 50-25-25% of acorn-pine-sawdust mixture ratio pellets, there were fewer in the C-III crack category as size increased, but the number in the C-I category also decreased apart from in class 45 mm < PL. Most C-IV cracks was found in class 40 mm < PL ≤ 45. In

each mixture, most C-I cracks was found in class 45 mm < PL.

Distribution in the Whole Pellet Sample

The first five rows in Table 3, which are arranged according to crack categories in both mixtures apart from the 3.15 mm < PL ≤ 20 mm class, were the same for both mixture ratios. For all samples, the length class 20 mm < PL ≤ 35 mm and C-II cracks were the most frequent. It was calculated that in the 66.5-33.5% acorn-pine mixture pellets, the proportions of

C-I, C-II, C-III and C-IV cracks were 20.2%, 31.83%, 8.32% and 0.44% respectively, while they were 13.12%, 28.83%, 7.52% and 0.64% for the 50-25-25% acorn-pine-sawdust mixture.

The increase from C-I cracks to C-II cracks reduces mechanical durability. C-III cracks is not preferable for high mechanical durability, but also, C-IV cracks are definitely not desirable. Pellet durability will decrease because of this length class which was calculated in the acorn-pine mixture and the acorn-pine-sawdust mixture respectively as 39.21% and 49.91%.

Table 3. Distribution of Length Classes by Crack Categories in the Whole Pellet Sample and 66.5-33.5% Acorn-Pine and 50-25-25% Acorn-Pine-Sawdust Mixture Ratios

Series	Pellet Type 1		Pellet Type 2	
	%	Length Class and Crack Category	%	Length Class and Crack Category
1	39.21	PL1, C-I,II,III,IV	49.91	PL1, C-I,II,III,IV
2	21.56	PL2, C-II	22.31	PL2, C-II
3	14.37	PL2, C-I	10.38	PL2, C-I
4	6.01	PL2, C-III	6.45	PL2, C-III
5	3.56	PL5, C-II	2.01	PL5, C-II
6	3.02	PL3, C-II	1.88	PL6, C-II
7	2.18	PL5, C-I	1.70	PL3, C-II
8	1.94	PL4, C-II	1.00	PL6, C-I
9	1.75	PL6, C-II	0.93	PL4, C-II
10	1.59	PL6, C-I	0.70	PL3, C-I
11	1.50	PL3, C-I	0.70	PL5, C-I
12	0.66	PL5, C-III	0.43	PL2, C-IV
13	0.58	PL3, C-III	0.34	PL4, C-I
14	0.56	PL4, C-I	0.34	PL5, C-III
15	0.56	PL6, C-III	0.32	PL3, C-III
16	0.51	PL4, C-III	0.25	PL6, C-III
17	0.16	PL2, C-IV	0.16	PL4, C-III
18	0.09	PL5, C-IV	0.14	PL5, C-IV
19	0.07	PL4, C-IV	0.05	PL3, C-IV
20	0.07	PL6, C-IV	0.02	PL4, C-IV
21	0.05	PL3, C-IV	0.00	PL6, C-IV
	100	Total	100	Total

Length – Diameter – Weight Measurements

For 66.5-33.5% acorn-pine mixture ratio pellets, the following measurements were found: length (mm), maximum 50.15, minimum 12.14, mean 25.80, standard deviation 9.44; diameter (mm), maximum 8.10, minimum 7.62, mean 7.84, standard deviation 0.12; weight (g), maximum 2.82, minimum 0.57, mean 1.35, standard deviation 0.53, while for the acorn-pine-sawdust pellets, the measurements were length (mm), maximum 53.89, minimum 8.57, mean 21.90, standard deviation 9.28; diameter (mm), maximum 8.29, min 7.52, mean 7.92, standard deviation 0.17;

weight (g), maximum 2.92, minimum 0.40, mean 1.09, standard deviation 0.52.

Deviations in pellet diameter were greater in the 50-25-25% acorn-pine-sawdust pellets than in the 66.5-33.5% acorn-pine mixture ratio pellets.

Mechanical Durability by Length and Crack Categories

Pellet Durability Tester Results

The mechanical durability test results showed that, with the 66.5-33.5% acorn-pine mixture ratio pellets, only the 20 mm < PL ≤ 35 mm-C-I pellets were within the 97.5% mechanical durability limit of the

ENplus Standard [13]; however, the other classes met the minimum PFI standard [12] mechanical durability limit of 95% except for 3.15 mm < PL ≤ 20 mm-all cracks and 20 mm < PL ≤ 35 mm-C-III. With the 50-25-25% acorn-pine-sawdust mixture ratio pellets, none of the pellet classes were within the mechanical durability limit of the ENplus Standard, and only the 20 mm < PL ≤ 35 mm-C-I, 20 mm < PL ≤ 35-all cracks, 40 mm < PL ≤ 45-all cracks and 45 mm < PL

mixed cracks classes were within the mechanical durability limit of the PFI standard (Table 4).

With both pellet mixtures, even though pellets of the ideal pellet group of 20 mm < PL ≤ 35 mm were a mixture of all crack categories, they met ENplus or PFI standards. However, when only crack categories C-II and C-III are considered, mechanical durability progressively falls.

Table 4. Mechanical Durability of Pellets

Pellet Type 1: 66.5-33.5% Acorn-Pine Mixture Ratio				
Length Classes and Crack Categories	Pellet Sample Weight Before Test (g)	Pellet Sample Weight After Test (g)	Weight Loss (g)	Mechanical Durability (%)
PL1,2,3,4,5,6 C-I,II,III,IV	502.70	481.74	20.96	**95.83
PL1 – C-I,II,III,IV	500.16	469.15	31.01	*93.80
PL2 – C-I	500.39	489.92	10.47	***97.91
PL2 – C-II	500.11	483.99	16.12	**96.78
PL2 – C-III	250.54	233.63	16.91	*93.25
PL2 – C-I,II,III,IV	500.50	487.44	13.06	**97.39
PL3 – C-I,II,III,IV	350.77	339.55	11.22	**96.80
PL4 – C-I,II,III,IV	220.40	210.26	10.14	**95.40
PL5 – C-I,II,III,IV	500.07	485.72	14.35	**97.13
PL6 – C-I,II,III,IV	375.67	361.78	13.89	**96.30
Pellet Type 2: 50-25-25% Acorn-Pine-Sawdust Mixture Ratio				
PL1,2,3,4,5,6 C-I,II,III,IV	500.91	471.16	29.75	*94.06
PL1 – C-I,II,III,IV	500.38	462.36	38.02	*92.40
PL2 – C-I	364.43	352.68	11.75	**96.78
PL2 – C-II	500.59	472.35	28.24	*94.36
PL2 – C-III	200.61	185.72	14.89	*92.58
PL2 – C-I,II,III,IV	500.49	476.99	23.50	**95.30
PL3 – C-I,II,III,IV	168.04	159.54	8.50	*94.94
PL4 – C-I,II,III,IV	106.63	100.18	6.45	*93.95
PL5 – C-I,II,III,IV	243.43	227.27	16.16	*93.36
PL6 – C-I,II,III,IV	282.49	268.38	14.11	**95.01
***Pellets met the ENplus (EU) standard mechanical durability limit of 97.5%				
**Pellets met the minimum PFI (American) standard mechanical durability limit of 95%				
* Mechanical durability of pellets was lower than 95%				

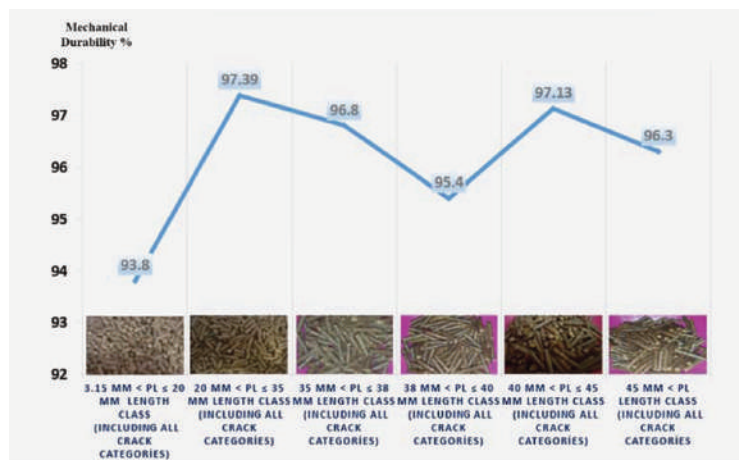


Figure 6. 66.5-33.5% Acorn-Pine Mixture Ratio Pellet Mechanical Durability by Length Classes

Some samples were found to be under 500 g. In these samples it was expected that the PDI value determined by the durability tester would be somewhat higher [15].

According to Figures 6 and 7, in which the mechanical durability of pellet lengths was examined against all crack categories, general mechanical durability fell with both mixtures between the length classes $20\text{ mm} < \text{PL} \leq 35\text{ mm}$ and $38\text{ mm} < \text{PL} \leq 40\text{ mm}$.

mm. However, the lowest mechanical durability in both mixtures was found in the length class $20\text{ mm} < \text{PL} \leq 35\text{ mm}$. This is thought to arise from the large number of cracks in small pellets. Generally, it was found that the durability of 66.5-33.5% mixture pellets was higher than that of 50-25-25% mixture pellets. Adding sawdust to the pellet mixture had a negative effect on mechanical durability.

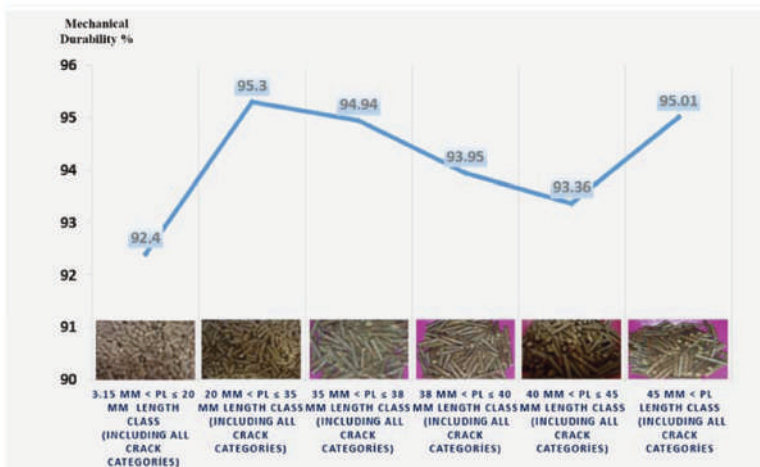


Figure 7. 50-25-25% Acorn-Pine-Sawdust Mixture Ratio Pellet Mechanical Durability by Length Classes

Free Fall Test Results

Three pellets were to be taken from each of the six length classes and crack categories, so that a total of 72 pellets were to be examined from each mixture. However, pellets of the class $3.15\text{ mm} < \text{PL} \leq 20\text{ mm}$ was not separated into crack categories, there were few or no examples of C-IV cracks, and some of pellets had been used in the mechanical durability tests, and so as a result of that 52 samples of 66.5-33.5% acorn-pine mixture ratio pellets and 50 of the 50-25-25% acorn-pine-sawdust mixture ratio pellets were examined.

According to the results, all length classes generally showed the same results for the two types of pellet mixes, namely that C-I pellets did not break into pieces easily, fragmentation and loss of weight of C-II and C-III pellets was greater than that of C-I, and C-IV pellets broke into pieces at the first fall and their loss of weight was determined as higher than the other categories. $3.15\text{ mm} < \text{PL} \leq 20\text{ mm}$ class did not break into pieces because of their short length, but their mechanical durability was calculated to be the lowest in the durability tester results as shown in Table 4. Breaking and weight loss increased with increase in length. In general, longer pellets began to break from the end. (Figure 8). Breaking into four pieces was most commonly seen in 50-25-25% acorn-

pine-sawdust mixture ratio pellets of the $40\text{ mm} < \text{PL} \leq 45\text{ mm}$ length class (Figure 9).



Figure 8. Longer pellets beginning to break from the end



Figure 9. 50-25-25% Acorn-Pine-Sawdust mixture ratio $40\text{ mm} < \text{PL} \leq 45\text{ mm}$ Length Class Pellet

It was calculated from the results of the free fall test when 66.5-33.5% oak-pine mixture ratio pellets of the C-I crack category, which had shown the best mechanical durability, were examined by length class, that weight loss was 0.023 g in the $20\text{ mm} < \text{PL} \leq 35\text{ mm}$ class, 0.037 g in the $35\text{ mm} < \text{PL} \leq 38\text{ mm}$ class, 0.043 g in the $38\text{ mm} < \text{PL} \leq 40\text{ mm}$ class, and 0.050 g in the $40\text{ mm} < \text{PL} \leq 45\text{ mm}$ and $45\text{ mm} < \text{PL}$ classes. In the 20 mm

< PL ≤ 35 class, only one pellet broke up; as length increased pellets broke into two, and in the 45 mm < PL class, some pellets were seen to break into three pieces (Table 5).

Table 5. 66.5-33.5% Acorn-Pine Mixture Ratio Pellets: Free Fall Test Results of C-I Cracks by Length

20 mm < PL ≤ 35 C-I												
Pellet No	Before 1 st Fall (g)	After 1 st Fall (g)	After 2 nd Fall (g)		After 3 rd Fall (g)		After 4 th Fall (g)		After 5 th Fall (g)		Total Weight Loss (g)	Pieces
1	1.46	-	-	-	-	-	-	-	1.44	0.02	0.02	1
2	1.17	-	-	-	-	-	-	-	1.15	0.02	0.02	1
3	1.39	-	-	-	-	-	-	-	0.72	0.64	0.03	2
35 mm < PL ≤ 38 C-I												
1	1.90	-	1.21	0.69	-	-	-	-	1.20	0.67	0.03	2
2	1.96	-	1.05	0.90	-	-	-	-	1.02	0.89	0.05	2
3	1.91	-	-	-	-	-	-	-	0.90	0.98	0.03	2
38 mm < PL ≤ 40 C-I												
1	2.06	-	1.40	0.63	-	-	-	-	1.38	0.62	0.06	2
2	2.02	-	-	-	-	-	-	-	1.05	0.94	0.03	2
3	1.94	-	-	-	0.89	1.03	-	-	0.88	1.02	0.04	2
40 mm < PL ≤ 45 C-I												
1	2.25	-	1.57	0.64	-	-	-	-	1.56	0.63	0.06	2
2	2.28	-	-	-	1.35	0.90	-	-	1.34	0.90	0.04	2
3	2.21	-	1.06	1.12	-	-	-	-	1.05	1.11	0.05	2
45 mm < PL C-I												
1	2.55	-	-	-	1.88	0.65	-	-	1.87	0.64	0.04	2
2	2.35	-	-	-	1.73	0.62	-	-	1.05	0.63	0.61	3
3	2.60	-	-	-	1.75	0.84	-	-	1.18	0.54	0.83	3

Pellets were weighed after each free fall, but the table shows only the weight when a pellet broke, and the final weight. Lines indicate that there was no change.

Crack Photographs

As seen in Figure 10, cracks on the surface of pellets increased in size from C-II to C-IV. An increase in

pellet storage time or storage in unsuitable conditions increased deterioration, and cracks became progressively larger [16].



Figure 10. Photos of crack categories taken by digital microscope

4. Conclusions

Mechanical durability has great importance for pellet quality under market conditions, and there are many factors such as raw material properties, moisture content, pellet length and surface cracks which affect the mechanical durability of pellets.

Generally, if the length of pellets increases, the mechanical durability decreases, but pellet length and surface cracks should be investigated together. Even if the ideal pellet length shows high mechanical durability, mechanical durability will decrease as a result of an increasing percentage of C-III and C-IV cracks.

The shortest pellets showed low mechanical durability. In our opinion, pellets in this group are parts of longer ones. Also, some of the longer pellets showed high mechanical durability according to durability test results, but they easily broke into pieces in the free fall tests. This indicates that the results of durability and free fall tests must be evaluated together.

Also, considering that longer pellets have a lower burning efficiency and have higher emission values [17], producers should adjust the cutting knives of their pelletizing machines according to the maximum length limits given in pellet standards.

References

- [1] **Turkish General Directorate of Forestry.:** 2015. Türkiye Orman Varlığı 2016-2017 [Forests in Turkey 2016-2017]. Republic of Turkey Ministry of Forestry and Water Management, pp. 36.
- [2] **Turkish General Directorate of Forestry.:** 2013. Orman Atlası [Forest Atlas]. Republic of Turkey Ministry of Forestry and Water Management, pp. 116.
- [3] **NIIR Board of Consultants & Engineers.:** 2011. Leather Processing & Tanning Technology Handbook, NIIR Project Consultancy Services, pp. 467. ISBN: 9788190568593
- [4] **Wickens G. E.:** 1995. Non-Wood Forest Products 5 Edible Nuts, Food And Agriculture Organization Of The United Nations, pp. 129. ISBN 92-5-103748-5
- [5] **Rosengarten, F. Jr.:** 2004. The Book of Edible Nuts. pp. 268. ISBN-10: 0486434990
- [6] **Erten A. P., Önal S.:** 1985. Ağaç Türlerimizin Odun ve Kabuklarının Değerlerinin Saptanmasına İlişkin Araştırmalar [Determination of Caloric Value of Native Spectes Woods and Barks]. Or. Araş. Ens. Dergisi, Temmuz, Vol. 31, No. 62, pp. 91-110.
- [7] **Garcia-Maraver A., Perez-Jimenez J. A., Zamorano M.:** 2015. Biomass Pelletization, Chapter 1, Background. pp. 2-20. ISBN 978-1-78466-062-8.
- [8] **Garcia-Maraver A., Carpio M.:** 2015. Biomass Pelletization, Chapter 2, Factors Affecting Pellet Quality. pp. 21-35, ISBN 978-1-78466-062-8
- [9] **Küçükyavuz O.:** 2002. Valeks İmalatı Sanayi Profili [Profile of the Valonia Production Industry]. T.C Sanayi Ve Ticaret Bakanlığı, Sanayi Araştırma ve Geliştirme Genel Müdürlüğü - [Republic of Turkey Ministry of Industry and Trade, General Directorate of Industry Research and Development], pp. 23.
- [10] **Govett R., Mace T., Bowe S.:** 2010. A Practical Guide For The Determination Of Moisture Content Of Woody Biomass, University of Wisconsin, pp. 20.
- [11] **Kofman P. D.:** 2007. Simple ways to check wood pellet quality, Processing/ Products No. 11, pp. 2.
- [12] **Pellet Fuels Institute.:** 2015. Pellet Fuels Institute Standard Specifications for Residential/Commercial Densified Fuel, July 9, 2015, pp. 10.
- [13] **European Pellet Council.:** 2015. ENplus Handbook, Part 3: Pellet Quality Requirements, European Pellet Council (EPC), Version 3.0, August 2015, pp. 10.
- [14] **ASABE.:** 2012. Densified Products for Bulk Handling — Definitions and Method. ASAE S269.5, October 2012.
- [15] **Stark C., Fahrenholz A.:** 2015. Evaluating Pellet Quality, Kansas State University Agricultural Experiment Station and Cooperative Extension Service, July 2015, Published Online: MF3228, pp. 4.
- [16] **Grahama S., Eastwick C., Colin Snape C., Quick W.:** 2017. Mechanical degradation of biomass wood pellets during long term stockpile storage. Fuel Processing Technology, Vol. 160, No. 1, pp. 143-151. <http://dx.doi.org/10.1016/j.fuproc.2017.02.017>
- [17] **Wöhler M., Jaeger D., Reichert G., Schmidl C., Pelz S. K.:** 2017. Influence of pellet length on performance of pellet room heaters under real life operation conditions. Renewable Energy, Vol. 105, pp. 66-75. <http://dx.doi.org/10.1016/j.renene.2016.12.047>

CONTENTS OF NO 32/2017

A REVIEW OF PERFORMANCE HYBRID PHOTOVOLTAIC/THERMAL SYSTEM FOR GENERAL - APPLICATIONS

M.H.R. Alktranee
Department of Mechanical,
Technical Institute of Basrah,
Southern Technical University, Basrah, Iraq.5

EXAMINATION OF THE HUNGARIAN AGRICULTURAL MACHINERY MANUFACTURERS' PRODUCT PLANNING, QUALITY MANAGEMENT TECHNIQUES AND PRODUCTION COORDINATION

A. Goda – V. Medina – L. Zsidai
Faculty of Mechanical Engineering,
Szent István University16

CLASSIFICATION MODELS OF HUNGARIAN HONEY SAMPLES BASED ON ANALYTICAL AND PHYSICAL CHARACTERISTICS

T. Kaszab¹ – Zs. Bodor² – Z. Kovacs¹ – Cs. Benedek²
¹Department of Physics and Control,
Faculty of Food Science, Szent István University,
Somlói út 14-16., Budapest, H-1118, Hungary
²Department of Dietetics and Nutrition,
Faculty of Health Sciences, Semmelweis University,
Vas u. 17., H-1088 Budapest, Hungary22

AXIAL FLOW TURBINE FOR SOLAR CHIMNEY

W. M.A Elmagid¹ – I. Keppler²
¹Institute of Environmental Systems,
Szent István University, Páter Károly street 1,
Gödöllő, H-2103, Hungary
²Institute of Mechanics and Machinery,
Szent István University, Páter Károly street 1,
Gödöllő, H-2103, Hungary29

PREDICTION OF MAIN ANALYTICAL AND PHYSICAL PARAMETERS OF HONEY WITH ELECTRONIC TONGUE

F. A. Koncz¹ – Zs. Bodor² – T. Kaszab¹ – I. Kertész¹ –
J. L. Z. Zaukuu¹ – Cs. Benedek² – Z. Gillay¹ –
Z. Kovacs¹
¹Department of Physics and Control,
Szent István University, Somlói út 14-16., Budapest,
H-1118, Hungary
²Department of Dietetics and Nutrition,
Faculty of Health Sciences, Semmelweis University,
Vas u. 17., H-1088 Budapest, Hungary38

A NEW SHAKER HEAD DESIGN FOR REDUCING BARK INJURIES ON FRUIT TREES

Z. Láng
Technical Department, Szent István University,
H-1118 Budapest, Villányi street 3144

THE FEASIBILITY OF MODELLING ROCKS IN ENGINEERING APPLICATIONS WITH THE USE OF DISCRETE ELEMENT METHOD

Á. Orosz – K. Tamás – J. P. Rádics
Department of Machine and Product Design,
Budapest University of Technology and Economics
Műegyetem rkp. 3., Budapest, H-1111, Hungary51

NON-DESTRUCTIVE POSTHARVEST MATURITY EVALUATION OF GOLDEN DELICIOUS APPLE

V. Zsom-Muha¹ – L. Ember² – G. Hitka² – L. Baranyai¹ –
L.L.P. Nguyen³ – D. Nagy¹ – T. Zsom²
¹Department of Physics and Control,
Faculty of Food Science, Szent István University,
Villányi út 29-43., Budapest, H-1118, Hungary
²Department of Postharvest Science and Sensory
Evaluation, Faculty of Food Science,
Szent István University, Villányi út 29-43., Budapest,
H-1118, Hungary
³Department of Refrigeration and Livestock Products
Technology, Faculty of Food Science,
Szent István University, Villányi út 29-43., Budapest,
H-1118, Hungary56

EFFECTS OF LENGTH ON MECHANICAL DURABILITY OF VARIOUS WOOD PELLETS

R.C Akdeniz¹ – O. Esmer²
¹Ege University, Faculty of Agriculture,
Department of Machinery and Technologies
Engineering, Bornova/Izmir, 35100, Turkey
²Ege University, Graduate School of Natural and
Applied Science Institute,
Agricultural Machinery and Technologies Engineering,
MSc, Bornova/Izmir, 35100, Turkey62